Design and Characterisation of Polyhydroxyalkanoate Bead-Alginate Hybrid Materials

A dissertation presented in partial fulfilment of the

requirements of the degree of

Master of Science

in

Microbiology

at Massey University, Manawatū,

New Zealand.

Kampachiro Ogura

2018

Abstract

Encapsulation is a technique to entrap a material of interest within a carrier material, and it has been used in a wide range of industries such as biopharmaceutical and biotechnological companies. Among biopolymers used for the carrier material, alginate has been widely used due to its attractive properties of biodegradability, biocompatibility and ease of gelation under mild conditions. In this study, a novel hybrid micro- or millisphere composed of functionalised polyhydroxyalkanoate (PHA) beads and alginate was fabricated through ionotropic gelation methods. The selected functional proteins displayed on PHA beads were the IgG binding domain (ZZ) of Protein A from *Staphylococcus aureus*, and organophosphate hydrolase (OpdA). The effect of alginate encapsulation on their functionality was assessed. In addition, alginate millispheres encapsulating PHA beads were assessed for their ability to remove lipophilic compounds from an aqueous solution. This utilised the hydrophobic polyester core of the PHA beads and was assessed by using the lipophilic dye, Nile red, as the reporter.

The results of IgG binding assays using PHA beads encapsulated in alginate microspheres showed no significant difference compared with negative controls, and no elution of bound IgG was observed. However, the alginate encapsulation enhanced IgG binding to the PhaC derived proteins on PHA beads within alginate microspheres. In contrast, alginate encapsulation limited the activity of PHA beads displaying OpdA when compared to free PHA beads. The qualitative data obtained from phase contrast and fluorescence microscopy suggested that the enzyme displayed on PHA beads was active within alginate microspheres. The lipophilic dye removal by PHA beads encapsulated in alginate millispheres was influenced by different parameters used in the millisphere preparation. The adsorption kinetics aligned with a pseudo second-order kinetic model, and the equilibrium adsorption data was in agreement with the Freundlich isotherm model.

This study has provided preliminary data for fabrication of a hybrid material of functionalised PHA beads with alginate. The development of combinations of highly functional PHA beads with other biomaterials is expected to expand the application field of PHA beads.

Acknowledgments

I would like to thank my supervisor Professor Bernd Rehm for giving me the opportunity to do my Masters project under his guidance and supervision. Without your guidance and encouragement, this project would not be possible.

I would also like to thank my co-supervisor Dr. Zoe Jordens for accepting the sudden request to be co-supervisor. Thank you for your time, guidance and encouragement to complete this thesis. Without your help, this thesis would not have been completed.

I would like to thank everyone at the Institute of Fundamental Science and the Manawatu Microscopy and Imaging Centre who offered me their time, support and technical expertise when needed.

I am grateful to be a member of the Rehm lab. I would like to thank all my colleagues for their advice and assistance. Also, thanks to the former staffs from Polybatics Ltd. for giving me support and technical advice for my project.

Last but not the least, I must express my very profound gratitude to my family for providing me with continuous support and encouragement throughout my years of study. This accomplishment would not have been possible without them.

Table of Contents

List of Figures

List of Tables

List of Abbreviations

°	Degree
°C	Degree Celsius
(aq)	Aqueous solution
Ag85A	Diacylglycerol acyltransferase from *Mycobacterium tuberculosis*
ANOVA	Analysis of variance
Ap^r	Ampicillin resistance
APS	Ammonium persulfate
b	Langmuir isotherm constant
BCA	Bicinchoninic acid
BET	Brunauer–Emmett–Teller
Bis-Tris	Bis(2-hydroxyethyl)amino-tris(hydroxymethyl)methane
BL21_69	BL21 (DE3) *Escherichia coli* harbouring pMCS69
BPA	Bisphenol A
BSA	Bovine serum albumin
CAT	Chloramphenicol acetyltransferase
C_e	Equilibrium concentration of the aqueous phase
Cm^r	Chloramphenicol resistance
Coumaphos	O, O-diethyl O-3-chloro-4-methyl-2-oxo-2H-chromen-7-yl phosphorothioate
cP	Centipoise
CPS	Counts per second
D10	The size of particle below which 10% of the sample lies
D50	Median particle size
D90	The size of particle below which 90% of the sample lies
Da	Dalton
DETP	Diethylthiophosphate
DMSO	Dimethyl sulfoxide
DsRedEC	A fluorescent protein
DNA	Deoxyribonucleic acid
EDTA	Ethylenediaminetetraacetic acid
Em.	Emission
Ex.	Excitation
FT-IR	Fourier transform infrared spectroscopy
g	Grams
g	G-force(s)
(g)	gas
G	Gauge
GFP	Green fluorescent protein from *Aequorea victoria*
GG	Homopolymeric G-monomer block
GRAS	Generally recognised-as-safe
3-HB	3-hydroxybutyrate
HEPES	4-(2-hydroxyethyl)-1-piperazineethanesulfonic acid

HPLC	High performance liquid chromatography
I	Internal gelation
I+E	Double gelation
IFN-α 2b	Human interferon alpha 2b, without signal peptide
IgG	Immunoglobulin G
IL-2	Interleukin-2
IPTG	Isopropyl-β-D-thiogalactopyranoside
k_1	The rate constant of first-order adsorption
k_2	The rate constant of second-order adsorption
k_{cat}	Catalytic rate
K_F	An indicator of adsorption capacity
K_M	The Michaelis-Menten constant
kDa	Kilo Daltons
kg	Kilogram
(l)	Liquid
LB	Luria-Bertani broth
LactC2	Phospholipid-binding domain of lactadherin
LacZ	β-galactosidase
µg	Microgram
µl	Microlitre
µm	Micrometre
µM	Micromolar
M	Molar
m^2	Square metre
MBP	Maltose binding protein
MG	Heteropolymeric G and M monomer block
MG/MG	A junction formed by MG-blocks via interaction with divalent cation
mA	Milliampere
mg	Milligram
ml	Millilitre
mm	Millimetre
mM	Millimolar
MM	Homopolymeric M-monomer block
MOPS	3-(N-morpholino) propanesulfonic acid
mPa.s	Millipascal-second
Mw	Molecular weight
n	Adsorption intensity
ng	Nanogram
nm	Nanometre
NemA	N-ethylmaleimide reductase
N.S.	Not significant
OD	Optical density
OmpA	Outer membrane protein A

OmpF	Outer membrane protein F
OpdA	Organophosphate hydrolase
PBS	Phosphate-buffered saline
PEG	Polyethylene glycerol
PHA	Polyhydroxyalkanoate
PhaA	β-ketothiolase
PHA_{LCL}	Long chain length (more than C14) PHA
PHA_{MCL}	Medium chain length (C6-14) PHA
PHA_{SCL}	Short chain length (C3-5) PHA
PHA bead-alginate microspheres	PHA beads encapsulated in alginate microspheres
PHA bead-alginate millispheres	PHA beads encapsulated in alginate millispheres
PhaB	Acetoacetyl-CoA reductase
PhaC	PHA synthase
phaCAB	PHA biosynthesis gene operon
PhaC PHA bead-alginate microspheres/ PhaC-ALG	PhaC PHA beads encapsulated in alginate microspheres
PhaC-OpdA	OpdA fused to the C-terminus of PhaC
PhaC-OpdA PHA beads	PHA beads displaying OpdA
PhaC-OpdA PHA bead-alginate microspheres	PhaC-OpdA PHA beads encapsulated in alginate microspheres
PhaE	Type III PHA synthase subunit
PhaF	PHA synthesis regulatory protein from *Pseudomonas oleovorans*
PhaI	PHA synthesis regulatory protein from *Pseudomonas oleovorans*
PhaM	Regulatory protein
PhaP	Phasin protein
PhaR	Transcriptional regulator protein that controls the transcription of Phasin/ Type IV PHA synthase subunit
PhaZ	Intracellular PHA depolymerase
PHB	Poly(3-hydroxybutyric acid)
PHBV	Poly(3-hydroxybutyrate-co-3-hydroxyvalerate)
p*I*	Isoelectric point
q_e	Equilibrium adsorption of solid phase
q_m	Maximum adsorption capacity
R^2	Correlation coefficient
rpm	Revolutions per minute
(s)	Solid
ScFv	Single-chain variable fragment antibody
SD	Standard deviation
SDS	Sodium dodecyl sulphate
SDS-PAGE	Sodium dodecyl sulphate polyacrylamide gel electrophoresis
SE	Standard error of mean
SEM	Scanning electron microscopy
Span80	Sorbitan monooleate

T7 promoter	Promoter for T7 RNA polymerase
T7 terminator	Transcription terminator for T7 RNA polymerase
TBS	Tris buffered saline
TEM	Transmission electron microscopy
TEMED	N, N, N', N'-tetramethylethyl-endiamine
Tet^r	Tetracycline resistance
TNF-α	Human tumour necrosis factor
Tris	Trishydroxymethylaminomethane
Triton X-100	4-(1,1,3,3-Tetramethylbutyl)phenyl-polyethylene glycol
V	Volts
V_0	Initial sorption rate
V_{max}	Maximum reaction rate
v/v	Volume per volume
w/o	Water-in-oil
w/v	Weight per volume
ZZ	Two IgG binding Z domain of protein A from *Staphylococcus aureus*
ZZC	ZZ domain fused to the N-terminus of PhaC
ZZC PHA beads	PHA beads displaying ZZ domain
ZZC PHA bead-alginate microspheres/ ZZC-ALG	ZZC PHA beads encapsulated in alginate microspheres

Abbreviations for ions

As^{5+}	Arsenic (V) or arsenic ion
Ba^{2+}	Barium (II) or barium ion
Ca^{2+}	Calcium (II) or calcium ion
Cd^{2+}	Cadmium (II) or cadmium ion
Co^{2+}	Cobalt (II) or cobalt ion
Cr^{2+}	Chromium (II) or chromium ion
Cu^{2+}	Copper (II) or cupric ion
Mg^{2+}	Magnesium (II) or magnesium ion
Mn^{2+}	Manganese (II) or manganous ion
Na^{+}	Sodium (I) or sodium ion
Ni^{2+}	Nickel (II) or nickel ion
Pb^{2+}	Lead (II) or lead ion
Sr^{2+}	Strontium (II) or strontium ion
Zn^{2+}	Zinc (II) or zinc ion

Chapter 1: Introduction

1.1 Encapsulation in polymers

Encapsulation is a technology of packaging solids, liquids, or gaseous materials within a natural or synthetic polymeric matrix (Desai & Park, 2005). This technology has been used in numerous applications in a wide range of industrial areas, such as the pharmaceutical, agricultural, medical, and food industries (Leong *et al.*, 2016). The encapsulation techniques have been used to (1) immobilise materials within the polymer matrix, (2) separate the encapsulated material from the external environment to avoid possible incompatibilities while the semi-permeable membrane allows the transport of low molecular weight compounds, and (3) extend the viability, or shelf life, of the encapsulated material (Singh *et al.*, 2010; Gasperini *et al.*, 2014; Dragostin *et al.*, 2017). Particularly in the drug delivery field, there have been extensive studies on the controlled release of the encapsulated material at the target destination (Singh *et al.*, 2010). Moreover, in the tissue-engineering field, polymer matrices have been used to provide a three-dimensional scaffold for the encapsulated cells (Nicodemus & Bryant, 2008; Elabd *et al.*, 2016; Bryant & Vernerey, 2018). Various types of polymers have been investigated for use in encapsulation applications including natural polymers such as alginate, chitosan, and agarose (Gasperini *et al.*, 2014; Rehm *et al.*, 2016) and synthetic polymers such as silica, polyacrylate, and polyethylene glycerol (PEG) (Gill & Ballesteros, 2000; Olabisi, 2015; Rehm *et al.*, 2016). Amongst the various available polymers, alginate is widely used in the encapsulation process due to its outstanding physical properties. Alginate has the properties of biocompatibility, biodegradability, low toxicity, as well as easily forming gels using divalent cations under mild and safe conditions (Lee & Mooney, 2012; Gasperini *et al.*, 2014; Paques, 2015).

1.2 Alginate

1.2.1 Chemical structure

Alginate is a naturally occurring anionic and hydrophilic polysaccharide that is composed of β-D-mannuronic acid (M) and α-L-guluronic acid (G) monomer residues linked via the β-1,4-glycosidic bond (Figure 1). The monomers are linked in highly variable distribution patterns, and the proportions of M and G-residues give different properties to the alginate polymer. The arrangement of monomer blocks can be homopolymeric (GG and MM) and

heteropolymeric (MG) (Donati & Paoletti, 2009; Ching *et al.*, 2017). The main source of alginate is brown algae (Gasperini *et al.*, 2014), but some bacteria also produce alginate (Remminghorst & Rehm, 2006). The different species produce different proportions and distributions of the monomers that affects the molecular weight and physical properties of the alginate. In most cases, alginate is available as the sodium, potassium or ammonium salts (Ching *et al.*, 2017).

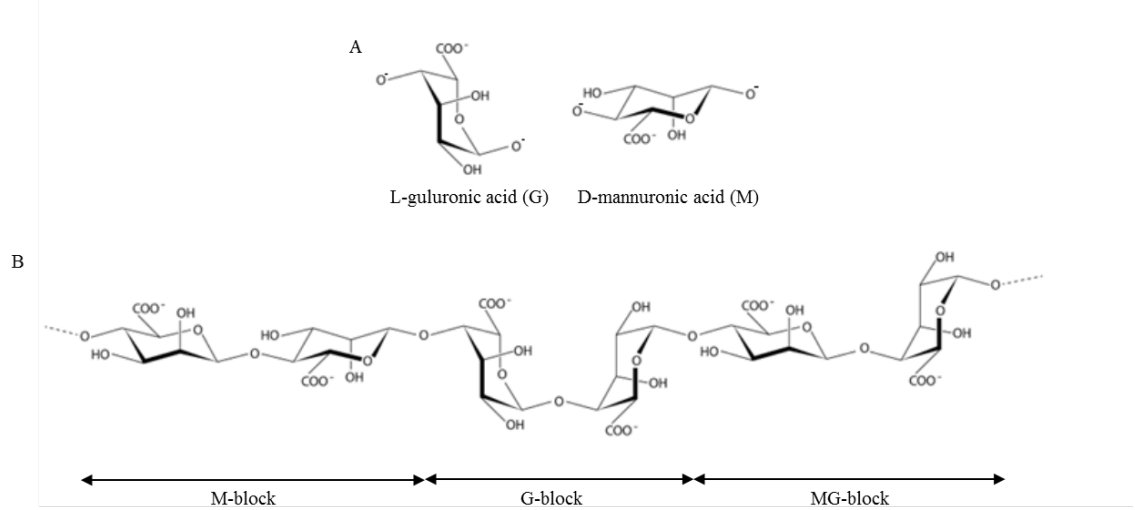

Figure 1: Chemical structure of alginate. A: Chemical structure of alginate monomers; M, mannuronic acid; G, guluronic acid. B: Sequences of an alginate polymer; M-block, G-block, and MG-block linked via a β-1,4-glycosidic bond.

1.2.2 Alginate gel matrix (Hydrogels)

Alginate hydrogels are hydrophilic three-dimensional polymer networks, which can be formed through physiological and chemical cross-linkage of the polymers (Lee & Mooney, 2012). The physical properties of an alginate hydrogel are largely influenced by the chemical composition, the distribution and ratio of G and M residues, and the concentration of alginate in the preparation (Donati & Paoletti, 2009; Lee & Mooney, 2012; Paques, 2015). The advantage of using alginate for the encapsulation process, especially for sensitive materials, is that alginate gelation can occur under mild conditions and uses nontoxic compounds during the preparation (Paques, 2015). Moreover, in comparison to other polysaccharide-based hydrogels, such as gelatin or agar, alginate gel formation is less dependent on temperature (Draget & Skja˚k-Bræk, 2011). Therefore, alginate is an ideal option for encapsulating sensitive materials. There have been a number of methods developed to prepare alginate hydrogels, including ionic cross-linking,

thermal gelation, cell-cross-linking, free radical polymerisation, and the click reaction (Sun & Tan, 2013). The most common gelling method used in the preparation of alginate spheres is the ionic cross-linking method (Ching *et al.*, 2017). Alginate hydrogel prepared with the ionic cross-linking gelation is described below.

1.2.2.1 Ionic gelation

Ionic cross-linking with various divalent cations is the most commonly used gelation method in alginate hydrogel preparation. The binding of multivalent cations to alginate is a highly selective process as it depends on the composition of the alginate, such as the presence of G blocks, and the binding affinity of the divalent cations used (Draget & Skja˚k-Bræk, 2011; Paques, 2015; Ching *et al.*, 2017). The binding affinity of various cations in increasing order is as follows: $Mg^{2+}<Mn^{2+}<Zn^{2+}<Ni^{2+}<Co^{2+}<Ca^{2+}<Sr^{2+}<Ba^{2+}<Cd^{2+}<Cu^{2+}<Pb^{2+}$ (Donati & Paoletti, 2009; Ching *et al.*, 2017), and the affinity directly influences the strength of the gel matrix as a higher binding affinity produces a stronger hydrogel (Smidsrød, 1974; Smidsrød & Skja˚k-Bræk, 1990). Among the various available divalent cations, calcium is the most commonly used for the ionotropic gelation of alginate. This is because the calcium ion is non-toxic, readily available, and relatively inexpensive (Paques, 2015; Ching *et al.*, 2017). In the presence of divalent cations, there is an ion exchange of the sodium ions from the G residue of the alginate polymer with the divalent cations, and gelation occurs by the cooperative interaction between the divalent cation and the oxygen atoms from the carboxyl groups of G residue block regions of the alginate polymers (Sun & Tan, 2013; Zia *et al.*, 2015). Each cation binds with four G residues forming a characteristic “egg-box” calcium linked junctions (Figure 2) (Draget & Skja˚k-Bræk, 2011; Ching *et al.*, 2017), which results in the interlinking of the alginate chains and forms a three-dimensional gel network.

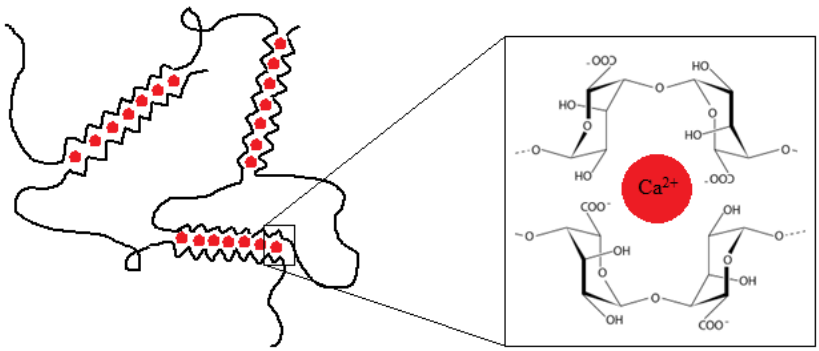

Figure 2: Alginate polymer binding with calcium ion to form an "egg-box" junction model.

1.2.2.1.1 External gelation

The external gelation method is the most widely used mechanism of ionotropic gelation for alginate sphere preparation because of its simple one-step process. When an alginate droplet contacts a divalent cation-containing cross-linkage solution, the divalent cation instantaneously cross-link with the alginate polymer at the periphery of the droplet, resulting in the formation of a solid membrane surrounding the liquid droplet in the core. Extended immersion in the cross-linking solution allows diffusion of the divalent cations across the membrane and ultimately towards the centre of the droplet. Therefore, this method is also referred to as the "diffusion method" (Chan *et al.*, 2006; Paques, 2015). As a result, this method produces a heterogeneous gelling profile with more alginate and cation networks formed at the peripheral regions compared with the centre of the sphere (Figure 3) (Chan *et al.*, 2006). To solve the inhomogeneity, a low concentration of non-gelling cations, such as Na^+ or Mg^{2+} ions, added in the cross-linking solution with calcium ions during gelation, have been shown to produce a homogeneous alginate hydrogel matrix (Skjåk-Bræk *et al.*, 1989; Donati & Paoletti, 2009). In an attempt to reduce the particle size of alginate spheres, an emulsification method with external gelation was conducted. In this method, alginate solution was added to an oil phase and dispersed to produce micron-sized droplets. Subsequently, the alginate droplets were externally gelled by adding $CaCl_2$ solution into the emulsion. The productivity of alginate spheres (microspheres) increased, however, clustering of alginate microspheres occurred, and multiple emulsion (water-in-oil-in-water, w/o/w) formed (Poncelet *et al.*, 1992). Therefore, the emulsification method predominantly uses internal gelation as later described. However, a recent study demonstrated that the formation of clusters and multiple emulsions were minimised by dispersing $CaCl_2$ nanoparticles in the oil phase of the emulsion instead of adding $CaCl_2$ solution directly to initiate gelation externally (Paques *et al.*, 2013).

1.2.2.1.2 Internal gelation

Alginate hydrogels prepared by the internal gelation method use insoluble calcium, such as calcium carbonate ($CaCO_3$), calcium citrate ($Ca_3(C_6H_5O_7)_2$), or calcium sulfate ($CaSO_4$) as the cross-linker in alginate polymers. The insoluble calcium compound is mixed with alginate solution, then dispersed into oil to form alginate droplets containing the insoluble calcium compounds. Calcium ions are then released in the alginate droplet

by dissolution of the insoluble calcium. This is achieved by reduction of the pH through acid addition, e.g. CH_3COOH. The reaction occurs as follows: $CaCO_3(s)+2H^+(aq)\rightarrow Ca^{2+}(aq)+H_2O(l)+CO_2(g)$. In contrast to the alginate hydrogel prepared by external gelation, internal gelation generates evenly distributed cations in the alginate hydrogel, thereby forming a more homogeneous gel network (Figure 3) (Poncelet *et al.*, 1992; Reis *et al.*, 2006; Zhao *et al.*, 2007; Andersen *et al.*, 2015; Paques, 2015).

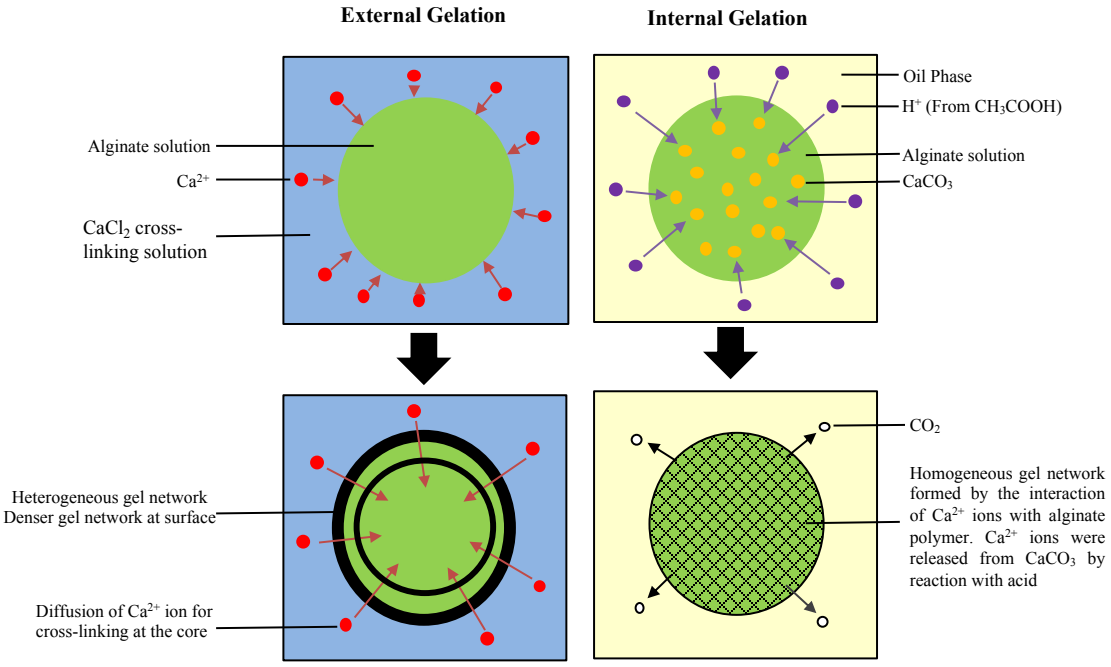

Figure 3: Schematic image of alginate hydrogels prepared by external and internal gelation. Based on Leong *et al.* (2016).

1.2.3 Physical properties of alginate hydrogel

The strength of alginate hydrogel prepared by ionic cross-linking is influenced by the G-block content and the level of calcium ion interaction with the alginate polymer (Smidsrød, 1974; Gombotz & Wee, 2012). Alginate with high G-block content tends to produce a stiff hydrogel while alginate with high M-block content produces a soft hydrogel. However, from the mechanical property point of view, the alginate hydrogel prepared with high G-block content is brittle while high M-block content is elastic (Thu *et al.*, 1996; Gombotz & Wee, 2012; Ching *et al.*, 2017). Higher concentrations of calcium ion give a greater extent of interaction with alginate polymer, influencing the gel strength as denser gel network will be formed (Draget *et al.*, 1993). In addition, the type of divalent

cation chosen in the ionic cross-linkage also influences the gel strength. For instance, barium ion has higher affinity for alginate than calcium ion, and binds to both M and G-blocks, while calcium ion does not bind to M-block (Mørch *et al.*, 2006). Moreover, the molecular weight of alginate also contributes to the mechanical strength of alginate hydrogel when calcium ion concentration is low. At low concentrations of calcium ion, higher molecular weight alginate contributes to stronger mechanical strength in which the intra-molecular covalent bonds of alginate polymer backbone are stronger than the inter-molecular ionic bonds formed by calcium ion cross-linking (Kuo & Ma, 2001; Draget *et al.*, 2005; Lee & Mooney, 2012). However, by increasing the concentration of calcium ion, there will be more interactions between calcium ions and alginate polymer making this a more significant contributor to the mechanical strength than molecular weight (Qiu *et al.*, 2011). Meanwhile, in the presence of excess calcium ions, it has been shown that contribution of molecular weight to the mechanical strength occurs up to 150 kDa. With alginate molecular weight higher than 150 kDa, there was only a slight increase in mechanical strength when the calcium ion and alginate polymer interaction was saturated (Draget *et al.*, 1993). The gelation rate controls the uniformity and strength of hydrogel as slower gelation produces hydrogel with more uniform structure and greater mechanical integrity (Kuo & Ma, 2001). For instance, gelation at low temperature reduces the rate of gelation, in turn, the mechanical strength of the hydrogel is enhanced (Augst *et al.*, 2006).

The alginate hydrogel preparation method, either internal or external gelation, significantly influences the porosity and permeability of the alginate hydrogel in the resulting alginate spheres (Chan *et al.*, 2006). The porous structure is a significant feature of alginate hydrogel as it allows substrates to diffuse in and out of the hydrogel (Smidsrød & Skja˚k-Bræk, 1990; Holte *et al.*, 2006). Studies using various analytical methods such as electron microscopy, size extrusion, diffusion studies, and gel chromatography have shown that alginate gel pore size ranges from 5-200 nm (Klein *et al.*, 1983; Stewart & Swaisgood, 1993; Simpliciano *et al.*, 2013). However, these values are highly variable, and gel pore size can be modulated by several factors. The concentrations and monomer composition of alginate influences porosity of the hydrogel. An increase of alginate concentration in the preparation reduces pore size of alginate hydrogel (Tanaka *et al.*, 1984). Alginate with a high G-block content creates a more open structure by interaction with calcium ions, creating larger pore sizes (Martinsen *et al.*, 1991). The concentration of calcium ion is also important to control the pore size, hence influencing the

permeability of the hydrogel. A higher concentration of calcium ion influence alginate polymer gelling to a greater extent. Therefore, it produces a higher gel density, creating smaller pore sizes, which in turn reducing the gel permeability (Ching *et al.*, 2017). The type of gelation mechanism influences the pore size of the gel matrix. As described above, the alginate spheres prepared by external gelation results in an inhomogeneous distribution of calcium ions with a denser gel at the surface than the interior of the sphere (Figure 3). Meanwhile, the alginate spheres prepared by internal gelation results in a homogeneous distribution of calcium ion in the spheres (Andersen *et al.*, 2015; Paques, 2015). This leads to an alginate hydrogel prepared by external gelation having a smaller pore size at the surface, resulting in higher resistance to diffusion of the substrate compared to internal gelation (Liu *et al.*, 2002). There have been a number of molecules tested for diffusability into alginate hydrogel. Small molecules such as glucose, ethanol, ammonia, or vitamin B12 can diffuse across the alginate membrane regardless of the molecular weight of alginate (Martinsen *et al.*, 1991; Gautier *et al.*, 2011). Meanwhile, the transfer of large molecules, such as albumin, is hindered by the porous structure. However, several proteins, including immunoglobulin G (IgG), fibrinogen, haemoglobin and insulin have been reported to transfer through the porous structure of alginate (Tanaka *et al.*, 1984; Liu *et al.*, 2002; Mørch *et al.*, 2006; Gombotz & Wee, 2012).

Syneresis and swelling are physical characteristics that can occur with alginate hydrogels. Syneresis is the shrinkage of alginate hydrogels resulting from the loss of water molecules from the hydrogel (Donati & Paoletti, 2009). In an alginate hydrogel, water molecules are entrapped within the alginate hydrogel through hydrogen bonding. Upon an increase in the level of ionic cross-linking, an external force is applied that contracts the hydrogel, and the release of water molecules from the hydrogel is induced. As a result, there is a decrease in dimensions of the alginate hydrogel (Donati & Paoletti, 2009; Helgerud *et al.*, 2009). The composition and sequence of alginate polymer significantly influence the degree of syneresis. Long G-blocks contribute to a decrease in syneresis as it forms stronger irreversible junctions than shorter G-blocks, meanwhile alternating MG-blocks give flexible elastic properties to alginate hydrogel, leading to a higher degree of syneresis (Martinsen *et al.*, 1989). In addition to this, the length of alternating MG-blocks has been shown to determine the extent of collapse of the hydrogel, leading to syneresis, by forming MG/MG junction upon an increase in calcium ion concentration (Donati *et al.*, 2005). Moreover, the degree of syneresis increases with increasing concentration of

calcium ion, gelation time, and alginate molecular weight. (Martinsen *et al.*, 1989; Draget *et al.*, 2001; Donati & Paoletti, 2009). Swelling of an alginate hydrogel occurs under different external stimuli. It has been demonstrated that alginate hydrogels shrink in low pH and swell at close to neutral pH and above (Han *et al.*, 2007; Matyash *et al.*, 2014; Ching *et al.*, 2017). In addition, ionic concentrations in a buffer also influence the degree of swelling of the alginate hydrogel (Matyash *et al.*, 2014). By dispersing alginate spheres in physiological solution, such as saline and PBS, the cross-linked calcium ion will be replaced with sodium ions, which have no cross-linking property. This phenomenon, namely "ion exchange", results in the destabilisation of the hydrogel networks, which in turn leads to water influx (Mørch *et al.*, 2007; Wu *et al.*, 2010). The mechanism of hydrogel shrinkage in low pH is still unclear (Ching *et al.*, 2017). It is known that low pH induces proton catalysed hydrolysis of alginate polymer, leading to a lower molecular weight of alginate (Haug *et al.*, 1963). However, it has also been shown that the low pH condition suppresses the disassociation of the carboxyl group of the alginate polymer (Yotsuyanagi *et al.*, 1990; Wu *et al.*, 2010). Therefore, it is suggested that the protonated carboxyl group at low pH forms a thick gel matrix due to reduced electrostatic repulsion (You *et al.*, 2001). In term of alginate hydrogel preparation, it has been reported that swelling capacity of alginate hydrogel can be reduced with an increase in calcium concentration, as well as increased amounts of G-block in the alginate polymer (Gao *et al.*, 2009). In addition, the type of divalent cations used to cross link the alginate polymer influences the swelling capacity, for instance, barium ions significantly reduced the swelling capacity compared with calcium ion (Smidsrød & Skja˚k-Bræk, 1990).

1.2.4 Preparation methods for alginate spheres

To select the appropriate alginate sphere preparation method for a particular application, it is important to consider the particle size of the alginate spheres required (Leong *et al.*, 2016). In this section, two methods of alginate sphere preparations widely used to produce micron- and macro-sized alginate spheres are reviewed.

1.2.4.1 Simple extrusion dripping method

The simple extrusion dripping method is the most widely used method to prepare alginate spheres because of its simple procedure. In general, this method involves an alginate solution loaded in a syringe, and alginate droplets are added dropwise into the cross-linking solution. This method is usually used together with the external gelation method

(Sun & Tan, 2013; Ching *et al.*, 2017). Alginate spheres produced by the simple dripping method are generally in the 1-2 mm size range (Ching *et al.*, 2017), these are similar in size to those made from gelatin and called gelatin millispheres (Yamashita *et al.*, 2009), hence will be called alginate millispheres here. The alginate viscosity, diameter of the needle tip opening, flow rate of alginate solution, and the height of needle tip from the cross-linking solution may all influence the particle size of the millispheres (Lee *et al.*, 2013). The distance between needle tip and the cross-linking solution affects the particle sphericity as when alginate viscosity and its droplet surface tension are not able to overcome the surface tension exerted by the cross-linking solution, the droplet may be deformed from a perfect sphere (Chan *et al.*, 2009). To overcome this, surface-active compounds, such as methanol, may be added to reduce the surface tension of the cross-linking solution (Skjermo *et al.*, 1995; Thu *et al.*, 1996). The advantage of the simple extrusion dripping method is its simplicity. The drawback of this method is that alginate spheres are large and there is low process productivity (in term of sphere number per unit time) (Ching *et al.*, 2017). In addition, even though gelation occurs as soon as droplets are added into the cross-linking solution, diffusion of cations into the interior of the droplet takes a longer time, eventually creating a gradient of the gel network (Paques, 2015). To overcome these shortcomings, several modified techniques, which aimed to produce smaller alginate droplets using mechanical apparatus, have been developed (Ching *et al.*, 2017). These include: Electrostatic atomisation (Huang *et al.*, 2011), vibration method (Zhou *et al.*, 2009), jet cutting method (Paulo *et al.*, 2017), spinning disk/nozzle method (Nagata *et al.*, 2001), spraying method (Tritz *et al.*, 2010), and impinging aerosol method (Hariyadi *et al.*, 2010).

1.2.4.2 Emulsification

In the emulsification method, alginate solution is dispersed in an oil phase and homogenised to produce a water-in-oil (w/o) emulsion. Subsequently, gelation is slowly initiated by addition of either cross-linking solution ($CaCl_2$) (external gelation, Section 1.2.2.1.1) or acid (internal gelation, Section 1.2.2.1.2) (Paques *et al.*, 2013; Paques *et al.*, 2014b; Paques, 2015). However, as described above (Section 1.2.2.1), the emulsification method is often used together with the internal gelation method as the external gelation method may result in microspheres clustering and double emulsion formation. The particle size of alginate spheres prepared with the emulsification method is generally in the range of 100-1,000 μm in diameter (microspheres) (Ching *et al.*, 2017), or even

smaller particle sizes may be obtained (Paques, 2015). The particle size distribution of the alginate microspheres is influenced by various factors involved in the preparation, including alginate property and its concentration, water to oil ratio in the emulsion, emulsifier type and its concentration, homogeniser shear force, as well as environmental factors . The advantage of using this method is that it increases the productivity of alginate spheres in comparison to the simple dripping method (Reis *et al.*, 2006; Zuidam & Shimoni, 2010). However, there are some drawbacks using the emulsification method. They are: (1) random alginate droplet coalescence may occur during emulsification that leads to a wider particle size distribution; (2) high shear force and heat generated in the method may affect the encapsulated material; and (3) collection of alginate microspheres from the emulsion usually requires centrifugation followed by extensive washing procedures to remove oil, in some cases using organic solvents (Zhao *et al.*, 2007; Nagpal *et al.*, 2012; Ching *et al.*, 2017).

1.2.5 Applications of alginate

Owing to its attractive properties, alginate has been employed in a wide range of applications. The most common application is found in the food industry as a viscosifying, stabilising, emulsifying and gelling agent as well as a moisture retainer in products (Donati & Paoletti, 2009). The properties of alginate meet the requirements for use in the high-value niche of biomedical and pharmaceutical applications. It has been used in the production of wound dressings, dental impressions, and formulation with bicarbonate for gastric reflux prevention (Donati & Paoletti, 2009). Moreover, applications of alginate in hydrogel form to encapsulate a material of interest within the three-dimensional hydrogel have been demonstrated. For example, it has been used in various fields such as controlled drug delivery (Shelke *et al.*, 2014), cell encapsulation (Gasperini *et al.*, 2014), and tissue engineering for regenerative therapy (Rinaudo, 2014).

1.2.5.1 Alginate encapsulation

Due to its properties of biocompatibility, biodegradability, and its ability to easily form gels by addition of divalent cations under mild and safe conditions, alginate has been used to produce hydrogel (i.e. micro-/milli-spheres) to encapsulate various materials. These materials include proteins, enzymes, volatile compounds, cells, DNA, and various drugs (Chan *et al.*, 2000; Nicodemus & Bryant, 2008; Al-Mayah, 2012; Gombotz & Wee, 2012). The encapsulation in alginate hydrogel provides various advantages to the encapsulated

materials. These are: (1) providing a relatively inert environment within the gel matrix; (2) forming gels in mild conditions without harmful organic solvents; (3) enhancing the stability and function of the encapsulated material; (4) allowing diffusion of small and large molecules through the porous gel structure; (5) being able to control the porous structure by simple coating procedures; and (6) dissolving and degrading under normal physiological conditions (Raj & Sharma, 2003; Holte *et al.*, 2006; Gombotz & Wee, 2012). For instance, in particular, (1) to (4) are important factors for cell encapsulation and (1) to (6) are important factors for drug delivery systems. In the encapsulation of enzymes into alginate hydrogel, the encapsulated enzymes typically improve their mechanical and thermal stability (Rehman *et al.*, 2013), and alginate encapsulation may create the ideal physio-chemical microenvironment for the enzyme (Mohamad *et al.*, 2015). However, the practical use of enzyme-encapsulated alginate hydrogel is rather limited, as the hydrogel matrix tends to incur limitations in mass transfer of the substrate to the active site of the enzyme. In addition, leakage of the encapsulated enzyme through the porous gel structure may occur during the process (Blandino *et al.*, 2001; Mohamad *et al.*, 2015). Recently, Zhao and co-workers have shown that hybrid beads composed of chemically reduced graphene oxide and alginate effectively prevented the leakage of the encapsulated enzyme (Zhao *et al.*, 2015).

Alginate has shown to be an effective adsorbent for the removal of heavy metal ions, such as Cd^{2+}, Cu^{2+}, Cr^{6+}, Pb^{2+}, and Zn^{2+} from aqueous solution utilising its chelating property (Lim & Chen, 2007; Pandey *et al.*, 2007; Deze *et al.*, 2012). Recently, it has also been used as a support polymer material to prepare active material/alginate composite hydrogel for more efficient removal of diverse water pollutants (Jiao *et al.*, 2016; Jung *et al.*, 2017; Huang & Wang, 2018). For example, Asthana and co-workers prepared silver nanoparticles encapsulated in alginate beads for removal of Fe^{2+} from aqueous solution (Asthana *et al.*, 2016). Moreover, the encapsulation of graphene oxide within alginate hydrogel has been widely demonstrated as an efficient adsorbent for water treatment applications. It has been shown that it successfully removed heavy metal ions such as Cu^{2+}, Pb^{2+}, Cr^{6+}, and As^{5+} (Jiao *et al.*, 2016; Vu *et al.*, 2017), and organic pollutants such as methylene blue, phenol, tetracycline, and bisphenol A (BPA) (Wu *et al.*, 2014; Feng *et al.*, 2017; Gan *et al.*, 2018) from aqueous solution. Similar to this, activated carbon encapsulated in alginate hydrogel demonstrated the ability to remove organic pollutants

as well as heavy metal ions from aqueous solution (Lin *et al.*, 2005; Park *et al.*, 2007; Cataldo *et al.*, 2016).

1.2.5.2 Protein purification

Alginate has been shown to be useful in protein purification (Jain *et al.*, 2006). For example, in affinity precipitation using a polymer, the polymer is often conjugated with an affinity ligand. When the ligand conjugated polymer is added to a crude mixture of proteins, it selectively forms a complex with the target proteins. The polymer-protein complex is then precipitated by an appropriate stimulus, in the case of alginate, the addition of calcium ions. Subsequently, the precipitated complex is collected by low speed centrifugation, and the target protein can be obtained by a suitable dissociation step (Roy & Gupta, 2000; Jain *et al.*, 2006). Somers and co-workers observed that alginate beads bind pectinase, and the bound enzyme could be eluted off with a moderate concentration of sodium chloride (Somers *et al.*, 1989). Based on this observation, pectinase was purified from *Aspergillus niger* by affinity precipitation (Gupta *et al.*, 1993). Moreover, pre-treatment of alginate by microwaves enhanced the selectivity of alginate for pectinase and resulted in higher purification of the enzyme (Mondal *et al.*, 2004). These affinity precipitations were conducted without conjugating an affinity ligand to alginate, giving an advantage for alginate in protein purification as a simple and an economical procedure, as well as motivating further investigations to look for other enzymes to be selectively purified by alginate. Several proteins have been shown to be selectively purified by alginate, such as α-amylase (Sharma *et al.*, 2000a), β-amylase (Teotia *et al.*, 2001a), glucoamylase (Teotia *et al.*, 2001b), lipase (Sharma & Gupta, 2001), phospholipase D (Sharma *et al.*, 2000b), and α-galactosidase (Celem *et al.*, 2009). In addition, alginate in bead form used in expanded bed affinity chromatography also purified several proteins listed above without an affinity ligand conjugated on the alginate bead (Roy *et al.*, 2004; Jain *et al.*, 2006).

Alginate has also been used as immobilised metal ion affinity chromatography resin, similar to commercially available agarose resin charged with metal ions (Jain *et al.*, 2006). Gupta and co-workers produced zinc chelated alginate (Zn-alginate) beads for purifying soybean trypsin inhibitor from a crude extract of soybean flour. The Zn-alginate beads successfully purified the protein, however, 6 mM metal ion was needed throughout the procedure to maintain the integrity of the bead, and the metal ion caused the precipitation

of other proteins (Gupta *et al.*, 2002; Jain *et al.*, 2006). To overcome this problem, alginate beads were cross-linked with epichlorohydrin, in which the hydroxyl groups of alginate reacted with epichlorohydrin while carboxyl groups were left free for coordinating to metal ions (Jain *et al.*, 2006). The epichlorohydrin cross-linked alginate bead charged with Cu^{2+} ion was used to purify goat IgG in a packed bed, resulting in high purification and recovery of IgG from goat serum (Jain & Gupta, 2004).

1.3 Polyhydroxyalkanoate beads

As described above (Section 1.2.5), alginate has been employed for applications in various industries owing to its unique and valuable properties. This study focused on the alginate encapsulation application. The material of interest to encapsulate within the alginate hydrogel in this study was polyhydroxyalkanoate (PHA) beads. PHAs are natural biopolyesters of hydrophobic nature that are produced by a wide range of microorganisms as spherical inclusion bodies for their carbon and energy storage (Grage *et al.*, 2009). Recently, genetic engineering of bead-associated proteins allowed display of various functional protein at the beads' surface, producing functionalised nano-beads (Parlane *et al.*, 2017). Below provides a brief summary of PHAs, bead-associated proteins, and bead formation. In addition, protein immobilisation on PHA beads and their current applications are described.

1.3.1 Polyhydroxyalkanoate

Polyhydroxyalkanoates (PHAs) are natural biopolymers that are produced by a wide range of bacteria, some archaea, as well as some yeast cells (Rehm, 2007; Priji *et al.*, 2016). PHAs are synthesised and deposited in the cytoplasm of bacterial cell as spherical water insoluble inclusion bodies, also known as PHA beads (Rehm, 2010). PHA beads are formed in unbalanced nutrient conditions in which carbon source is available in excess while the other nutrients, such as nitrogen, oxygen, and phosphorus, are depleted (Steinbüchel & Valentin, 1995; Muhammadi *et al.*, 2015). The primary function of the bead is to serve as the carbon and energy source by depolymerising the PHA in conditions of carbon starvation (Steinbüchel *et al.*, 1992). The particle size of PHA beads ranges between 50-500 nm in diameter (Rehm, 2007; Grage *et al.*, 2009). In general, bacteria accumulate 5-10 PHA beads per cell, and are capable of accumulating more than 80% of their cellular dry weight as beads (Figure 4A) (Grage *et al.*, 2009; Tan *et al.*, 2014; Muhammadi *et al.*, 2015). In naturally synthesised (native) PHA beads, an amorphous

hydrophobic polyester core is surrounded by attached or embedded proteins on its surface that are involved in structural and regulatory functions. The surface proteins include PHA synthase (PhaC) that catalyses the polymerisation of PHA and remains covalently attached to the polyester core, as well as PHA depolymerase (PhaZ), structural proteins (Phasins), and regulatory proteins (PhaR) bound to the polyester core by hydrophobic interactions (Figure 4B) (Rehm, 2007; Parlane *et al.*, 2017). However, it has been demonstrated that apart from the PHA biosynthesis genes the other bead-associated proteins are not necessary to produce PHA beads in recombinant (non-native) PHA producing cells or plants (Poirier *et al.*, 1992; Wang *et al.*, 1999; Parlane *et al.*, 2017).

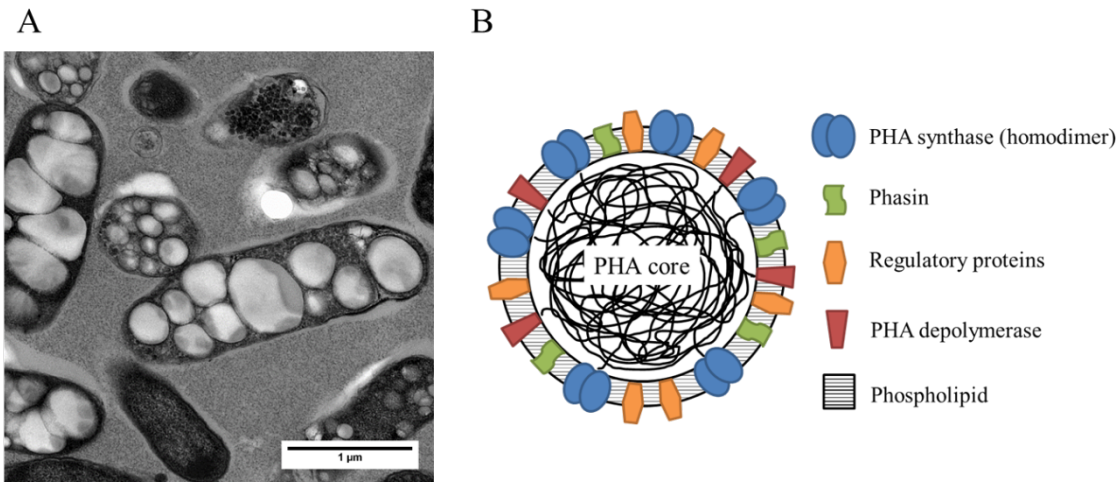

Figure 4: PHA bead inclusions. A, Transmission electron microscopic image of PHA inclusions in recombinant *E. coli*; B, Schematic view of a native PHA bead. TEM image (A) from K. Ogura taken by the Manawatu Microscopy and Imaging Centre (Palmerston North, New Zealand)

The most commonly found form of PHA in bacteria is poly(3-hydroxybutyric acid) (PHB), which is synthesised from 3-hydroxybutyrate (3-HB) monomers. This was the first bacterial PHA polymer identified and was found in the cytoplasm of *Bacillus megaterium* in 1926 (Maestro & Sanz, 2017). Currently, over 150 different (R)-3-hydroxy fatty acids as PHA constituents have been reported and the number is growing (Steinbüchel & Valentin, 1995; Parlane *et al.*, 2017). Many factors may influence the monomer content in the resulting PHA polymer. This includes strains, cultivation conditions and carbon sources (Park *et al.*, 2012; Jia *et al.*, 2016). In addition, genetic or metabolic engineering of PHA-producing strains have been explored to produce tailor-made monomers or monomer precursors which in turn contribute to the increase in the

number of PHA constituents available (Madison & Huisman, 1999; Chen *et al.*, 2015). Moreover, direct chemical or physical modifications to the existing PHA polymers have also been demonstrated (Levine *et al.*, 2016; Wang *et al.*, 2016). The monomer diversity and ability to modify PHA polymers make it possible to synthesise PHAs with different thermal and mechanical properties. PHAs occur as either homopolymers or copolymers and are classified into three major groups based on the monomer size (Rehm, 2007; Maestro & Sanz, 2017). These are: short chain length PHAs (PHA_{SCL}), which are produced by a wide range of bacteria and archaea, and consist of 3-5 carbon atoms in the monomer; medium chain length PHAs (PHA_{MCL}), which are primarily produced by *Pseudomonas* species, and consist of 6-14 carbon atoms in the monomer; and long chain length PHAs (PHA_{LCL}) that consist of more than 14 carbon atoms but they are scarcely found (Rehm, 2007; Grage *et al.*, 2009; Maestro & Sanz, 2017). From a materials property point of view, PHA_{SCL} is hard but brittle with a high melting point and high crystallinity. In contrast, PHA_{MCL} is more elastomeric but has less tensile strength with a low melting point and low crystallinity (Rehm, 2007).

PHAs have been extensively studied in various industries due to their attractive properties compared with synthetic plastics. PHAs are biocompatible, biodegradable, chemically and physically modifiable, and can be produced from renewable sources. In comparison, traditional synthetic plastics are produced from crude oil, are non-renewable and non-biodegradable. Therefore, PHAs are expected to be used increasingly as alternatives to the petroleum-based plastics (Philip *et al.*, 2007; Chen, 2009). However, due to fermentation and purification cost, it is still more expensive to produce PHA-based plastics compared to conventional petroleum-based plastics. Hence, the current market niche for PHAs is in high-value applications, especially in the biomedical field (Chen & Wu, 2005; Grage *et al.*, 2009). The biocompatible property of PHA allows its use in biomedical materials such as sutures (Shishatskaya *et al.*, 2004), bone scaffolds (Lim *et al.*, 2017), and drug delivery systems (Francis *et al.*, 2011). However, these biomaterials are based on extracted PHA polymers, thus the PHA bead loses its natural form, as do any bead-associated proteins. In contrast, the application of the natural form of PHAs as a protein-coated bead has been exploited to produce functionalised nano-beads. In this technology, the bead-associated proteins are genetically engineered to display functional proteins on the surface of the PHA beads (Rehm, 2007; Grage *et al.*, 2009; Draper & Rehm, 2012; Parlane *et al.*, 2017).

1.3.1.1 PHA biosynthesis

There are three major metabolic pathways to synthesise PHA in native bacteria. The most well characterised pathway, namely pathway I, is utilised to synthesise short chain length PHAs (PHA_{SCL}) by bacteria, such as *Cupriavidus necator*, while pathways II and III are utilised by bacteria such as *Pseudomonas aeruginosa*, to synthesise medium chain length PHAs (PHA_{MCL}) (Rehm, 2007; Grage *et al.*, 2009; Zou *et al.*, 2017).

The biosynthesis of PHB (PHA_{SCL}) in *C.necator* requires three key enzymes: PHA synthase (PhaC), β-ketothiolase (PhaA), and acetoacetyl-CoA reductase (PhaB), which are encoded by *phaC*, *phaA*, and *phaB* genes, respectively. These biosynthesis genes are clustered in a single *phaCAB* operon in the bacterial genome (Rehm, 2007; Grage *et al.*, 2009). The precursor ((R)-3-hydroxybutyryl-CoA) is synthesised by β-ketothiolase (PhaA) and acetoacetyl-CoA reductase (PhaB). β-ketothiolase (PhaA) condenses two molecules of acetyl-CoA to form acetoacetyl-CoA, with subsequent reduction to (R)-3-hydroxybutyryl-CoA by NADH-dependent acetoacetyl-CoA reductase (PhaB). Eventually, PhaC catalyses the polymerisation of (R)-3-hydroxybutyryl-CoA monomers into PHB with the release of CoA (Rehm, 2007; Muhammadi *et al.*, 2015). The pathways II and III in *P. aeruginosa* for PHA_{MCL} synthesis utilises metabolic intermediates from the fatty acid *de novo* synthesis ((R)-3-hydroxyacyl-ACP) and fatty acid β-oxidation (enoyl-CoA) to convert them into (R)-3-hydroxyacyl-CoA thioester monomer, which is subsequently polymerised into PHA_{MCL} by PhaC (Tsuge *et al.*, 2003; Philip *et al.*, 2007; Rehm, 2007).

1.3.1.2 PHA bead formation: self-assembly

Although *in vitro* synthesis of PHAs and self-assembly into spherical beads has been demonstrated using purified PHA synthases and substrates (Gerngross & Martin, 1995), the exact molecular events of PHA bead assembly *in vivo* have not been fully elucidated (Parlane *et al.*, 2017). Currently, three models of PHA bead assembly *in vivo* have been proposed, namely: the micelle model, the budding model (Rehm, 2007; Grage *et al.*, 2009), and the scaffolding model (Parlane *et al.*, 2017).

The micelle model is currently considered the most favoured model. In this model, soluble PhaC forms a dimer, and the dimerised PhaC interacts with the substrate in the cytoplasm to initiate the polymerisation process. During the polymerising process, the dimer remains

covalently attached to the growing hydrophobic polymers, forming an amphipathic molecule. Subsequently, several amphipathic molecules undergo self-assembly by aggregation via hydrophobic interactions to form a micelle-like structure (Gerngross *et al.*, 1993; Grage *et al.*, 2009). Phasin and other bead-associated proteins (PhaZ and PhaR) that are involved in the regulation and metabolism of PHA beads interact with the intracellularly formed PHA beads by hydrophobic interaction (Parlane *et al.*, 2017). This model is supported by studies of the *in vitro* PHA bead formation, where the cytoplasmic membrane is absent (Gerngross & Martin, 1995; Hiraishi *et al.*, 2005).

In contrast to the micelle model, the membrane budding model arose from the observation in electron microscopic studies showing membrane-like material surrounding PHA beads in intact cells and isolated beads (Boatman, 1964; Lundgren *et al.*, 1964; Dunlop & Robards, 1973; Mayer *et al.*, 1996). In this model, soluble PhaC and phasin protein localise to the inner side of the cytoplasmic membrane, either inherently or as soon as PHA chains emerge from PhaC protein. The polyester chains are growing into the inter-membrane space, forming PHA inclusions surrounded by a phospholipid monolayer with other bead-associated proteins attached, which then eventually bud off the membrane into the cytoplasm (Jendrossek *et al.*, 2007; Thomson *et al.*, 2010). Studies using fluorescent techniques support the membrane budding model. In these studies, they have shown that PHA beads in native and recombinant PHA bead-producing bacteria are not randomly distributed in the cytoplasm, but are predominantly located at, or near, the cytoplasmic membrane (Jendrossek, 2005; Jendrossek *et al.*, 2007). However, recent findings have provided evidence against this model. For example, high-resolution images of PHA bead synthesis in *C. necator* using electron cryotomography revealed that PHA beads of different sizes are distributed towards the centre of the cytoplasm, and their surface was a discontinuous layer with no lipid monolayer present on the surface of the bead (Beeby *et al.*, 2012). Further confirmation for the absence of phospholipid layer on the PHA bead was conducted using fluorescence microscopy (Bresan *et al.*, 2016). In this study, DsRed2EC and other fluorescent proteins fused with the phospholipid-binding domain of lactadherin (LactC2) were tested with three native PHA bead producers (*C. necator*, *Pseudomonas putida*, and *Manetospirillum gyphiswaldense*). The fluorescence microscopy showed the fusion protein co-localised only with the cytoplasmic membrane, but not with the PHA beads (Bresan *et al.*, 2016). This observation is not consistent with the membrane budding model, as it should contain phospholipid as previously described.

The scaffolding model was suggested by the observation of PHA bead synthesis in *C. necator* using transmission electron microscopy (Tian *et al.*, 2005). These authors observed that PHA beads localised close to the dark-stained structure or "mediation elements" in the centre of the cell. It was undefined at the time, however, the authors proposed that the mediation elements serve as scaffolds to initiate bead formation (Tian *et al.*, 2005). Nowadays, the mediation element is believed to be bacterial nucleoid (Parlane *et al.*, 2017). A regulatory protein, PhaM, has been shown to bind not only to PhaC but also to DNA and nucleoid both *in vitro* and *in vivo* (Pfeiffer *et al.*, 2011). Moreover, supporting evidence for the scaffolding model was demonstrated as PhaM mediated the binding of PHA bead with nucleoid, and overproduction of the protein caused the attachment of small PHA beads to the nucleoid region in *C. necator* (Wahl *et al.*, 2012). However, *phaM* deletion in *C. necator* strain still has shown to produce PHA beads. Therefore, PhaM mediated scaffolding event may be unnecessary for bead formation (Pfeiffer *et al.*, 2011).

1.3.1.3 PHA synthases

PHA synthase is the critical enzyme for PHA synthesis. The enzyme catalyses the polymerisation of (*R*)-hydroxyacyl-CoA thioester monomers into PHAs with the concurrent release of CoA. Currently, genome sequencing technology has identified over 90 PHA synthase genes in a number of different bacterial species. PHA synthases are classified into four different classes based on their substrate specificity, subunit composition, and primary structure (Rehm, 2003; Rehm, 2007; Grage *et al.*, 2009; Parlane *et al.*, 2017).

1.3.1.3.1 Classification of PHA synthase

Class I and II PHA synthases, with representatives from *C. necator* and *P. aeruginosa* respectively, consist of a single PhaC subunit with a molecular weight ranging between 61-73 kDa (Timm & Steinbüchel, 1992; Qi & Rehm, 2001; Rehm, 2003; Philip *et al.*, 2007). Class III and IV PHA synthases, with representatives from *Allochrimatium vinosum* and *Bacillus megatrium* respectively, are composed of two subunits (Parlane *et al.*, 2017). In the class III PHA synthases, there are two subunits, PhaC and PhaE, of similar molecular weight (40 kDa), however, they show no homology based on their primary structure. The PhaC subunit exhibits 21-28% similarity to the class I and II PhaC

while PhaE has no similarity to PhaC (Qi *et al.*, 2000; Qi & Rehm, 2001). The class IV PHA synthases are similar to the class III PHA synthase, except the PhaE subunit is replaced with PhaR subunit (20 kDa) (Tsuge *et al.*, 2015). In term of substrate specificities, class I, III, and IV PHA synthases prefer to catalyse the polymerisation of short chain length monomers (C3-C5) to generate PHA_{SCL}, while class II PHA synthase catalyses the polymerisation of medium chain length monomers (C6-C14) to generate PHA_{MCL} (Parlane *et al.*, 2017).

1.3.1.3.2 Structural features of PHA synthases

Purified PHA synthases have been shown to exist *in vitro* in equilibrium as monomeric and dimeric forms (Zhang *et al.*, 2003; Rehm, 2007). The presence of substrate induces dimerisation of PHA synthase, suggesting dimer formation is the active form of PHA synthase to polymerise substrates into PHAs (Rehm, 2007). Currently, the active form of PHA synthase is considered to be a homodimer for class I and II PHA synthases and heterodimers for class III and IV PHA synthases (Rehm, 2007).

Comparing amino acid sequences of all four classes of PHA synthases from different bacteria have shown six conserved amino acid blocks and eight conserved amino acid residues in all PHA synthases (Rehm *et al.*, 2002; Rehm, 2007). Also, a truncation study on class I PHA synthase from *C. necator* revealed that the first 100 amino acids of the N-terminus are highly variable and dispensable (Rehm *et al.*, 2002; Peters & Rehm, 2005). In contrast, the C-terminus appeared to be a highly conserved and hydrophobic feature among class I and II PHA synthases, suggesting a function in enzyme activity as well as the binding domain to facilitate the attachment of PHA synthase to the hydrophobic polyester core (Rehm *et al.*, 2002; Peters & Rehm, 2005; Rehm, 2007). In class III and IV, their PHA synthases do not contain a hydrophobic C-terminus, instead, their respective second subunit, PhaE and PhaR, possess a hydrophobic C-terminus, suggesting it facilitates the binding to the polyester core (Rehm, 2007). In addition, the amino acid alignment found that PHA synthase contains conserved PhaC box sequence ([G/S]-X-C-X-[G/A]-G) (Tsuge *et al.*, 2015) and a conserved cysteine-histidine-aspartate catalytic triad in the C-terminus of all classes of PHA synthases (Rehm, 2003). These features are homologous to lipase, a member of the α/β-hydrolase superfamily, which forms a core α/β-hydrolase fold that is composed of eight β-sheets surrounded by six α-helices (Ollis

et al., 1992), except the serine residue in the catalytic site of lipase is replaced with a cysteine residue in PHA synthase (Rehm, 2003; Rehm, 2007; Tsuge *et al.*, 2015)

1.3.1.4 Other PHA granule-associated proteins

PHA synthase (PhaC) is not the only protein presented on the surface of PHA beads. Three major types of proteins are also known to associate with PHA beads in native PHA producers, and these proteins play a role in PHA synthesis regulation, bead formation, and degradation. These are Phasin (PhaP), PHA depolymerase (PhaZ), and regulatory proteins, PhaR, PhaF, and PhaI (Grage *et al.*, 2009; Parlane *et al.*, 2017).

1.3.1.4.1 Phasin (PhaP)

Phasins are a group of proteins that are the most abundantly produced bead-associated protein and make up to 5% of the total cellular proteins. The molecular weight of the proteins ranges from 11 to 25 kDa, and they are non-covalently attached to PHA beads by hydrophobic interactions (Grage *et al.*, 2009). In the model PHA producer, *C. necator*, seven phasins (PhaP1-PhaP7) have been identified (Pfeiffer & Jendrossek, 2012). Their function is considered to be in the role of regulating PHA production level, bead size and number in the cell, and preventing nonspecific interaction of other proteins with PHAs (Grage *et al.*, 2009; Parlane *et al.*, 2017). Studies have demonstrated that phasins are not essential for PHA bead production, however, the absence of phasins led to a single large granule formation (Hanley *et al.*, 1999) while many small beads were produced in a cell with the overproduction of phasin (Pötter *et al.*, 2002). This observation was supported by other studies that demonstrated phasins stabilise the PHA beads by preventing the coalescence of individual beads by forming an amphiphilic layer on the surface of PHA beads (Parlane *et al.*, 2017).

1.3.1.4.2 PHA depolymerase (PhaZ)

PHA depolymerases are the main enzymes to catalyse the degradation of PHA polyesters by thiolysis under nutrient deficiency (Jendrossek *et al.*, 1996; Jendrossek & Handrick, 2002). The PHA depolymerases are classified into two groups by the location of enzyme activity: intracellular and extracellular PHA depolymerases. The intracellular PHA depolymerases are the PHA bead-associated protein that degrades the accumulated polyesters in the cytoplasm of bacteria (Handrick *et al.*, 2000). The extracellular PHA

depolymerases are secreted by many microorganisms into the environment to utilise the extracellular PHA sources (Mergaert & Swings, 1996). The PHA depolymerases have the substrate binding site at the C-terminus that interacts with PHA core by hydrophobic and chemical interactions (Jendrossek & Handrick, 2002). The four crucial amino acid residues (arginine, cysteine, histidine and serine) in the substrate-binding site, especially the positively charged histidine and arginine residues have been suggested to interact with the carbonyl group of PHAs by electrostatic interaction (Jendrossek & Handrick, 2002; Park *et al.*, 2005).

1.3.1.4.3 Regulatory Proteins (PhaR, PhaF, and PhaI)

PHA biosynthesis and phasin (PhaP) production are tightly regulated by the transcriptional repressor PhaR (Grage *et al.*, 2009; Parlane *et al.*, 2017). Studies in *Ralstonia eutropha* (Currently known as *C. necator*) and *Pseudomonas denitrificans* have shown that PhaR binds upstream of the *phaP* and *phaR* genes (Pötter *et al.*, 2002). A mutagenesis study in *R. eutropha* provided evidence that no phasins could be detected in a *phaC* deletion strain, whereas a *phaC/phaR* deletion strain and *phaR* deletion strain both produced a large amount of phasin proteins (York *et al.*, 2002). Based on these findings, the PhaP/PhaR autoregulation model has been proposed (Parlane *et al.*, 2017). The proposed mechanism of the autoregulation is as follows. Under non-PHA synthesis conditions, PhaR binds to the *phaP* promoter region and inhibits transcription. While under PHA synthesis conditions, PhaR binds non-covalently to the hydrophobic surface of newly synthesised PHA beads, reducing the concentration of PhaR in the cytoplasm below a threshold level for repressing the transcription of *phaP*. This then leads to the synthesis of phasins, and these proteins immediately interact with the PHA beads' surface. Once the bead reaches maximum size, the bead surface is covered by phasins, preventing further binding of PhaR to the bead. This results in an increase in the cytoplasmic concentration of PhaR, which results in binding of PhaR to the *phaP* promoter region once again and prevents transcription of *phaP* and *phaR* (Pötter *et al.*, 2002; York *et al.*, 2002; Grage *et al.*, 2009). In *Pseudomonas oleovorans*, it has been reported that PhaF and PhaI have a similar regulatory function to the PhaP/PhaR autoregulation model of *R. eutropha* (Prieto *et al.*, 1999; Parlane *et al.*, 2017).

1.3.1.5 Immobilisation of functional protein on PHA beads

Proteins for use in various biomedical applications often require purification from a complex protein mixture, ideally in a manner that does not affect their biological activity or altering their structure (Grage *et al.*, 2009). Affinity-based purification technologies have been used as protein purification methods, and these utilise the specific interaction of a protein of interest with its corresponding solid support (Arnau *et al.*, 2006). This interaction is often mediated by a genetically engineered purification tag, such as poly-histidine, to the protein of interest. The purification tag may provide some positive effects, for instance, enhanced solubility and production level of the protein (Esposito & Chatterjee, 2006). However, the drawbacks of the purification tag are that they may affect the protein's intrinsic properties, such as solubility, net charge, and protein folding (Waugh, 2005; Arnau *et al.*, 2006). Enzymatic cleavage of the purification tag may overcome this issue (Esposito & Chatterjee, 2006), however, the protein may revert to an insoluble form (Waugh, 2005). Therefore, affinity-based protein purification requires optimisation for purification of each protein, as well as expensive enzymatic cleavage and multiple separation steps, making this method costly and time-consuming (Grage *et al.*, 2009; Parlane *et al.*, 2017).

Protein immobilisation to a solid material has been shown to enhance the stability and activity of the protein of interest (Hanefeld *et al.*, 2013). However, conventional approaches of immobilisation need a purification of both the protein of interest and the solid material separately and then proteins attached to the solid material by non-specific adsorption or chemical cross-linking (Hanefeld *et al.*, 2009). As these multiple steps are costly and time-consuming, it is desirable that bacteria produce the protein of interest and the solid material simultaneously, with the protein directly displayed on the solid material *in vivo*. The subsequent cell disruption and centrifugation can readily purify the protein of interest displayed on the solid material (Steinmann *et al.*, 2010).

In vivo produced PHA bead-based protein immobilisation and purification strategies have been developed as a cost-effective approach to purify proteins by genetically engineering bead-associated proteins on the surface of PHA beads. Among the bead-associated proteins, PHA synthase (PhaC), Phasin proteins (PhaP) and regulatory protein (PhaR) have been used for recombinant protein production and purification. (Rehm, 2007; Grage *et al.*, 2009; Parlane *et al.*, 2017). In 2005, Banki and co-workers developed a protein

purification method that combined intracellular PHA synthesis and intein-mediated self-cleaving (Figure 5A). In this method, gene constructs were made to give the protein of interest fused to the C-terminus of PhaP from *C. necator*, which acts as the affinity tag to bind to the PHA bead. The fusion protein and PHA beads were co-produced in *E. coli* resulting in the *in vivo* production of the fusion protein bound to PHA beads. Subsequent cell disruption and centrifugation, followed by mild washing steps and self-cleavage of intein allowed purification of the protein of interest. This method successfully purified several model proteins, including maltose binding protein (MBP), β-galactosidase (LacZ), chloramphenicol acetyltransferase (CAT), and NusA (Banki *et al.*, 2005). A similar strategy was demonstrated in *C. necator* by Barnard *et al.* (2005), and Wang *et al.* (2008) who produced PhaP tag fused with a protein of interest *in vivo*, and purified the PhaP tag fused with the protein of interest by subsequent attachment on separately synthesised PHA beads *in vitro* (Figure 5B).

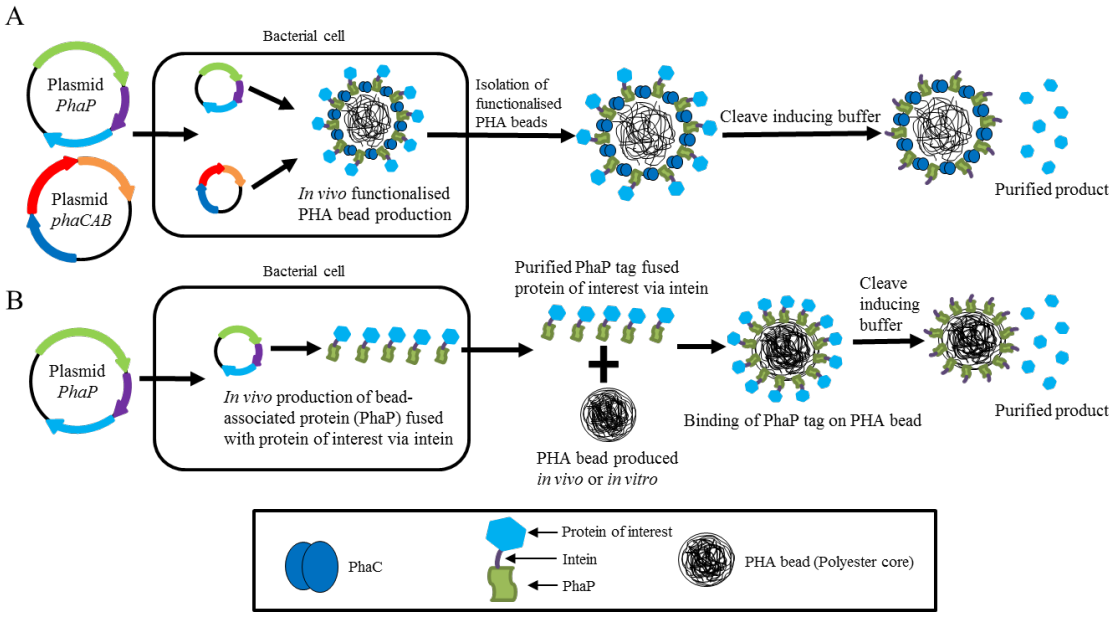

Figure 5: Schematic images of functionalised PHA bead production *in vivo* and protein purification via PhaP.

Genetic engineering to give the fusion of green fluorescent protein (GFP) to the N-terminus of PHA synthase (PhaC) from *C. necator* was also successfully shown not to affect PHA bead formation (Peters & Rehm, 2005). The authors subsequently immobilised the enzyme β-galactosidase onto PHA beads via PHA synthase from *P. aeruginosa* and showed it was highly functional with enhanced stability in comparison to

free β-galactosidase (Peters & Rehm, 2006). The main advantages of making gene constructs to give fusion proteins with PHA synthase over other bead-associated proteins are: (1) PHA synthase remains covalently attached to the polyester core; and (2) it allows a simple recombinant production system which only needs critical PHA biosynthesis genes (i.e. *phaC*, *phaA*, and *phaB*) in the recombinant cells (Grage *et al.*, 2011). Hence, the protein fusions to PHA synthase are commonly targeted for protein immobilisation (Figure 6).

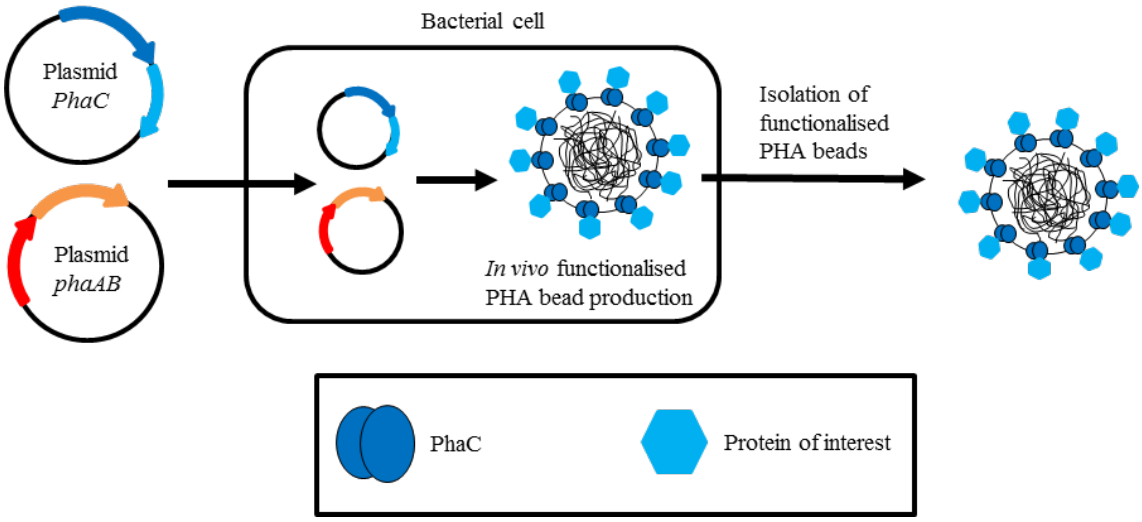

Figure 6: Schematic image of functionalised PHA bead production *in vivo* and protein immobilisation via PhaC.

1.3.1.6 Applications of PHA beads as bio-beads displaying functional proteins

The increasing knowledge of structural and biochemical properties of bead-associated proteins has enabled genetic engineering of these proteins to provide PHA beads with various functional proteins attached while retaining the primary role of the bead-associated proteins (Rehm, 2007; Grage *et al.*, 2009; Parlane *et al.*, 2017). Therefore, the bead-associated proteins serve as a versatile platform for the display of a range of functional proteins on the surface of beads. Figure 7 summarises the currently demonstrated applications of PHA beads via PHA synthase (PhaC) in various fields, and the following section describes several examples of PHA beads displaying functional proteins.

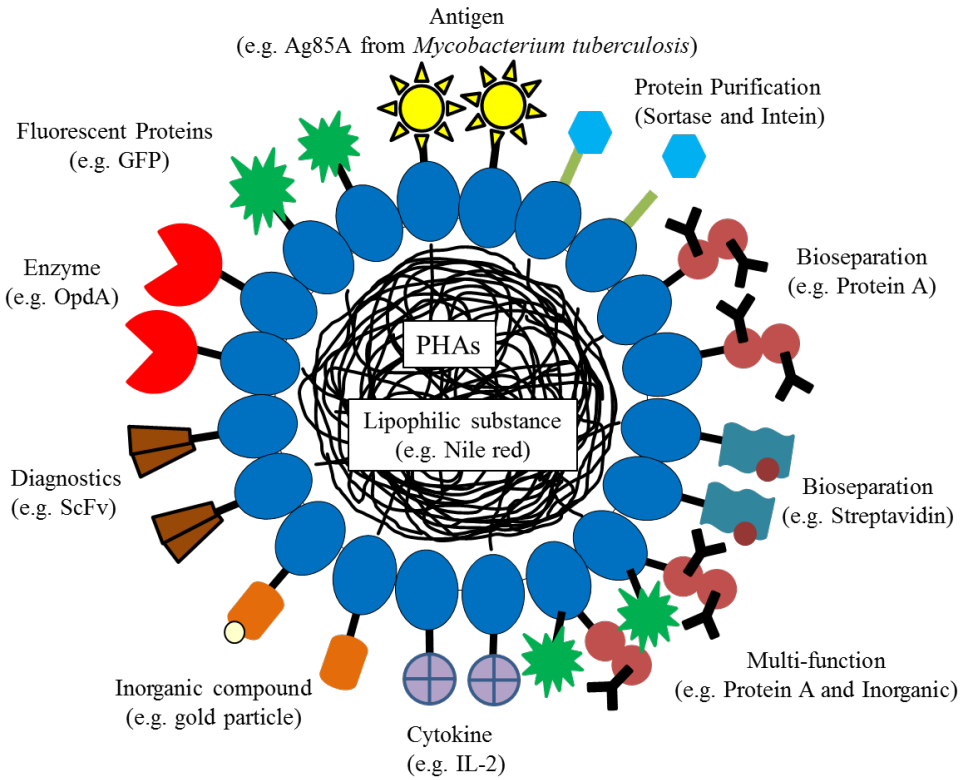

Figure 7: Schematic overview of immobilised functional proteins on PHA bead via PHA synthase. Based on Parlane *et al.* (2017).

1.3.1.6.1 Bioseparation

The purification of immunoglobulin G (IgG) was demonstrated by PHA beads displaying immunoglobulin G binding ZZ domain of protein A from *Staphylococcus aureus*, which was fused to N-terminus of the PHA synthase (Brockelbank *et al.*, 2006). The ZZ domain-displaying PHA beads showed efficient IgG purification from human serum and performed similarly to that of commercially available protein A-Sepharose chromatography beads with regards to purity and yield (Brockelbank *et al.*, 2006). Also, a subsequent study produced ZZ domain-displaying PHA beads in the generally recognised-as-safe (GRAS) and endotoxin free bacterium *Lactococcus lactis* and *Bacillus megaterium* for antibody purification production designed for biopharmaceutical applications (Mifune *et al.*, 2009; Grage *et al.*, 2017). Similarly, streptavidin fused to C-terminus of PHA synthase resulted in streptavidin-displaying PHA beads that were capable of binding biotin (Peters & Rehm, 2008). The streptavidin-displaying PHA beads

were successfully applied to the purification of biotinylated antibodies and DNA, as well as to enzyme immobilisation and flow cytometry (Peters & Rehm, 2008).

1.3.1.6.2 Enzyme

Since the first enzyme (β-galactosidase) immobilisation onto the PHA beads mentioned above (Section 1.3.1.5) (Peters & Rehm, 2006), there have been several enzymes immobilised onto PHA beads. Immobilisation of α-amylase by fusion to the N-terminus of PHA synthase (PhaC) from *C. necator* showed a Michaelis-Menten constant (K_M) of 5 μM and a maximum turnover rate (V_{max}) of 506 mU/mg of protein which is similar to the free state enzyme. Moreover, the enzyme activity remained stable up to 85 °C and showed the capacity of repeated use in starch liquefaction process (Rasiah & Rehm, 2009). The organophosphate hydrolase (OpdA) from *Agrobacterium radiobacter* fused to the C-terminus of the PHA synthase showed the enzyme activity of reduced catalytic constant (k_{cat}) by 16.5 fold to 139 s^{-1} and increased K_M by 1.6 fold to 2.5×10^{-4} M relative to the free enzyme, indicating reduced enzyme activity level. However, the OpdA-displaying PHA beads showed increased thermal stability, and the beads were capable of degrading organophosphorus pesticides present in the environmental conditions of wool scour effluent (Blatchford *et al.*, 2012). Moreover, immobilisation of N-ethylmaleimide reductase (NemA) (Robins *et al.*, 2013) and lipase B (Jahns & Rehm, 2015) to PHA synthase have also been shown to enhance the stability of these enzymes.

1.3.1.6.3 Protein purification

Similar to a protein purification system utilising phasins (PhaP) developed by Banki *et al.* (2005), a PHA synthase (PhaC) based protein purification system has also been developed. Recently, PHA synthase-sortase-protein of interest system has been developed as a new tool to produce tagless recombinant proteins (Hay *et al.*, 2015). In this system, the addition of $CaCl_2$ and triglycine activates the sortase, and the protein of interest is released. This system has been shown to purify soluble proteins, including green fluorescent protein (GFP), maltose binding protein and the tuberculosis antigen Rv1626 (Hay *et al.*, 2015) as well as some therapeutic proteins such as human tumour necrosis factor (TNF-α) and human interferon α 2b (IFN-α 2b) Du & Rehm (2017b). Moreover, the PHA synthase-intein-protein of interest system allowed protein purification mediated by cleavage of the pH-sensitive intein fused to the PHA synthase (Du & Rehm, 2017a).

1.3.1.6.4 Vaccine

Development of PHA beads-based vaccines utilising the biocompatibility and biodegradability properties of PHA beads has attracted great interest (Parlane *et al.*, 2017). Several studies have demonstrated that PHA beads displaying antigens are immunogenic *in vivo* and successfully activated the immune response (Parlane *et al.*, 2009; Parlane *et al.*, 2011; Parlane *et al.*, 2012; Martinez-Donato *et al.*, 2016; Reyes *et al.*, 2016; Lee *et al.*, 2017a; Lee *et al.*, 2017b). It is critical to select an appropriate strain to produce PHA beads displaying the desired antigen, especially for vaccine production. This is due to the potential presence of endotoxin in the PHA beads produced in *E. coli*. Therefore, *L. lactis* or Clear*coli*™ BL21 (DE3) cells are often used as alternative strains to produce the PHA beads for vaccine purposes due to the lack of endotoxin production in these bacterium (Mifune *et al.*, 2009; Parlane *et al.*, 2012; Reyes *et al.*, 2016). In addition, Lee and co-workers used the target microbe as the production host (*P. aeruginosa*) to make its own antigen-displaying PHA bead vaccine and showed that this activated cellular immunity in mice (Lee *et al.*, 2017b).

1.3.1.7 Application of PHAs

PHA polymers have been shown to have a variety of applications. There is increased recognition of global environmental issues caused by synthetic non-degradable polymers, thus, PHA has been gaining attention as a potential substitute to replace synthetic polymers (Keshavarz & Roy, 2010). Currently, there has been a number of products made from PHAs, including bags, containers as well as coatings and packagings (Keshavarz & Roy, 2010; Muhammadi *et al.*, 2015; Keskin *et al.*, 2017). Moreover, there have been extensive studies to blend PHAs with other polymers to give new plastic properties. The blending changes the crystallinity and the crystallisation rate of the plastic, and ultimately changes the mechanical property of the material (Sharma & Ray, 1995; Muhammadi *et al.*, 2015). For instance, the blending of poly(3-hydroxybutyrate-co-3-hydroxyvalerate) (PHBV) and thermoplastic polyurethane improved the mechanical and barrier properties, as well as increased water vapour permeability of PHBV (Martinez-Abad *et al.*, 2016; Keskin *et al.*, 2017).

In the medical field, PHAs have received great attention since the polymer is biocompatible and biodegradable. PHB is known to be present in the blood (Reddy *et al.*,

2003) and the cell membrane of eukaryotes (Reusch, 2000). Thus, the biocompatible property allows PHAs to be used in various biomedical applications. For example, PHAs have been applied in wound management such as surgical sutures, implants, and swabs, as well as three-dimensional tissue scaffolding and drug delivery carriers (Muhammadi *et al.*, 2015). However, currently, there are still some limitations in the application of PHAs in the medical and pharmaceutical fields. This is due to their low tensile strength, minimal cell interaction capacity, and slow biodegradation and high hydraulic stability in sterile tissues (Wang & Bakken, 1998; Muhammadi *et al.*, 2015; Manavitehrani *et al.*, 2016). To overcome these issues, PHAs have been blended with other polymers, had inorganic compounds added, and been modified through chemical or physical modifications (Manavitehrani *et al.*, 2016).

PHAs have also been shown to have applications in water and wastewater treatment. It has been shown that PHAs can serve as the solid substrate, termed "solid-phase denitrification", to denitrify water and wastewater (Muhammadi *et al.*, 2015). There are several advantages of using PHAs in this method. They are: (1) PHAs have no potential risk of releasing dissolved organic carbons to cause deterioration of effluent quality; (2) PHAs serve as solid matrices for the development of microbial biofilms for bacterial denitrification; (3) the system is controlable as the biofilm is washed out when the supply of PHAs are used up; and (4) PHAs are subsequently degraded by PHA-degrading bacteria (Hiraishi & Khan, 2003). Moreover, the hydrophobic property of PHAs has been shown to have applications in removal of lipophilic organic pollutants from water (Muhammadi *et al.*, 2015). Zang and co-workers produced a biomimetic adsorbent, named PHBMA, prepared with PHB by a modified double emulsion solvent evaporation method, and demonstrated adsorption of a lipophilic organochlorine compound (chlorobenzene and *o*-nitrochlorobenzene) from wastewater (Zhang *et al.*, 2010a; Zhang *et al.*, 2010b). Similarly, Sudesh and co-workers developed PHA films that were excellent at absorbing oil, suitable for their application of the removal of lipophilic substances (Sudesh *et al.*, 2007).

1.4 Significance of this study

As described above, the PHA bead technology as a versatile platform to immobilise and display functional proteins is an attractive new tool for protein immobilisation. Although several studies have shown the effectiveness of utilising the technology, the state of the bead in a reaction medium may influence the level of the bead functionality. In any suspensions that PHA beads were dispersed, the beads have often been shown to form undesirable aggregates. As the functionality of the beads depends on the exposure of the functional protein on the bead to the outer environment, the formation of aggregates may limit the functionality level of the proteins. In addition, the bead would form a rigid precipitation in a stock medium during long time storage. A sonication and/or mechanical homogeniser may be applied to separate the beads from the aggregates, however, the protein on the surface may be damaged or degraded leading to the loss of its functionality. To address this, encapsulation techniques have been used to immobilise the beads within a polymer matrix to prevent further formation of bead aggregates. The encapsulation techniques have been extensively studied in drug delivery applications, however recent interest is to entrap and then immobilise materials of interest, such as cells, within a polymer matrix. As described above, the polymer matrix functions to immobilise as well as to form a three-dimensional scaffolding to support the materials encapsulated within. In addition, it also provides a controlled and supportive environment inside, with a barrier against several environmental factors for the encapsulated material to function effectively. Therefore, encapsulating PHA beads in a polymer matrix is expected to retain the dispersity and functionality of the bead within the polymer matrix.

PHAs have been applied to the removal of lipophilic organic pollutants from water. Therefore, utilising PHA in the bead from for this application has an advantage due to the size of the bead, which provides a higher specific surface area. However, a single PHA bead is hard to control due to its small particle size. For this reason, the immobilisation of PHA beads in an alginate hydrogel matrix would potentially have considerable advantages over existing materials.

The polymer material used in this study was alginate. Alginate has been shown to encapsulate a wide range of materials, as well as its favourable property of gelling under

mild conditions that should not adversely affect the activity of the protein displayed on the PHA beads during the hybrid material production.

1.5 Aim and objectives

The main aim of this study was to encapsulate PHA beads in an alginate hydrogel matrix by the ionotropic gelation method and assess the functionality of the hybrid material. To investigate this novel approach, this study aimed to encapsulate three different types of PHA beads within alginate hydrogels and assess their functionality. This study was divided into three distinct parts, which aimed to:

1. Encapsulate PHA beads displaying IgG binding domain in alginate microspheres and asess the functionality of the hybrid material, focusing on the IgG binding ability to the binding domain displayed on the PHA beads in the alginate polymer matrix.
2. Encapsulate PHA beads displaying OpdA (an organophosphate hydrolase) in alginate microspheres and asess the functionality of the hybrid material, focusing on the enzymatic activity of the fusion protein displayed on the PHA beads in the alginate polymer matrix.
3. Encapsulate PHA beads in alginate millispheres as a payload for lipophilic substances and assess the removal of a lipophilic substance from aqueous solution.

1.5.1 Alginate encapsulation of PHA beads displaying IgG binding domain

To achieve the first aim, the following objectives were planned:

- **Production and purification of PHA beads**:
    I. Use pPolyC (Hay *et al.*, 2017) and pET-14b zz(-) phaC (Brockelbank *et al.*, 2006) to transform a production *E. coli* strain, BL21 (DE3) harbouring pMCS69 (Amara & Rehm, 2003).
    II. Culture the transformed production strain under PHA accumulating conditions, and then isolate and purify the PHA beads.

- **PHA bead characterisations and functional assessment**:
    I. Characterise the morphology of *E. coli* cells accumulating PHA beads and isolated PHA beads by fluorescent microscopy, transmission electron microscopy (TEM), and scanning electron microscopy (SEM).
    II. Measure the particle size distribution by laser diffraction.
    III. Evaluate the fusion protein on PHA beads by sodium dodecyl sulfate polyacrylamide (SDS-PAGE).
    IV. Assess the IgG binding capacity of the fusion protein displayed on the PHA beads by IgG binding capacity assay (Brockelbank *et al.*, 2006).
- **Production of PHA beads encapsulated in alginate microspheres:**
    I. Encapsulate PHA beads in alginate microspheres using a water-in-oil (w/o) emulsion with internal gelation method. Subsequently, recover the alginate microspheres from the emulsion and further cross-link through exposure to a $CaCl_2$ cross-linking solution (double gelation).
- **Characterisation of the microspheres:**
    I. Assess the morphology by phase contrast microscopy, fluorescence microscopy and SEM, and particle size distribution by laser diffraction method.
    II. Assess the encapsulation efficiency of PHA beads in alginate microspheres by the combination of bicinchoninic acid (BCA) assay, SDS-PAGE, and calculate the amount of the PhaC derived protein on PHA beads.
    III. Assess the difference in particle size in different solutions by laser diffraction method.

- **Functional assessment of the microspheres:**
    I. Assess the IgG binding capacity of the alginate encapsulated PHA beads by IgG binding capacity assay in batch and column conditions.
    II. Quantify the bound IgG on PhaC derived protein on PHA bead by SDS-PAGE gel densitometry using BSA and IgG as the standard.

1.5.2 Alginate encapsulation of PHA beads displaying OpdA in alginate microspheres

To achieve the second aim, the following objectives were planned:

- **Production and purification of PHA beads:**
  I. Use pPolyC (Hay *et al.*, 2017) and pET-14b PhaC-linker-OpdA (Blatchford *et al.*, 2012) to transform a production *E. coli* strain, BL21 (DE3) harbouring pMCS69 (Amara & Rehm, 2003).
  II. Culture the transformed production strain under PHA beads accumulating conditions, and then isolate and purify the PHA beads.
- **PHA bead characterisations**
  I. Characterise morphology of *E. coli* cells accumulating PHA beads and isolated PHA beads by fluorescent microscopy, transmission electron microscopy (TEM), and scanning electron microscopy (SEM).
  II. Measure the particle size distribution by laser diffraction.
  III. Evaluate the fusion protein on PHA beads by sodium dodecyl sulfate polyacrylamide (SDS-PAGE).
- **Production of PHA beads encapsulated in alginate microspheres:**
  I. Encapsulate PHA beads in alginate microspheres using a water-in-oil (w/o) emulsion with internal gelation method.
- **Characterisation of the microspheres:**
  I. Assess the morphology by phase contrast microscopy, fluorescence microscopy and SEM, and particle size by laser diffraction.
  II. Assess the encapsulation efficiency of PHA beads in alginate microspheres by the combination of BCA assay, SDS-PAGE, and calculate the amount of the PhaC derived protein on PHA beads.
- **Functional assessment:**
  I. Assess the enzyme activity by measuring the change in fluorescence caused by the liberation of enzymatic product.

1.5.3 Alginate encapsulation of PHA beads as a lipophilic adsorbent

To achieve the third aim, the following objectives were planned:

- **Production of PHA beads encapsulated in alginate millispheres:**
    I. Encapsulate pPolyC PHA beads obtained in the first objective of the first aim (Section 1.5.1) in alginate millisphere by dripping droplets of a mixture containing alginate and PHA beads into $CaCl_2$ cross-linking solution.
- **Characterisation of the beads:**
    I. Assess the morphology on appearance, diameter, and wet weight. Assess the proportion of PHA in the alginate millispheres by the combination of BCA assay, SDS-PAGE, and then calculate the amount of PhaC protein on PHA beads.
- **Functional assessment:**
    I. Assess the adsorption capability of PHA beads in alginate millisphere to adsorb a lipophilic dye, Nile red, from an aqueous solution, and determine the residual concentration of Nile red in the solution by measuring the level of fluorescent intensity. Also, assess the effect of alginate concentrations, calcium ion concentrations, and PHA bead concentration used in the preparation on adsorption kinetic and isotherm of the millispheres.

Chapter 2: Materials and Methods

Unless indicated, all reagents were purchased from Sigma-Aldrich, Ajax Finechem, or Merck and used without further purification.

All shaking incubations at 37ºC were conducted on a Thermoline Scientific (Australia) model TLM-530 Chest orbital shaker.

2.1 Bacterial strains and plasmids

The bacterial strains and plasmids used in this study are listed in Table 1 and Table 2:

Table 1: Bacterial strains used in this study.

E.coli strains	Relevant characteristics	References/ Supplier
BL21 (DE3)	F^- *ompT hsdS*(r_B^- m_B^-) *dcm*+ Tet^{r}gal λ(DE3) *endA Hte*	Stratagene
XL1-Blue	*rec*A1 *end*A1 *gyr*A96 *thi*-1 *hsd*R17 *sup*E44 *rel*A1 *lac* [F′ *pro*AB l*ac*IqZΔM15 Tn10 Tet^r]	Stratagene

Tet^r, tetracycline resistance

Table 2: Plasmids used in this study.

Plasmid name	Relevant characteristics	References/ Supplier
pET-14b	Ap^r; T7 promoter; His-6tag	Novagen
pPolyC	Ap^r; T7 promoter, pET-14b derivative containing *phaC* gene fragment with a C-terminal linker	Hay *et al.* (2017)
pET-14b zz(-)phaC	Ap^r; T7 promoter pET-14b derivative containing *zz* gene fragment fused to 5' end of *phaC* without a signal sequence encoding region	Brockelbank *et al.* (2006)
pET-14b phaC-linker-OpdA	Ap^r; T7 promoter, pET-14b derivative containing *opdA* gene fragment fused to the 3' end of *phaC* via a linker sequence	Blatchford *et al.* (2012)
pMCS69	Cm^r; T7 promoter; pBBR1MCS derivative containing codon optimised genes *phaA* and *phaB* from *C. necator*	Amara & Rehm (2003)

Ap^r, Ampicillin resistance; Cm^r, Chloramphenicol resistance

2.2 Primers

Primers used in this study are listed in Table 3 and were used to confirm the DNA sequence of plasmids.

Table 3: Primers used in this study.

Primer name	Sequence from 5' to 3'	References/ Supplier
T7_promoter	TAATACGACTCACTATAGGG	Allan Wilson Centre
T7_terminator	GCTAGTTATTGCTCAGCGG	Integrated DNA Technologies (IDT)

2.3 Alginate

Medium viscosity alginic acid (sodium salt) from brown algae (A2033) was purchased from Sigma-Aldrich (USA). According to the manufacturer, the molecular weight of the alginate ranges between 80,000-120,000 Da, and the typical content of mannuronic acid (M) and guluronic acid (G) is approximately 61% and 39% respectively (M/G ratio of 1.56). The viscosity is ≥2,000 cP at 2% w/v in water at 25°C.

2.4 Media

2.4.1 Liquid media

Luria-Bertani (LB) medium (Neogen Corporation, USA) was prepared by adding 20 g per litre of distilled water and autoclaved at 121°C for 20 minutes.

2.4.2 Solid media

LB agar was prepared by adding agar (Neogen Corporation, USA) to 1.5 g per 100 ml LB medium and autoclaved at 121°C for 20 minutes.

2.5 Antibiotic stocks and concentrations

Antibiotics used in this study are listed below. They were sterilised by filtration using a 0.22 µm filter and stored at -20ºC for future use. For the preparation of solid media supplemented with an appropriate antibiotic, autoclaved solid media (Section 2.4.2) was cooled to approximately 50ºC before adding the antibiotic at the concentration outlined below. Antibiotics were added at 1 µl stock/1 ml medium.

Antibiotics	Stock concentration	Final concentration
Ampicillin (Sodium salt)	100 mg/ml in Milli-Q water	100 µg/ml
Chloramphenicol	50 mg/ml in absolute ethanol	50 µg/ml

2.6 Cultivation conditions

Cultivation of *E. coli* cells was performed in Erlenmeyer flasks containing sterile liquid LB medium supplemented with appropriate antibiotics and a carbon source. The flask was plugged with cotton wool plug. The culture was incubated at 37ºC with shaking at

200 rpm. The ratio of the flask to liquid medium volume was kept at 5:1 to maximise aeration.

2.6.1 PHA bead production in *E. coli*

Conditions for PHA bead production *in vivo* was performed as previously described (Hooks *et al.*, 2013). Recombinant pET expression vectors were used to transform *E. coli* BL 21 (DE3) production strain harbouring pMCS69 and incubated (Section 2.6) to provide overnight pre-cultures. This overnight pre-cultures was inoculated at 2% v/v into 1 L sterile LB medium supplemented with 1% v/v glucose, 100 µg/ml ampicillin, and 50 µg/ml chloramphenicol. This culture was incubated at 37ºC with shaking at 200 rpm for approximately 2 to 3 hours until the OD_{600} reached 0.4-0.5. IPTG was then added to the culture to a final concentration of 1 mM to induce gene expression and incubation continued at 25ºC for 48 hours with shaking at 200 rpm (TR225, INFOS HT, Switzerland).

	Stock concentration	Final concentration
IPTG	1 M in Milli-Q water	1 mM
D-Glucose	25% w/v in Milli-Q water	1% v/v

2.7 Long-term storage of bacterial strains

E. coli cells were incubated overnight in sterile LB medium containing appropriate antibiotics at 37ºC with shaking at 200 rpm. 1 ml of the overnight culture was mixed with 70 µl of filtrated dimethylsulfoxide (DMSO) in a 2 ml cryovial tube to give a final concentration of 6.5% v/v and stored at -80ºC for future use.

2.8 Revival of bacterial strains

The revival of *E. coli* cells was performed by removing a small chip from the frozen stock using a sterile pipette tip or a sterile inoculation loop, and inoculating into sterile LB liquid medium (Section 2.4.1) supplemented with appropriate antibiotics. The inoculated medium was incubated overnight at 37ºC with shaking at 200 rpm.

2.9 Competent cells preparation

Competent *E. coli* cells were prepared as described elsewhere (Hanahan, 1983). 50 ml of sterile LB medium (Section 2.4.1) was inoculated with 2% (1 ml) inoculum of an

overnight culture and incubated at 37ºC with shaking at 200 rpm until OD_{600} reached approximately 0.35. The cell culture was subsequently stored on ice for 15 minutes and harvested by centrifugation at 8,000×*g* for 15 minutes. The cell sediment was re-suspended in 16 ml of RF1 solution and incubated on ice for a further 30 minutes. Cells were then harvested again by centrifugation at 8,000×*g* for 15 minutes and re-suspended in 4 ml of RF2 solution. For future use, 200 µl of competent cells were aliquoted into microfuge tubes and stored at -80ºC. The composition of RF1 and RF2 solutions are outlined below:

RF1 solution:	
RbCl	100 mM
$MnCl_2$	50 mM
Potassium acetate	30 mM
$CaCl_2 \cdot 6H_2O$	10 mM
pH adjusted to pH 5.8 using acetic acid	

RF2 solution:	
RbCl	10 mM
MOPS	10 mM
$CaCl_2 \cdot 6H_2O$	75 mM
Glycerol	15 mM
pH adjusted to pH 5.8 using NaOH	

RF 1 and RF2 were sterilised by filtration using a 0.22 µm filter.

2.10 Plasmid isolation and DNA sequencing

2.10.1 High Pure Plasmid isolation kit

Plasmid isolation was performed by using the High Pure Plasmid isolation kit (Roche, Switzerland) according to the manufacturer's instructions.

2.10.2 Determination of plasmid concentration

Plasmid concentration was measured using NanoDrop 1000 (Thermo Fisher Scientific, USA) according to the manufacturer's instructions.

2.10.3 DNA sequencing

DNA sequencing of the plasmids was performed by the Massey Genome Service in Massey University, Palmerston North, New Zealand.

2.11 Transformation of *E. coli*

The frozen *E. coli* competent cells were allowed to warm from storage at -80 ºC (Section 2.9) on ice for 40 minutes. Subsequently, 3 µl of purified plasmid DNA was added and mixed thoroughly with the aliquot of competent cells, and then the mixture was incubated on ice for 20 minutes. To promote the uptake of the plasmid DNA into the cells, the mixture was gently mixed and heat-shocked at 42ºC for 90 seconds then immediately incubated on ice for 5 minutes. Cells were regenerated by adding 800 µl of sterile liquid LB medium (Section 2.4.1) and incubated at 37ºC for one hour. For the selection and isolation of transformants, 100 µl of the cell culture was spread on solid LB agar medium (Section 2.4.2) supplemented with appropriate antibiotics (Section 2.5). To maximise the yield of transformants, the remaining cells were collected by centrifugation at 6,000×*g* for 2 minutes using a Haeraeus™ Pico™ 17 (Thermo Fisher Scientific, USA), and re-suspended in 100 µl of sterile LB medium and plated on fresh solid LB agar medium containing appropriate antibiotics. The plates were incubated at 37ºC overnight. To make a frozen stock, a colony on the plate was inoculated into sterile LB medium supplemented with appropriate antibiotics and incubated overnight. The overnight culture was treated as described in Section 2.7.

2.12 PHA beads isolation and purification

2.12.1 Cell harvest

After 48 hours of culturing and PHA bead production at 25˚C (Section 2.6.1), cells were collected by centrifugation at 6,000×*g* for 20 minutes at 4˚C using a Sorvall RC-6+ (Thermo Scientific, USA). Before the centrifugation, 1ml of the cell culture was taken into centrifuge tubes for microscopy analysis (Section 2.13.1). The cell pellet was frozen at -20˚C overnight before completing a cell disruption procedure (Section 2.12.2).

2.12.2 Mechanical cell disruption

To extract PHA beads from *E. coli* cells, a Microfluidizer® (M110-P: Microfluidics, USA) was used. The frozen cell sediment (Section 2.12.1) was thawed at room

temperature and suspended completely in 0.5×lysis buffer, at 10% w/v concentration, using a homogeniser (MICCRA D-9: MICCRA, Germany). The mixture was then subjected to a mechanical cell disruption procedure with the Microfluidizer (Z type chamber) for 3 passes at 20,000 psi. The crude cell lysate was centrifuged at 9,000×*g* for 30 minutes at 4˚C. The pellet was washed once with the lysis buffer and then the beads purified as described in Section 2.12.3. The composition of the lysis buffer is outlined below:

0.5×Lysis buffer:

Tris	25 mM
EDTA	5 mM
SDS	0.04% w/v

pH adjusted to pH 9.5 using NaOH

2.12.3 Purification of PHA beads

PHA beads in the crude cell lysate (Section 2.12.2) were purified by the inclusion body purification method as described in Palmer & Wingfield (2012). PHA beads were re-suspended in 2M urea wash buffer at 10 % w/v concentration. The suspension was mixed well and homogenised for one minute using a MICCRA D-9 then PHA beads were collected by centrifugation at 9,000×*g* for 30 minutes at 4ºC. This procedure was repeated three times. Subsequently, the pellet containing the PHA beads was re-suspended in 70% ethanol at 10% w/v and incubated at room temperature with shaking overnight. The composition of the urea wash buffer is outlined below:

2 M Urea wash buffer:

Tris	100 mM
EDTA	5 mM
Urea	2 M
Triton X-100	2% v/v

pH adjusted to pH 9.5 using NaOH

2.12.4 PHA beads storage

After purification (Section 2.12.3), PHA beads were washed once with sterile Milli-Q water and then centrifuged at 9,000×*g* for 30 minutes at 4˚C. The PHA bead pellet was re-suspended in sterile Milli-Q water and stored at 15% w/v concentration at 4˚C for future use.

2.13 PHA beads characterisation

2.13.1 Detection of PHA beads in *E. coli* cells

2.13.1.1 Nile-red staining

The presence of PHA beads in cells was detected by a Nile-red staining method as previously described (Spiekermann *et al.*, 1999). Cell culture (1 ml) (Section 2.12.1) was harvested by centrifugation at 6,000×*g* for 5 minutes, and the supernatant was carefully removed. The cell pellet was mixed with 10 µl of Nile-red solution (0.25 mg/ml in DMSO), followed by the addition of 1 ml of 50 mM potassium phosphate buffer (pH 7.5) and mixed thoroughly. The mixture was then incubated in a dark room at room temperature for 15 minutes. After the incubation, the cells were harvested by centrifugation at 6,000×*g* for 5 minutes and washed once with 1 ml of 50 mM potassium phosphate buffer. The cell pellet was re-suspended in 1 ml of 50 mM potassium phosphate buffer, and 10 µl spotted on a glass slide and covered by a coverslip. The slide was analysed by fluorescent microscopy (Section 2.13.1.2).

50 mM potassium phosphate buffer:

K_2HPO_4 (Alkaline)	50 mM
KH_2PO_4 (Acidic)	50 mM

pH of K_2HPO_4 adjusted to pH 7.5 using KH_2PO_4

2.13.1.2 Fluorescence microscopy

Fluorescent microscopy was used to detect PHA beads in *E.coli* cells after staining by Nile-red (Peters *et al.*, 2007). The glass slide prepared in Section 2.13.1.1 was examined with an Olympus BX51 Fluorescence Light Microscope (Olympus, Japan) under 1,000× magnification with a U-MWIG2 filter unit (Ex. 520-550 nm; Em. 580 nm; Dichromatic

mirror 565 nm). Images were captured using MicroPublisher™ 5.0 RTV and analysed by Q-Capture Pro7 software (QImaging, Canada).

2.13.2 Transmission and Scanning electron microscopy

Transmission electron microscopy (TEM) and scanning electron microscopy (SEM) images were taken at the Manawatu Microscopy and Imaging Centre (MMIC, Massey University, Palmerston North, New Zealand). The samples were prepared by centrifuging 0.5 to 1 ml of sample (Section 2.12.1 and 2.12.4) in a microfuge tube, and a small pellet was sent to the MMIC. All subsequent processing on the samples was done by the MMIC.

2.13.3 Particle size analysis

The particle size distribution of PHA beads in the storage solution (Section 2.12.4) was measured by laser diffraction using a Mastersizer 3000 (Malvern Instruments, UK). The Mastersizer 3000 was equipped with an Hydro small volume sample dispersion unit and a dispersion unit controller (Malvern Instruments, UK). The particle refractive index of the PHA beads and the dispersion refractive index of water were set to 1.50 and 1.33, respectively. The particle absorption index of PHA beads was set to 0.01. The obscuration factor was set between 5-15% and aimed at 10%. The dispersion unit controller was set to 2,000 rpm. The particle size analysis was based on the Mie scattering model.

2.14 General methods for protein analysis

2.14.1 Determination of protein profile

2.14.1.1 Sodium dodecylsulfate polyacrylamide gel electrophoresis (SDS-PAGE)

2.14.1.1.1 SDS-PAGE gel preparation

Sodium dodecylsulfate polyacrylamide gel electrophoresis (SDS-PAGE) was performed in a vertical slab gel to evaluate and characterise protein samples. Each gel consisted of two layers with a separating gel (10% w/v polyacrylamide, pH 8.9) at the bottom and a stacking gel (4% w/v polyacrylamide, pH 6.8) on the top. The gel was made in Mini PROTEAN® glass plates (Bio-Rad Laboratories, USA, 1.0 mm thick gel). The separating gel solution was prepared and a few milligrams of Na_2SO_3 was added to help remove O_2 from the solution. The polymerisation was initiated by adding 30 µl of 40% w/v ammonium persulfate (APS) solution and 28 µl of N, N, N', N'–tetramethylethyl-

endiamin (TEMED) while mixing. The mixture was gently poured into the glass plates and a layer of isopropanol immediately added to the top of the gel. The gel was left for approximately one hour to complete the polymerisation. Once the gel had set, the isopropanol was removed and the gel washed once with Milli-Q water and drained using a paper towel. The composition of the separating gel (10% w/v) is outlined below:

3.5×Bis-tris gel buffer:	
Bis-tris	1.25 M
pH adjusted to pH 6.5 using HCl	

Separating gel (10% w/v):	(For four gels)
3.5×Bis-tris gel buffer	11.44 ml
30% Acrylamide	13.32 ml
Milli-Q water	15.24 ml

Ammonium persulfate (40% w/v), APS:	
APS	4 g
Milli-Q water	Make to 10 ml

The stacking gel solution was prepared and a few milligrams of Na_2SO_3 added to help remove O_2 from the solution. While mixing, 17 µl of 40% w/v APS and 19 µl of TEMED were added to initiate polymerisation. The solution was gently poured onto the separating gel. A plastic comb was immediately inserted into the glass plates to form wells. The gel was left for approximately 30 minutes to complete the polymerisation. The composition of stacking gel (4% w/v) is outlined below:

Stacking gel (4% w/v):	
3.5×Bis-tris gel buffer	2.9 ml
30% Acrylamide	1.5 ml
Milli-Q water	5.6 ml

2.14.1.1.2 Protein sample preparation for SDS-PAGE and electrophoresis conditions

SDS-PAGE sample preparation used 30 µl of a solution containing 33-50 µg (wet weight) of whole cell or PHA beads. Two volumes of protein solution were mixed with one volume of 3×SDS denaturing buffer in a microfuge tube and incubated on a heating block at 95ºC for 15 minutes. The denatured protein sample was then centrifuged at 17,000×*g* for 5 minutes to collect the polyester beads before loading onto the gel. GangNam-STAIN™ prestained protein ladder (iNtRON Biotechnology, Korea) was also loaded onto the gel and used for estimating the molecular weight of proteins on the gel. Running buffer was added to the electrophoresis tank. The electrophoresis conditions were electric current at a fixed 1,000 mA and voltage at 150 V until the loading dye had reached the end of the gel, which takes approximately 1 hour. The composition of 3×SDS denaturing buffer, 5×High molecular weight running buffer, and 200×Reducing agent are outlined below:

3×SDS denaturing loading buffer:

Tris	100 mM
SDS	8.0 g
EDTA	37.2 mg
Glycerol	40 ml
β-mercaptoethanol	20 ml
Bromothymol blue	10.0 mg
Milli-Q water	Make to 100 ml

pH adjusted to pH6.8 using HCl

5×High molecular weight running buffer:

MOPS	250 mM
Tris	250 mM
SDS	0.5 w/v
EDTA	5 mM

200×Reducing agent:

Sodium bisulfite	1 M

Running buffer:	
5x High molecular weight running buffer	100 ml
200x Reducing agent	2.5 ml
Milli-Q water	Make to 500 ml

Protein marker	**Molecular weights (kDa)**
Gangnam-STAIN prestained protein ladder	235, 170, 130, 93, 72, 53, 41, 30, 22, 18, 14, 9

Note: Molecular weights are in Bis-Tris 10 % MOPS buffer condition

2.14.1.1.3 Protein staining with Coomassie blue and destaining

The SDS-PAGE gel was carefully removed from the glass plates and stained with Coomassie brilliant blue staining solution for 15 minutes on a tilt shaker. After staining, the gel was washed with distilled water and then destained using destaining solution until protein bands were visible and the background stain was removed. The GEL-DOC 2000 (Bio-Rad Laboratories, USA) and Image Lab software (Bio-Rad Laboratories, USA) were used to obtain and to analyse the gel image.

Coomassie brilliant blue staining solution:	
Coomassie blue R-250	4 g
Ethanol	450 ml
Acetic acid	90 ml
Distilled water	460 ml

Destaining solution:	
Ethanol	600 ml
Acetic acid	200 ml
Distilled water	1,200 ml

2.14.1.1.4 Densitometry

Densitometry was used to determine the percentage of the fusion (PhaC derived) protein on the PHA beads from the total proteins in the bead suspension. Each SDS-PAGE gel image was analysed using Image Lab software (Bio-Rad Laboratories, USA).

2.14.2 Determination of protein concentration

2.14.2.1 Gel densitometry

Densitometry of SDS-PAGE gels was used to quantify the protein on the surface of PHA beads based on a serially diluted bovine serum albumin as the standard. PHA bead suspension was prepared at 5 µg/µl (0.5% w/v) bead concentration in a microfuge tube and eventually 3.33 µg/µl concentration after addition of 3×SDS denaturing loading buffer (Section 2.14.1.1.2). Bovine serum albumin (BSA: Thermo Fisher Scientific, USA) was prepared at 75 ng/µl then 50 ng/µl after addition of the loading buffer. Into the well of SDS-PAGE gel, BSA was loaded from 50-500 ng. PHA beads were loaded from 10-40 µg of PHA beads into the well. The sample preparation and conditions of SDS-PAGE were followed as described in Section 2.14.1.1.2. The amount of protein displayed on the surface of PHA beads was determined from a standard curve prepared from known BSA protein amounts shown on the gel. Similarly, the quantity of human IgG was determined on the SDS-PAGE gel using serially diluted human IgG (Equitech-Bio, USA) as a standard. Human IgG was prepared at 375 ng/µl then 250 ng/µl after addition of 3×SDS denaturing loading buffer. The quantity of human IgG bound per unit of protein was determined from a standard curve prepared from 250-2,500 ng of human IgG on the SDS-PAGE gel.

2.14.2.2 Bradford assay

Protein concentration in a suspension was determined using the Bradford assay method. 10 µl of standard or sample were prepared in a flat bottom well microtitre plate (Greiner Bio-One, Austria). A known concentration of serially diluted bovine serum albumin (BSA) or IgG (Equitech-Bio, USA) was used as the standard for the assay. Into each well containing 10 µl of standard or sample, 200 µl of filtered Bradford reagent was added. The plate was then incubated in the dark at room temperature for 5 minutes for colour development. After the incubation, the absorbance was measured at λ=595 nm using ELx808iu ultra microtiter plate reader (BIO-TEK Instruments Inc., USA). Protein concentration in the sample was determined from a standard curve. For the standard curve, BSA was prepared at 0.05-0.4 mg/ml, and IgG was prepared at 0.05-0.8 mg/ml.

2.14.2.3 Bicinchoninic acid (BCA) assay

The total protein concentration in PHA bead suspension was determined using BCA assay. The Pierse™ BCA protein assay kit (Thermo Fisher Scientific, USA) was used according to the manufacturer's instructions. A known concentration of BSA was used as the standard for this assay. PHA bead suspension was prepared to 2.5-10% w/v slurry. 60 µl of standard or sample was prepared in a microfuge tube, and then 480 µl of working solution was added. The tube was incubated at 37ºC for 30 minutes on an orbital rotator. After the incubation, the tube was centrifuged at 17,000×*g* for 5 minutes to pellet PHA beads. The supernatant fluid (200 µl) was transferred to a flat bottom well microtitre plate (Greiner Bio-One, Austria) and the absorbance was measured at λ=562nm by ELx808iu ultra microtiter plate reader (BIO-TEK Instruments Inc., USA). Protein concentration in the sample was determined from a standard curve prepared with known concentrations of BSA ranging from 0.125-2.0 mg/ml.

2.15 Assessment of the activity of fusion protein displayed on PHA beads

Determination of the activity of fusion protein displayed on the surface of PHA beads is described in Section 2.17.2.

2.16 Preparation of PHA beads encapsulated in alginate microspheres

2.16.1 Alginate solution preparation

Medium viscosity sodium alginate (Section 2.3) solution was prepared at 2.5% w/v in sterile Milli-Q water. Dried sodium alginate was mixed with sterile Milli-Q water in a sterile beaker and stirred with a magnetic stirrer. The alginate solution was heated and stirred at 80ºC until the dried alginate was fully dissolved. Once it had completely dissolved, the heat was turned off and the mixture stirred overnight at room temperature to ensure complete re-hydration. The alginate solution was then stored at 4ºC for future use. Alginate solution was equilibrated to room temperature before using for alginate sphere production.

2.16.2 Internal gelation

PHA beads encapsulated in alginate microspheres were produced by the water-in-oil (w/o) emulsion technique with internal gelation as described by Silva *et al.* (2005). Alginate solution prepared in Section 2.16.1 was mixed with a 15% w/v PHA bead suspension to produce the alginate-PHA bead mixture. Into this mixture, $CaCO_3$ (May & Baker, UK) solution (100 mg/ml) was also added to give final concentrations of each component in the mixture of 2% w/v alginate, 2% w/v PHA beads and 40 mM $CaCO_3$. For making blank alginate microspheres, an equal volume of sterile Milli-Q water was added instead of PHA bead suspension. The mixture was homogenised for 1 minute with a blade homogeniser (MSE, UK). The mixture was then dispersed into paraffin liquid (Paraffin liquid, water white, general purpose grade, Thermo Fisher Scientific, USA) containing Span 80 (Span 80 viscosity 1,000-2,000 mPa.s at 20ºC), a lipophilic surfactant, at 1% v/v by stirring at a preselected speed (Table 4) using a homogeniser equipped with blades (MSE, UK). The stirring speed of the homogeniser was monitored using a light tachometer (461895: EXTECH, USA). The w/o ratio was kept constant at 30/70 ratio (30 ml water phase and 70 ml oil phase, in total 100ml) throughout this study. After emulsifying for 15 minutes, glacial acetic acid was added at 2.5 molar ratio of acid/Ca^{2+} into the emulsion to reduce the pH in the water phase. An additional 15 minutes stirring was completed to ensure gelation. The oil dispersed alginate microspheres were recovered by washing with 100 mM acetate buffer (pH 5.5) and centrifuging by Centrifuge 5702 (Eppendorf, Germany) at 2,000×*g* for 15 minutes. The washing was continued until no more oil was detected under an optical microscope. After the acetate buffer washing, the microspheres were washed twice with sterile Milli-Q water. The microspheres were then dispersed in Milli-Q water and incubated at 4ºC overnight with tilt shaking to equilibrate the suspension. The microspheres were then collected by centrifugation at 2,000×*g* for 15 minutes and dispersed again in sterile Milli-Q water at 50% w/v and kept at 4ºC for future use. The schematic procedure of preparing alginate microspheres by w/o emulsion with internal gelation is shown in Figure 8, and the production parameters are summarised in Table 4:

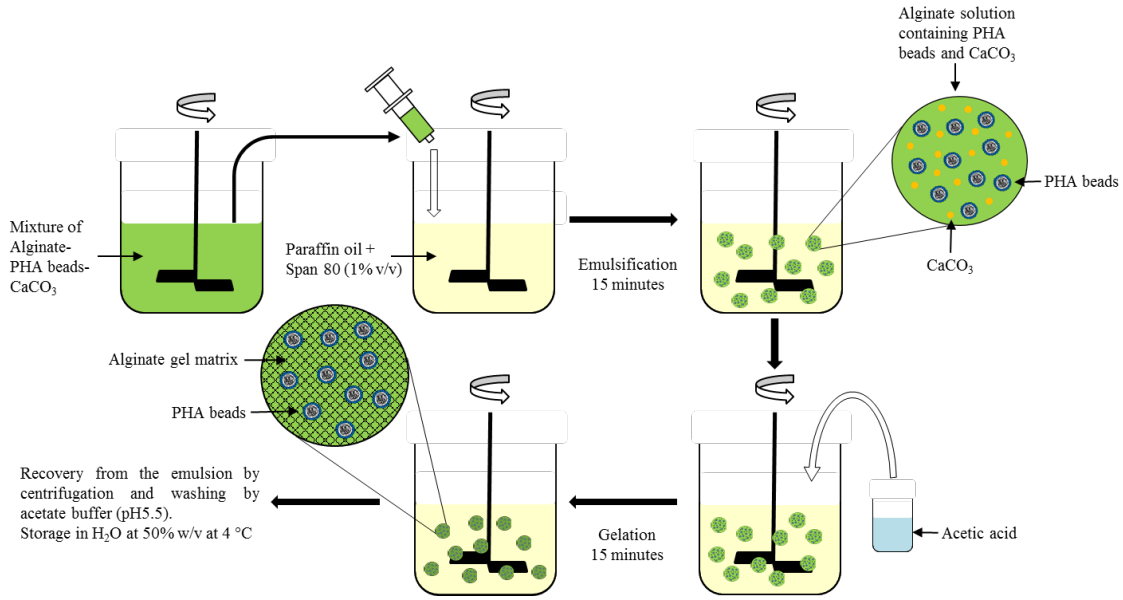

Figure 8: Schematic image of alginate microspheres preparation by water-in-oil emulsion method with internal gelation.

Table 4: Summary of formulation parameters in water-in-oil emulsion with internal gelation method.

Production parameters	
Oil phase	Paraffin liquid
Water phase	Alginate, PHA beads and $CaCO_3$ mixture
Emulsifier	1% v/v Span80 in paraffin liquid
Duration	15 minutes emulsification, 15 minutes gelation
Stirring speed	250-450 rpm (Section 3.1) 400 rpm (Section 3.2)
w/o ratio	30/70
Acid/Ca^{2+}	2.5 molar ratio
Washing buffer solution	100 mM Acetate buffer (pH 5.5)
Storage solution	Milli-Q water

2.16.3 Double gelation

The PHA beads displaying IgG binding domain encapsulated in alginate microspheres, prepared with internal gelation (Section 2.16.2), were subjected to an additional gelation in $CaCl_2$ cross-linking solution (Figure 9). Briefly, the 50% w/v suspension of alginate microspheres prepared with internal gelation were dispersed into 40 mM $CaCl_2$ cross-linking solution at a ratio of 1:1. The final concentration of $CaCl_2$ in the crosslinking solution was 20 mM after the addition of the microsphere suspension. The dispersion was then incubated with a magnetic stirrer at 300 rpm for 15 minutes at room temperature. After the incubation, the microspheres were collected by centrifugation at 2,000×*g* for 15 minutes. The pellet containing the microspheres was washed with sterile Milli-Q water for three times then dispersed in sterile Milli-Q water at 50% w/v and kept at 4ºC for future use.

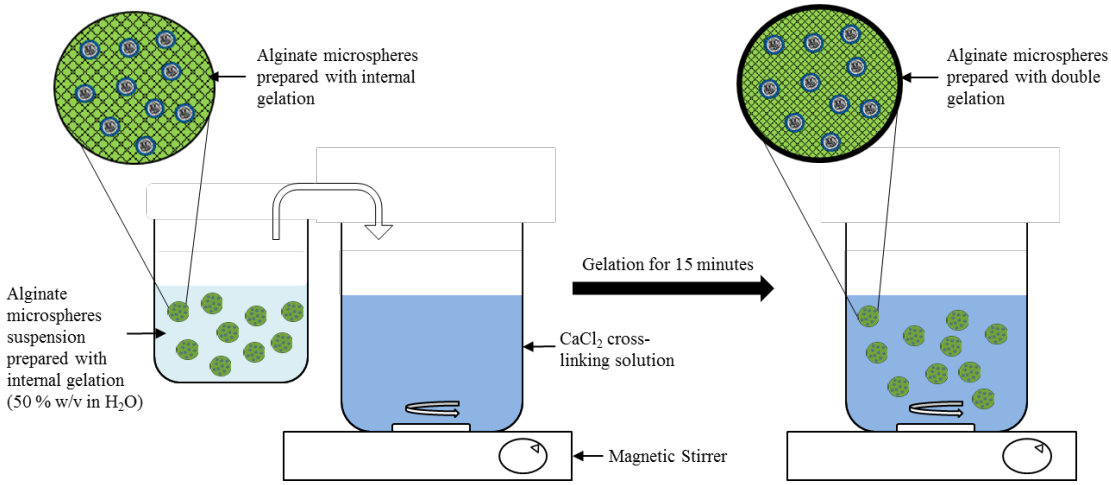

Figure 9: Schematic image of alginate microspheres preparation by double gelation.

2.16.4 External gelation

A simple extrusion dropping method was applied to produce PHA beads encapsulated in alginate millispheres (Zhao *et al.*, 2015). Alginate solution was mixed with a PHA bead suspension at a range of concentrations (Section 3.3). For making blank alginate millispheres, the same volume of sterile Milli-Q water was added instead of the PHA bead suspension. The alginate-PHA bead mixture was prepared in a 50 ml syringe (BD Plastipak, USA), then C-FLEX® Tubing L/S 14 (Masterflex, Germany) equipped with 23 G needle (TERUMO, Japan) was attached to the syringe. A peristaltic pump (BT300-2J pump, LongerPump, China) was used with the pumping speed of 5 rpm and the mixture added dropwise into a $CaCl_2$ cross-linking solution. The needle tip was set to 3 cm above the surface of the solution and perpendicular to the solution. The solution was stirred at 300 rpm with a magnetic stirrer. After all the alginate-PHA bead mixture had been added to the solution, millispheres were stirred for an additional hour before collection. The millispheres were washed three times with sterile Milli-Q water then stored hydrated in Milli-Q water at 4ºC for future use. A schematic image of alginate millisphere production is shown below (Figure 10).

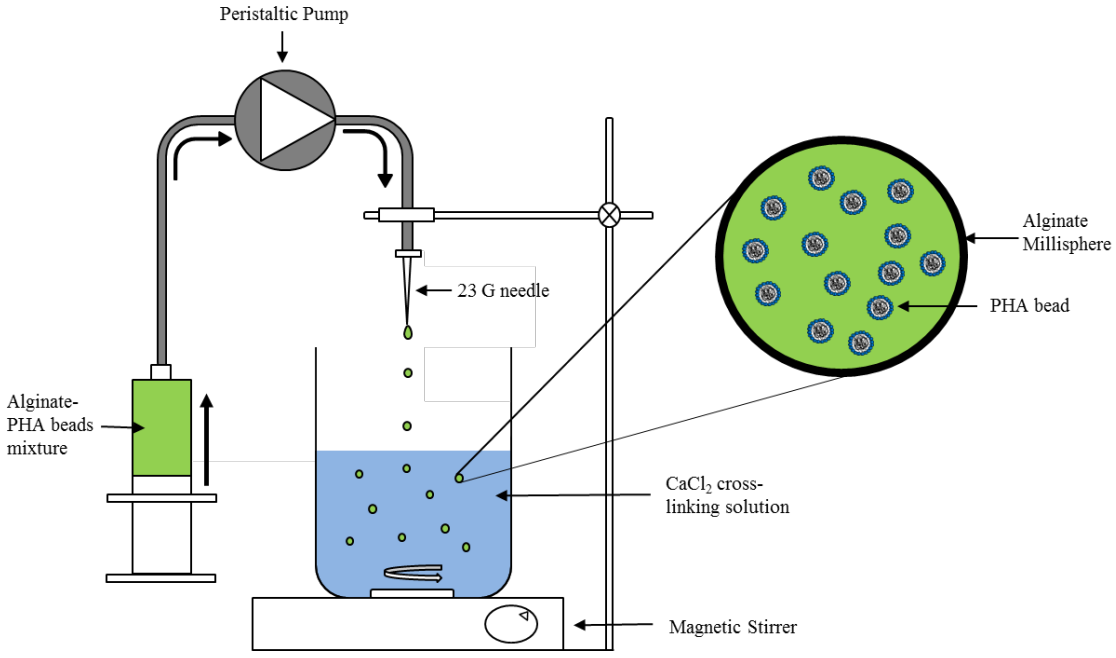

Figure 10: Schematic image of alginate millisphere preparation by a simple extrusion dripping method with external gelation.

2.17 Characterisation of PHA beads encapsulated in alginate microspheres and millispheres

2.17.1 Morphology analysis

2.17.1.1 Microscopic analysis of microspheres

Phase contrast microscopy (Leica, Germany) was used to observe the structure of alginate and PHA beads encapsulated in alginate microspheres. In the meantime, the same frame position was also analysed by fluorescence for the presence of PHA beads in the alginate microspheres using N 2.1 unit (Ex. 515-560 nm; Em. 590 nm; Dichromatic mirror 580 nm). The image was captured using a Leica DFC500 (Germany) and analysed by LAS AF Lite software (Leica, Germany). PHA beads in alginate microspheres were stained as previously described in Section 2.13.1 using Milli-Q water for washing instead of 50 mM potassium phosphate buffer.

2.17.1.2 Scanning electron microscopy

PHA beads encapsulated in alginate microspheres were collected by centrifugation at 2,000×g for 5 minutes in a microfuge tube. The supernatant was removed, and the pellet was mixed with absolute ethanol to dehydrate the pellet. The sample was then collected at 2,000×g for 5 minutes. The pellet was frozen at -80ºC then lyophilised. Millispheres were collected by filtration using Whatman 542 filter paper (Whatman, UK) and treated with absolute ethanol to dehydrate. The dehydrated millispheres were frozen at -80ºC then lyophilised. The sample was then processed at the MMIC as described in Section 2.13.2.

2.17.1.3 Particle size analysis

2.17.1.3.1 Microspheres

The particle size of alginate and PHA beads encapsulated in alginate microspheres was analysed by Mastersizer 3000 (Malvern instruments, UK) as also described for PHA beads in Section 2.13.3. The particle refractive index was set to 1.78, and the absorption index was set to 0.005, as given by optimal property optimizer in the Mastersizer software (Malvern instruments, UK). The dispersion refractive index was set to 1.35. The

obscuration was set between 5-15% and aimed at 10%. The dispersion unit was set to 1,500 rpm. The particle size analysis was based on the Mie scattering model.

2.17.1.3.2 Millispheres

The particle size (mm, diameter) of alginate millispheres produced by the simple extrusion dropping method (Section 2.16.4) was determined by measuring the diameter of 30 randomly picked spheres using a ruler (H-101C, SHINWA, Japan) as the standard.

2.17.1.4 Encapsulation efficiency

To determine the encapsulation efficiency of PHA beads in alginate microspheres, the combination of solubilising alginate microspheres, BCA assay for protein quantification (Section 2.14.2.3), and densitometry on SDS-PAGE gel for determining the proportion of protein (PhaC derived) on PHA beads (Section 2.14.1.1.4) were used. Microsphere suspension (300-500 µl) was collected in a microfuge tube by centrifugation at 6,000×g for 5 minutes, the supernatant discarded and 1,000 µl of solubilising buffer was added to the tube. The suspension was mixed well by vortex-mixing and centrifuged at 17,000×g for 5 minutes. The extracted PHA bead pellet was washed once with the solubilising buffer and twice with Milli-Q water or any buffer solution in the test. Finally, the PHA bead pellet was re-suspended at 10% w/v concentration. The PHA bead suspension was then tested by BCA assay for protein quantity and SDS-PAGE for protein proportion of PhaC derived protein on PHA beads. The encapsulation efficiency of PHA beads in alginate microspheres was determined by the following equation:

$$EE\ (\%) = \left\{ \left[\frac{(P_{BCA} \times P_{\%SDS}) \times V_{total}}{P_{PHA\ beads} \times v} \right] \div (C_{PHA\ beads} \times V_{PHA\ beads}) \right\} \times 100$$

Where *EE(%)* is the encapsulation efficiency, P_{BCA} is the protein amount of BCA assay (mg), $P_{\%SDS}$ is the protein proportion of the extracted PHA beads (%), $P_{PHA\ beads}$ is the amount of fusion protein on PHA beads (mg/mg), v is the volume used in microsphere solubilisation from stock suspension (ml), V_{total} is the total volume of the microsphere stock suspension (ml), $C_{PHA\ \text{beads}}$ is the theoretical concentration of initial PHA beads in stock bead suspension (mg/ml), and $V_{PHA\ beads}$ is the total volume of initial PHA bead stock suspension used (ml).

Solubilising buffer (TBS+EDTA):

Tris	50 mM
NaCl	150 mM
EDTA	50 mM

pH adjusted to pH 7.4 by HCl

For the millispheres prepared with external gelation (millimetre size), the NaCl concentration was 300 mM and EDTA was 100 mM. Millispheres were weighed and added to the solubilising buffer in a microfuge tube and incubated with orbital agitation for 1 hour at room temperature. The quantification of PHA beads in millispheres was followed as described above and the following equation was used:

$$PHA\ beads\ per\ g\ of\ millisphere\ (mg/g) = \left(\frac{P_{BCA} \times P_{\%SDS}}{P_{PHA\ beads}}\right) \div M_{millisphere}$$

Where P_{BCA} is the protein amount from BCA assay (mg), $P_{\%SDS}$ is the protein proportion of the extracted PHA beads (%), and $P_{PHA\ beads}$ is the amount of fusion protein on PHA beads (mg/mg), and $M_{millisphere}$ is the wet weight (g) of PHA beads encapsulated in the alginate millispheres (excess water removed, Section 2.17.2.3).

2.17.2 Functional assessment

2.17.2.1 IgG binding testing of PHA beads encapsulated in alginate microspheres

2.17.2.1.1 Batch IgG binding test

An IgG binding capacity test was conducted to assess the IgG binding capacity of the ZZ domain on the surface of free PHA and the PHA beads encapsulated in alginate microspheres in batch conditions (Jahns *et al.*, 2013) (Figure 11A). Approximately 50 mg of PHA beads and 300 µl of 50% w/v PHA beads encapsulated in alginate microspheres were collected in a microfuge tube. Samples were washed once with TBS (50 mM Tris-Cl and 50 mM NaCl, pH7.4) and centrifuged for 5 minutes at 6,000×*g*. After the initial wash, PHA beads encapsulated alginate microspheres were added to 1 ml TBS buffer and incubated at room temperature for 1 hour with orbital rotational agitation (to equilibrate to temperature and in the buffer) before addition of the IgG sample. The supernatant was carefully removed. All samples were dispersed in 1 ml of 3 mg/ml of human IgG

(Equitech-Bio, USA) in TBS and incubated at 25ºC for 30 minutes with orbital agitation. After incubation, the samples were collected by centrifugation for 5 minutes at 6,000×*g*, and the unbound IgG fraction in the supernatant was collected into a new tube. The pellets containing bound IgG were washed three times with TBS by pipetting and collected by centrifugation for 5 minutes at 6,000×*g* between each wash. Bound IgG on PHA beads and PHA beads encapsulated in alginate microspheres was eluted by the addition of 100 mM glycine (pH2.5) and incubation at 25ºC with orbital rotational agitation for 5 minutes. PHA beads and PHA beads encapsulated in alginate microspheres were centrifuged at 17,000×*g* and 6,000×*g* for 5 minutes, respectively, and then supernatant containing eluted IgG was collected into a new tube. The low pH supernatant was neutralised by the addition of 1 M K_2HPO_4 at 1:10 ratio, e.g. 100 µl of supernatant with 10 µl of K_2HPO_4 solution. The collected samples (unbound and eluted IgG fractions) were analysed by the Bradford assay as described in Section 2.14.2.2.

2.17.2.1.2 Column IgG binding test

IgG binding capacity of PHA beads encapsulated in alginate microspheres in column conditions was analysed with a Pierce™ Spin Cups Paper Filter column, and followed the manufacturer's instructions (Thermo Fisher Scientific, USA) (Figure 11B). The column was washed once with TBS. 50 µl of alginate microspheres suspension (50% w/v) was added to the column and washed with TBS. The column was centrifuged at 1,000×*g* for 5 minutes. Then, the alginate microspheres were re-suspended in TBS and incubated for 1 hour at 25°C with orbital rotational agitation. The microspheres in the column were washed with TBS three times. Human IgG in TBS (300 µl of 3 mg/ml) was added to the column and mixed well with the microspheres in the column by pipetting up and down, and then the columns incubated for 30 minutes at 25°C with orbital rotational agitation. The column was centrifuged at 1,000×*g* for 5 minutes and the flow through collected in a separate microfuge tube to analyse the unbound IgG. TBS (300 µl) was added to the column containing the microspheres and the column washed three times with TBS. Bound IgG was eluted by adding 300 µl of 100 mM glycine (pH2.5) and incubating at 25°C for 5 minutes. The column was transferred to a new microfuge tube containing 30 µl of K_2HPO_4 solution, and the eluted fraction was collected by 1,000×*g* for 5 minutes. The elution was repeated three times, and the collected samples (unbound and eluted IgG fractions) were analysed by the Bradford assay as described in Section 2.14.2.2.

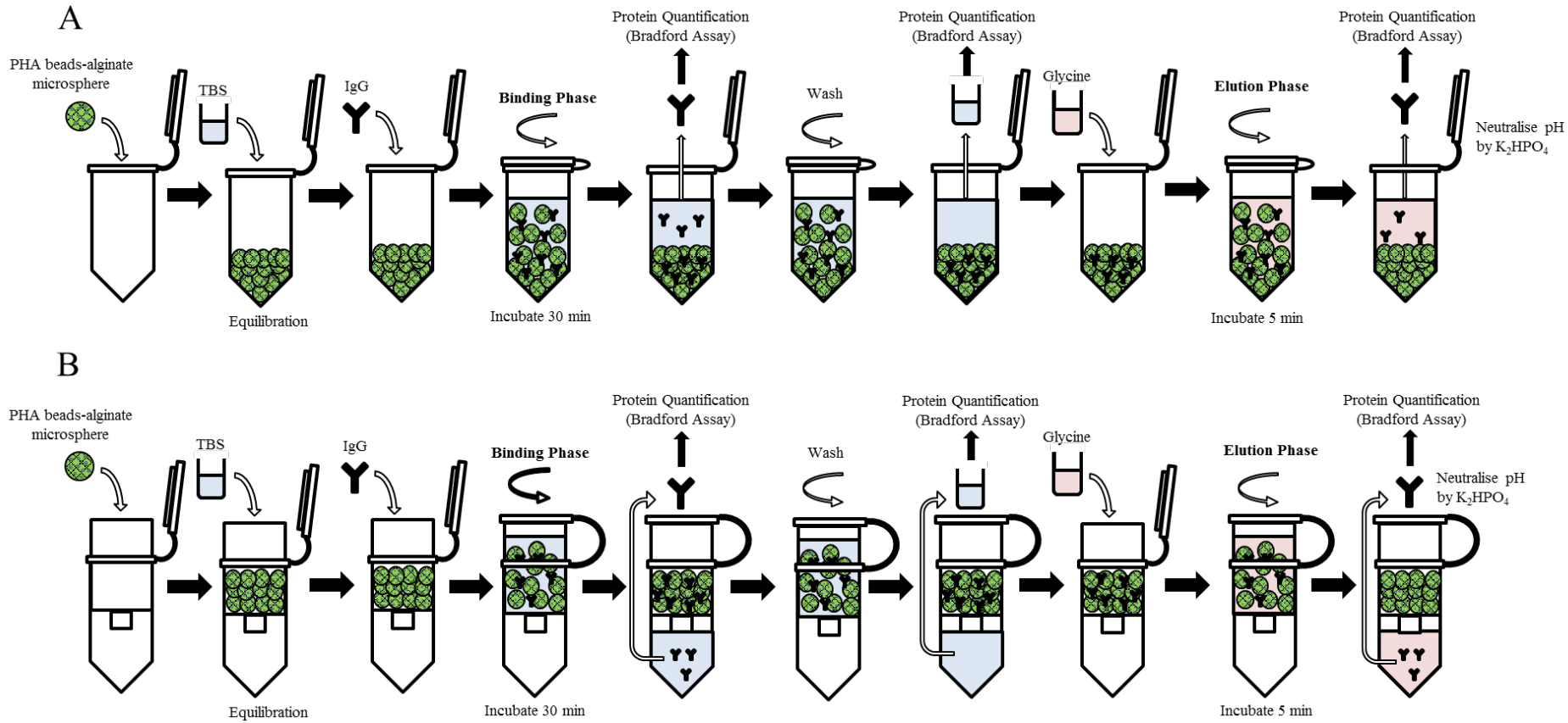

Figure 11: Schematic overview of batch (A) and column (B) IgG binding assay.

2.17.2.2 Enzyme activity assay of PHA beads encapsulated in alginate microspheres

Enzyme activity of free PHA beads displaying OpdA and the PHA beads encapsulated in alginate microspheres were assayed as described previously (Blatchford *et al.*, 2012). The amount of protein on the surface of the free and the encapsulated PHA beads were measured by SDS-PAGE gel densitometry, and 100 μg of the fusion protein on PhaC protein was used in each test. Coumaphos (O, O-diethyl O-3-chloro-4-methyl-2-oxo-2H-chromen-7-yl phophorothioate, Sigma-Aldrich, USA) was used as the substrate. The assay was conducted in 50 mM HEPES buffer at pH 8.0 containing 20% v/v methanol with 200 μM Coumaphos in a 3 ml cuvette. The enzyme activity was monitored for 4 hours by the increase of fluorescence intensity at a wavelength of Ex. 355 nm, and Em. 460 nm, using FluoroMax®-4 (HORIBA, Japan) equipped with Thermo Neslab RTE7 circulating chiller (Thermo, USA). The temperature was set at 25°C, and a small magnetic stirrer was added to the cuvette and stirred at level 3 on FluoroMax®-4 while monitoring.

2.17.2.3 Adsorption equilibrium test of PHA beads encapsulated in alginate millispheres

Batch adsorption equilibrium kinetic and isotherm test of blank alginate millispheres and PHA beads encapsulated in alginate millispheres were carried out at approximately 25ºC (a temperature controlled room) in an aluminium foil covered 50 ml flask shaking at 100 rpm. Millispheres were prepared by removing excess water using Whatman 542 filter paper (Whatman, UK) until no watermarks were visible on the blotting paper. The millispheres were measured in wet weight in this test. The test was done in triplicate for each millisphere type.

2.17.2.3.1 Adsorption kinetic test

Millispheres (0.2g) and 20 ml of Nile red solution prepared at 70 ng/ml in Milli-Q water containing 10 % v/v DMSO were added to an aluminium foil covered conical flask. The flask was covered with aluminium foil cap. Samples were taken at preselected time intervals (1, 2, 4, 8, 12, 18, and 24 hours) then the residual concentration of Nile red in the solution was measured (Section 2.17.2.3.3)

2.17.2.3.2 Adsorption isotherm test

0.2 g millispheres and 20 ml of Nile red solution (serially diluted) were added to an aluminium foil covered conical flask. The concentration of Nile red prepared in Milli-Q water containing 10% v/v DMSO was serially diluted to cover the range from 10-100 ng/ml. The flask was covered with aluminium foil cap. The flask was incubated for 24 hours as adsorption was assumed to reach equilibrium. After 24 hours contact time, the sample was analysed for residual Nile red concentration (Section 2.17.2.3.3).

2.17.2.3.3 Analysis of residual Nile red

Residual concentration of Nile red in the solution was measured by fluorescent intensity induced by Nile red reacting with a lipophilic substance. 20 µl of sample was withdrawn from the flask to a non-binding flat bottom black well microtiter plate (Greiner Bio-One, Austria). 200 µl of filtered 2% v/v Tween-20 in Milli-Q water was added to the plate. The plate was incubated in the dark for 15 minutes. Then, the fluorescence intensity in the plate was analysed at the wavelength of Ex. 544 nm, and Em. 612 nm, using FLUOstar galaxy (BMG labtechnologies, Germany). Milli-Q water containing 10% v/v DMSO was used as the blank. The concentration of Nile red in the solution was determined by the standard curve prepared from 7.5-120 ng/ml Nile red solution containing 10% v/v DMSO. The amount of Nile red in the solution at equilibrium, q_e, was calculated using the following equation:

$$q_e = \frac{(C_i - C_e) \times V}{m}$$

Where C_i and C_e are the initial and equilibrium Nile red concentration in the solution (ng/ml), respectively. V is the volume of the solution (ml), and m is the wet weight of adsorbent used (mg).

2.17.2.3.4 Quality control test

Nile red solution in an aluminium foil covered flask without beads (blank) was also prepared to assess the interference between Nile red in the solution and glassware. The experimental conditions were as described in Section 2.17.2.3.1 and Section 2.17.2.3.2. The residual concentration of Nile red in the solution was analysed as described in Section 2.17.2.3.3. All tests were conducted in triplicate.

2.18 Statistical analysis

Experiments were done in triplicate (n=3) and were presented as means±standard deviation. The mean difference was analysed by one-way ANOVA (Minitab® version 17, Minitab Inc., USA) to determine statistical significance, and the difference is considered significant when $p<0.05$.

Chapter 3: Results

3.1 PHA beads displaying IgG binding domain (ZZ) encapsulated in alginate microspheres

3.1.1 Preparation of PHA beads displaying IgG binding domain (ZZ)

3.1.1.1 *In vivo* production of PHA beads

To produce alginate microspheres encapsulating PHA beads (PHA bead-alginate microspheres) and to assess their functionality, the following plasmids constructed in previous studies were selected, pPolyC (Hay *et al.*, 2017) encoding PhaC and pET-14b zz(-)phaC (Brockelbank *et al.*, 2006) encoding IgG binding ZZ domain fused at N-terminus of PhaC. Both plasmids were confirmed by DNA sequencing (Section 2.10.3) before being used to transform a production strain of BL21 (DE3) *E. coli* harbouring plasmid pMCS69 (Amara & Rehm, 2003). pMCS69 plasmid encodes PhaA and PhaB from *C. necator* that are required for PHA precursor substrate synthesis. After the confirmation, plasmids were used to transform the production strain and plated on LB agar containing 100 µg/ml ampicillin and 50 µg/ml chloramphenicol for selection of transformants (Section 2.11). The recombinant strains were cultivated for *in vivo* PHA beads production under beads accumulating conditions (Section 2.6.1). The production *E. coli* strain transformed with pET14b expression vector was used as the negative control for the PHA beads production.

The presence of PHA beads in the *E. coli* cells was confirmed by Nile red staining (Section 2.13.1.1) and visualised using fluorescence microscopy (Section 2.13.1.2). The intracellular accumulation of PHA beads was observed as fluorescence (Figure 12), therefore indicating the activity of PHA synthase under the PHA bead accumulation conditions. Further confirmation was done using TEM analysis on PHA bead accumulating *E.coli* cells (Figure 13). The TEM images showed the accumulation of white circular PHA beads in *E.coli* cells harbouring pPolyC and pET-14b zz(-)phaC plasmids (Figure 13B and C) while no intracellular accumulation was detected in *E.coli* cells harbouring pET14b plasmid (Figure 13A).

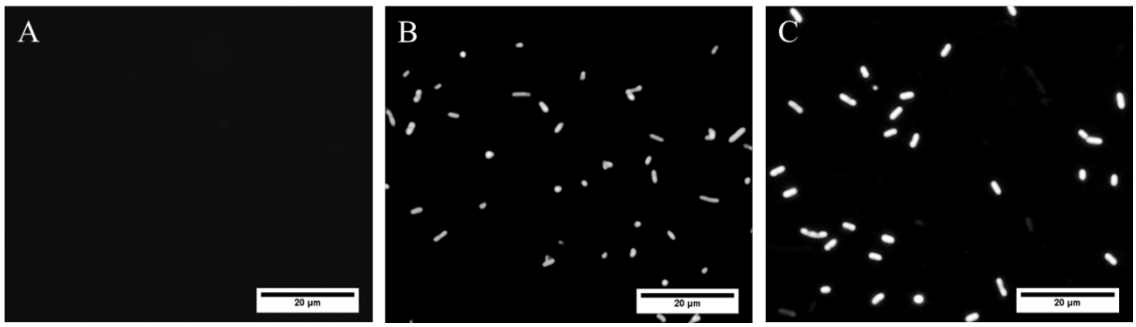

Figure 12: Fluorescence microscopy images of PHA beads produced in recombinant *E.coli* cells. A: BL21 (DE3) *E.coli*+pMCS69 (BL21_69) harbouring pET14b (negative control); B: BL21_69+pPolyC; C: BL21_69+pET-14b zz(-)phaC.

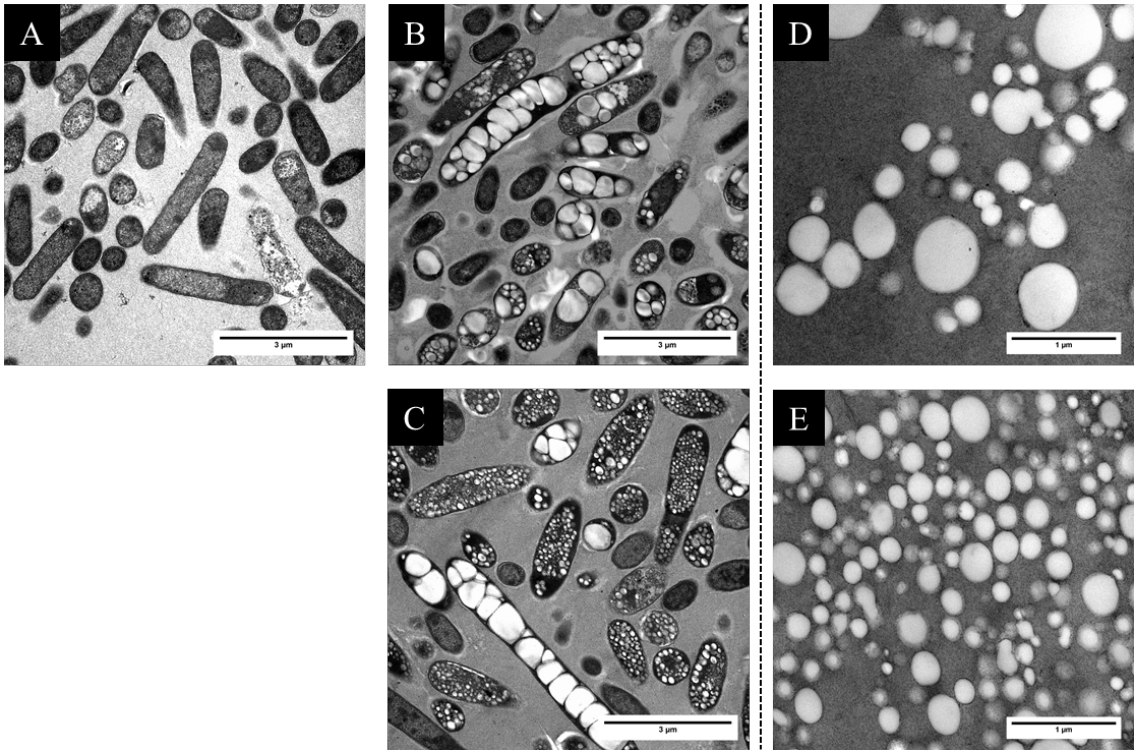

Figure 13: TEM analysis of recombinant *E.coli* cells accumulating PHA beads, and isolated and purified PHA beads. A: BL21 (DE3) *E.coli*+pMCS69 (BL21_69)+pET14b (negative control); B: BL21_69+pPolyC; C: BL21_69+pET-14b zz(-)phaC; D: PhaC PHA beads, E: ZZC PHA beads.

3.1.1.2 Characterisation of PHA beads displaying the IgG binding domain

The *E.coli* cells containing PHA beads were subjected to mechanical cell disruption (Section 2.12.2). The morphology of PHA beads isolated from cells was assessed by TEM and SEM analyses (Section 2.13.2). TEM images confirmed that PHA beads were successfully isolated from *E. coli* cells (Figure 13D and E), and further observation by SEM images showed that spherical or slightly irregular shaped beads were isolated from typical rod-shaped *E. coli* cells (Figure 14).

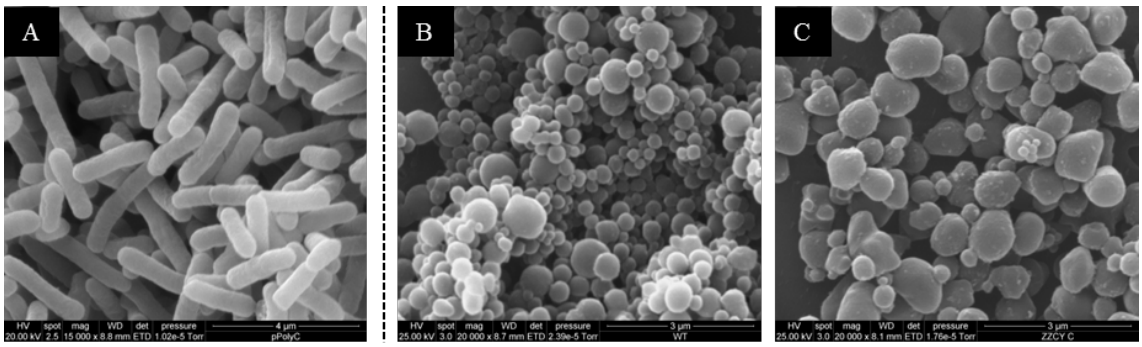

Figure 14: SEM analysis of recombinant *E.coli* cells accumulating PHA beads, and isolated and purified PHA beads. A: BL21 (DE3) *E.coli*+pMCS69 (BL21_69)+pPolyC; B: PhaC PHA beads (WT) ; C: ZZC PHA beads (ZZCYC).

The particle size distribution of the PHA beads as a stock solution (Milli-Q water) was analysed by the laser diffraction method using a Mastersizer 3000 (Section 2.13.3). The particle size was reported as bead diameters. Particle size distributions of both PhaC (wild type) and ZZC PHA beads showed two major peak distributions (Figure 15). The first peak of both PHA bead types was observed at 0.56 µm, and the second peak was observed at 7.17 µm and 3.78 µm, respectively. Moreover, the median particle size (D50) of PhaC and ZZC PHA beads was 6.23 µm and 2.17 µm, respectively (Table 10, Appendix I). However, the particle size of the single PHA beads was shown to be less than 1 µm from TEM and SEM images (Figure 13 and Figure 14). This indicated that the first peak can probably be attributed to a single PHA bead or possibly small bead aggregates, and the second peak can probably be attributed to larger aggregates of the beads. The SPAN factor indicates the width of the distribution that can be calculated using the following equation: $SPAN\ factor = \frac{D_{90}-D_{10}}{D_{50}}$. Due to the broader particle size distribution, ZZC PHA beads

showed higher SPAN factor than that of PhaC PHA beads. However, ZZC PHA beads had a higher specific surface area due to the higher volume density in smaller particle sizes (specific surface of PhaC and ZZC PHA beads were 2,211 and 6,085 m^2/kg, respectively) (Table 10, Appendix I).

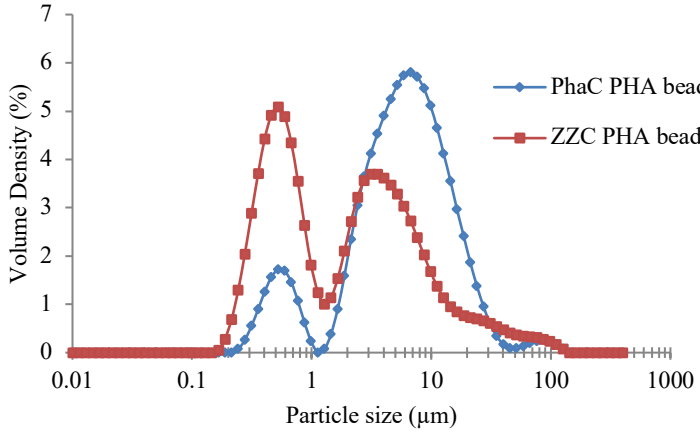

Figure 15: Particle size distribution of PhaC and ZZC PHA beads in water.

The protein profile of the fusion protein on the PHA beads was analysed by SDS-PAGE (Section 2.14.1), and the protein was quantified by densitometry on SDS-PAGE gel using BSA as the protein standard (Section 2.14.2.1). The theoretical molecular weight of recombinant fusion protein was calculated using the ProtParam tool in the ExPASy Proteomics Server (http://www.expasy.org/). The protein profile of whole cell lysate showed dominant protein bands observed at the theoretical molecular weight of 67 kDa for PhaC protein and 79 kDa for ZZC protein while *E.coli* transformed with pET14b showed no dominant protein band (Figure 16). Therefore, this indicated fusion proteins were overproduced in *E.coli* cells transformed with pPolyC and pET14b-zz(-) phaC plasmid, respectively. Densitometry analysis (Section 2.14.1.1.4) after isolation and purification procedure (Section 2.12) showed that the PhaC derived protein in the total protein from each suspension accounted for 36.9 % in pPolyC PHA bead, and for 26.2 % in the ZZC PHA bead. Protein quantification of the fusion protein on the wet weight PHA bead was 5.4±0.2 mg/g for PhaC PHA beads and 2.1±0.3 mg/g for ZZC PHA beads (Table 10, Appendix I).

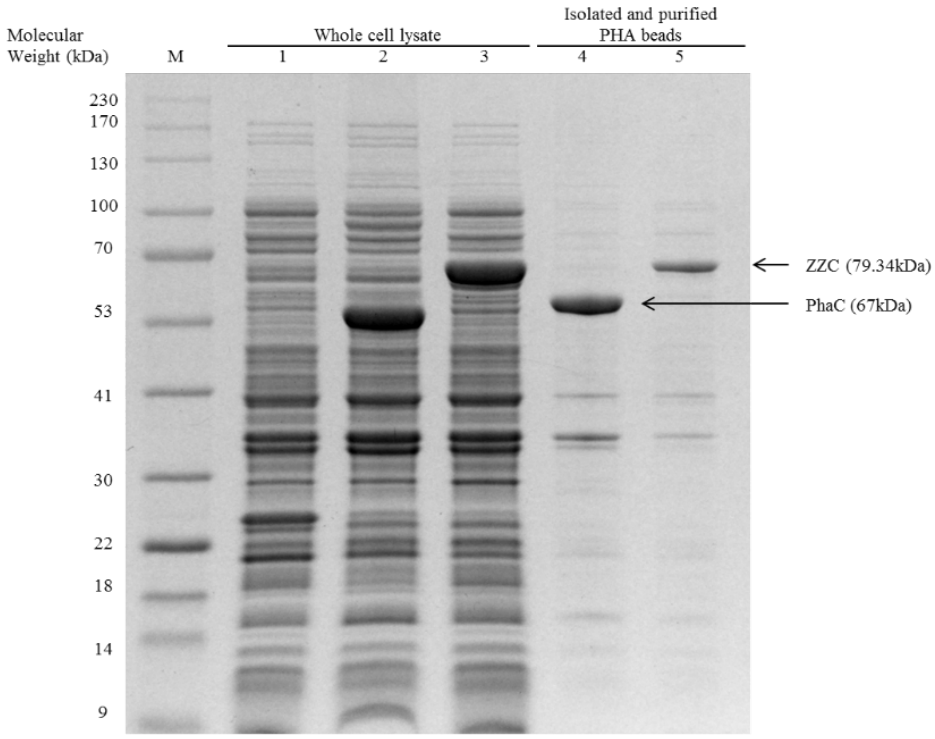

Figure 16: SDS-PAGE protein profile analysis of whole-cell proteins from *E.coli* cells accumulating PHA beads, and isolated and purified PHA beads. Lane M, molecular weight ladder (GangNam-STAIN prestained protein ladder); lane 1, BL21 (DE3) *E.coli* strain+pMCS69 (BL21_69) harbouring pET14b (negative control); lane 2, BL21_69+pPolyC; lane 3, BL21_69+pET14b-zz(-)phaC; lane 4, PhaC PHA beads (67 kDa); lane5, ZZC PHA beads (79.34 kDa).

3.1.1.3 Functional assessment of PHA beads displaying IgG binding domain

The activity of the IgG binding domain (ZZ) displayed on the surface of PHA beads was confirmed before the beads were encapsulated in alginate microspheres. The binding capacity of the IgG binding domain was determined by an IgG binding assay (Section 2.17.2.1.1) which utilised the following equation: $IgG\ binding\ capacity = \frac{(Feed\ IgG - Unbound\ IgG)}{Protein\ amount\ on\ PHA\ beads}$. The protein quantification of unbound and eluted fractions was completed using by the Bradford assay (Section 2.14.2.2). The IgG binding capacity of ZZC PHA beads was significantly higher at 3.95 fold than PhaC PHA beads ($p<0.05$). This indicated that IgG showed a binding affinity towards the IgG binding domain (ZZ) on the PHA beads. However, it also showed non-specific binding to the negative control PhaC PHA beads, which do not display the IgG binding domain (Figure 17A).

Unbound and eluted fractions from the functional assessment of the IgG binding domain (ZZ) were analysed by SDS-PAGE (Section 2.14.1.1) to check the purity of the IgG from

the eluted fractions. SDS-PAGE gel image showed two bands at approximately 50 and 25 kDa, which corresponded to the molecular weight of heavy and light chains of IgG, respectively (Figure 17B). The eluted fraction from ZZC PHA beads showed a greater band intensity than that of the eluted fraction from PhaC PHA beads, indicating that PHA beads displaying IgG binding domain were capable of purifying more IgG in comparison to the negative control (PhaC PHA beads).

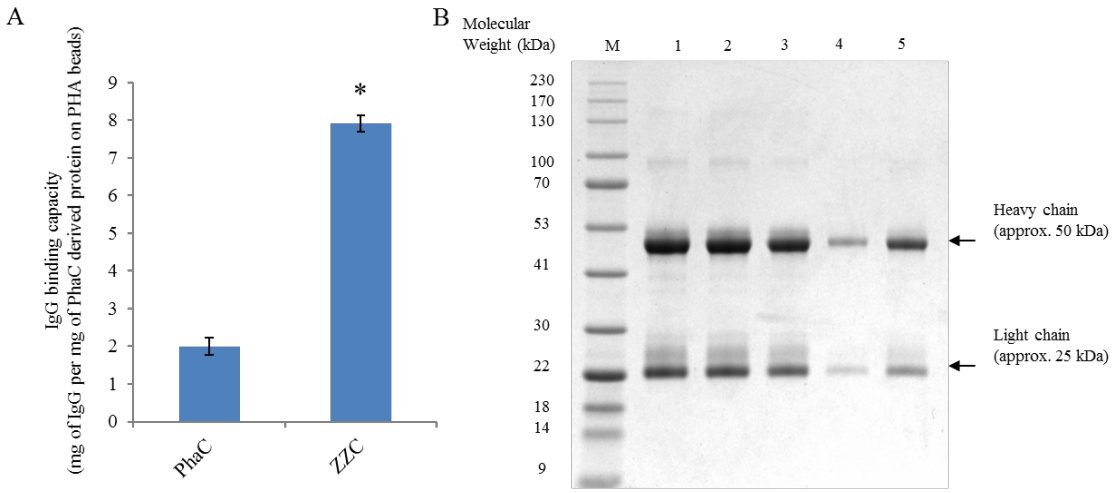

Figure 17: IgG purification performance of PHA beads displaying IgG binding domain. A, Comparative IgG binding capacity analysis of PhaC and ZZC PHA beads. PHA beads were incubated in 3 mg/ml human IgG in TBS at 25°C with orbital rotational agitation.* Indicates the statistically significant difference ($p<0.05$). B, Protein profile of unbound and eluted fractions of IgG binding test on PhaC and ZZC PHA beads. PHA beads were incubated in 3 mg/ml human IgG in TBS, pH 7.4 and eluted by 100 mM Glycine, pH2.5, at 25°C. The molecular weight of IgG heavy chain and light chain are 50 and 25 kDa, respectively. Lane M, molecular weight ladder (GangNam-STAIN prestained protein ladder); lane 1, Human IgG; lane 2, Unbound IgG of pPolyC PHA beads; lane 3, Unbound IgG of ZZC PHA beads; lane 4, Eluted IgG from pPolyC PHA beads; lane 5, Eluted IgG from ZZC PHA beads.

3.1.2 IgG binding domain displaying PHA beads encapsulated in alginate microspheres

3.1.2.1 Characterisation of the microspheres

The PHA beads encapsulated in alginate microspheres (namely, PHA bead-alginate microspheres) were prepared initially by the water-in-oil (w/o) emulsion with internal gelation method (2.16.2), then a further gelation completed on the microspheres (Section 2.16.3). The morphology of the alginate microspheres was assessed using phase contrast

microscopy (Section 2.17.1.1). The alginate microspheres without PHA beads (negative control) were clear spheres while both PhaC and ZZC PHA bead-alginate microspheres showed particulates enclosed within (Figure 18A, B, and C). For further confirmation that PHA beads were encapsulated in the alginate microspheres, the microspheres were stained using Nile red and observed under fluorescence microscopy (Section 2.17.1.1). Red fluorescence at the positions corresponding to the microspheres in the phase contrast images indicated the presence of PHA beads (Figure 18). This showed that the encapsulation of PHA beads within alginate microspheres by w/o emulsion with internal gelation followed by an additional gelation step (double gelation) was successful. In addition, no aggregation of the microspheres was observed. Further morphological analysis by SEM showed that the blank alginate microspheres had a smooth surface while the surface of PHA bead-alginate microspheres was rough (Figure 19).

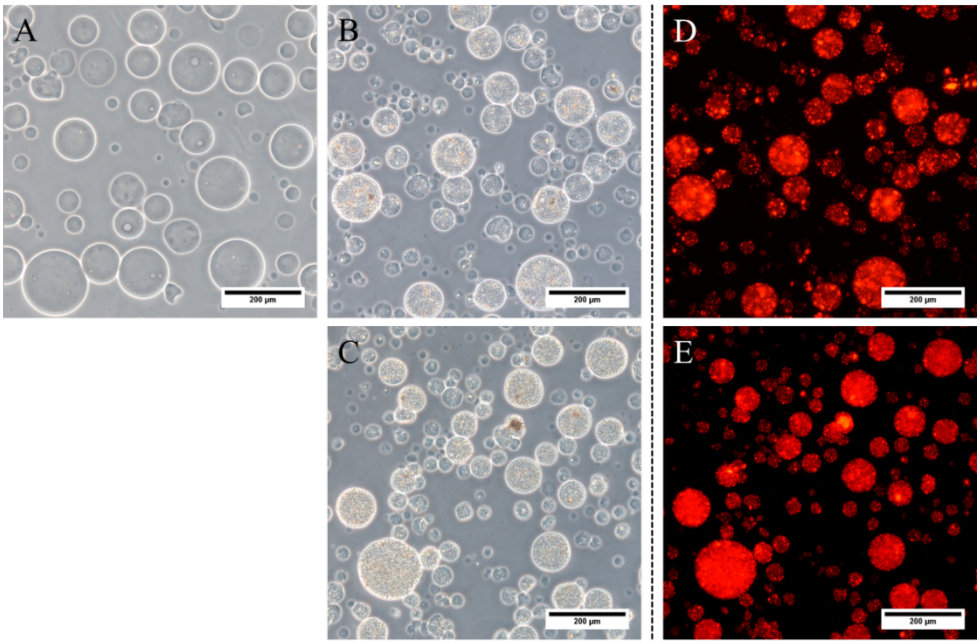

Figure 18: Microscopic images of alginate microspheres encapsulating PHA beads prepared with double gelation. A-C: phase contrast microscopic images; A: blank alginate microspheres; B: 2% w/v PhaC PHA bead-alginate microspheres; C: ZZC PHA bead-alginate microspheres. D and E: fluorescence microscopic images of corresponding alginate microspheres encapsulated PHA beads; D: 2% w/v PhaC PHA bead-alginate microspheres; E: ZZC PHA bead-alginate microspheres.

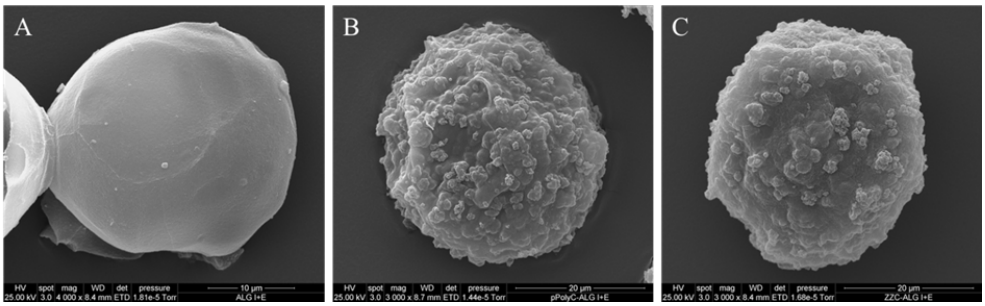

Figure 19: SEM analysis of lyophilised blank alginate microspheres and PHA bead-alginate microspheres prepared with double gelation. The microspheres were prepared with w/o emulsion/internal gelation with additional gelation. A, Blank alginate microspheres; B, PhaC PHA bead-alginate microspheres; C, ZZC PHA bead-alginate microspheres

According to the manufacturer's product description, Pierce™ Spin Cups Paper Filter column has pore sizes less than 10 µm. Therefore, the aim was to produce alginate microspheres above this pore size so they would be suitable for retention on these spin columns. Alginate microspheres were prepared from w/o emulsions using stirring speeds of 250, 350 and 450 rpm. The particle size distribution (diameter) of alginate microspheres prepared in these different stirring speeds was measured by laser diffraction (Section 2.17.1.3.1). A comparison of median particle size values (D50) showed the microspheres prepared at 250 rpm were 1.34-1.48 times larger in diameter than those prepared at 350 rpm and 2.06-2.28 times larger than those prepared at 450 rpm. Similarly, microspheres prepared at 350 rpm were 1.52-1.55 times larger than those prepared at 450 rpm (Table 12, Appendix II). A comparison of the particle size diameter difference between microspheres prepared with only internal gelation, and microspheres prepared with internal gelation followed by an additional gelation step was also analysed. According to the median particle size value (D50), the extra gelation step resulted in a reduction in particle size of 33-56% for blank alginate microspheres, 52-71% for PhaC PHA bead-alginate microspheres, and 58-75% for ZZC PHA bead-alginate microspheres. Moreover, the microspheres prepared at a lower stirring speed demonstrated a larger particle size reduction than the alginate microspheres prepared with a higher stirring speed. For example, the reduction of particle size based on the median particle size (D50) for blank alginate microspheres prepared at 250, 350, and 450 rpm was 56, 45, and 33 %, respectively. The particle size distribution was compared in water (control), TBS (50 mM Tris, 50 mM NaCl, pH7.4), and 100 mM glycine (pH2.5), and showed the largest particle size in TBS and followed by 100 mM glycine (Figure 20 and Table 12, Appendix II).

These results showed that alginate microspheres react differently when dispersed in different solutions.

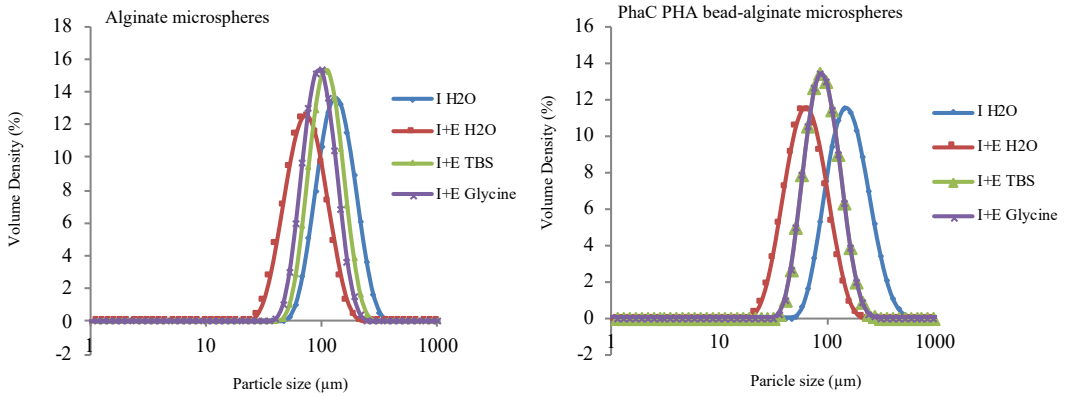

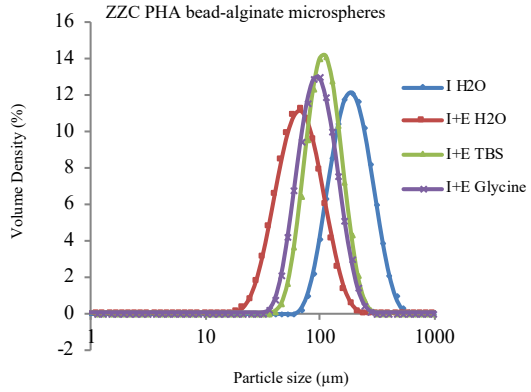

Sample (350rpm)	D(10)	D(50)	D(90)	SPAN	Uniformity
Alginate microspheres					
I - H_2O	87.5	138	220	0.96	0.296
I+E - H_2O	46.3	76.3	125	1.037	0.323
I+E - TBS	76	114	173	0.851	0.263
I+E - Glycine	66.5	99.6	151	0.846	0.262
PhaC PHA bead-alginate microspheres					
I - H_2O	95.9	163	289	1.184	0.367
I+E - H_2O	38.8	67.2	117	1.159	0.359
I+E - TBS	70.5	109	170	0.913	0.282
I+E - Glycine	60	95.1	154	0.985	0.304
ZZC PHA bead-alginate microspheres					
I - H_2O	117	197	332	1.092	0.334
I+E - H_2O	39.5	69.8	123	1.192	0.368
I+E - TBS	72.6	113	177	0.926	0.286
I+E - Glycine	62.1	100	163	1.007	0.313

Figure 20: Summary of particle size distribution of blank alginate and PHA bead-alginate microsperes prepared at 350 rpm. The particle size of microspheres was measured in water, TBS (pH7.4), and 100 mM glycine (pH2.5). I: Internal gelation, I+E: double gelation.

The encapsulation efficiency of PHA beads in alginate microspheres was assessed by examining the PhaC derived protein (PhaC or ZZC) displayed on the PHA beads. The combination of extracting PHA beads by solubilising the alginate microspheres, total protein quantification of the extracted PHA bead fraction, and protein profiling by SDS-PAGE was conducted (Section 2.17.1.4). The initial PhaC derived protein proportion from the total protein in the stock suspensions for PhaC, and ZZC PHA beads before encapsulating in alginate microspheres was 36.9% and 26.6%, respectively (Table 10, Appendix I). After encapsulation in alginate microspheres prepared with internal gelation, the protein proportion was increased by 2.8% for PhaC PHA beads and 3.1% for ZZC PHA beads. The encapsulation efficiency of alginate microspheres prepared in the internal gelation phase was slightly higher in PhaC PHA beads than ZZC PHA beads, but both beads showed high encapsulation efficiency (98.4±0.5% and 92.6±2.6%,

respectively). The additional gelation on the internally gelled microspheres showed an increase in the proportion of PhaC derived proteins by 4.1% for PhaC PHA beads and 2.7% for ZZC PHA beads compared to the alginate microspheres prepared with internal gelation only. In total, the proportion of PhaC derived proteins after double gelation resulted in an increase by 6.9% for PhaC PHA beads and 5.8% for ZZC PHA beads from the initial protein proportion in the stock suspension. However, the encapsulation efficiency was significantly reduced after the additional gelation step, compared to the microspheres prepared with internal gelation only, with encapsulation efficiency reduced by 34% and 26.1% for PhaC PHA bead-alginate microspheres and ZZC PHA bead-alginate microspheres, respectively (Table 5).

Table 5: The encapsulation efficiency of PhaC and ZZC PHA beads in alginate microspheres.

		Internal gelation only		Double gelation	
PHA bead types	Initial PhaC proportion (%)*	PhaC proportion (%)*	Encapsulation efficiency (%)	PhaC proportion (%)*	Encapsulation efficiency (%)
PhaC	36.9	39.7	98.4±0.5	43.8	64.4±1.0
ZZC	26.6	29.7	92.6±2.6	32.4	66.5±1.9

Note: * The protein proportion obtained from densitometry on SDS-PAGE gel

3.1.2.2 Functional assessment of the microspheres: IgG binding capacity

The IgG binding assay was conducted to assess the IgG binding capacity of the PHA bead-alginate microspheres (Section 2.17.2.1). The IgG binding capacity of the alginate microspheres in the batch test is shown in Figure 21A. All the alginate microsphere types (the blank, PhaC PHA bead- and ZZC PHA bead-alginate microspheres) demonstrated a similar binding capacity level with no significant differences ($p>0.05$). Similarly, the alginate microspheres tested in the column test showed similar binding capacity among all the type of alginate microspheres tested ($p>0.05$) (Figure 21B). In comparison with the IgG binding capacity of the alginate microspheres in the column test, the binding capacity of the batch test was approximately half of the column test (approximately 2.5 μg/mg versus 5.0 μg/mg.). To avoid interference by the residual IgG in the elution result, the IgG concentration in the supernatant (batch) and flow through liquid (column) was measured prior to the elution phase and confirmed at negligible concentration levels (approximately 1% of initial IgG concentration). The elution procedure was completed

three times to ensure the release of bound IgG from the microspheres. Nevertheless, both batch and column test conditions resulted in very low, and almost no, IgG eluted (Figure 21A and B). Therefore, the results of the IgG binding assay showed that alginate microspheres had a binding affinity with IgG, however, the bound IgG could not be eluted.

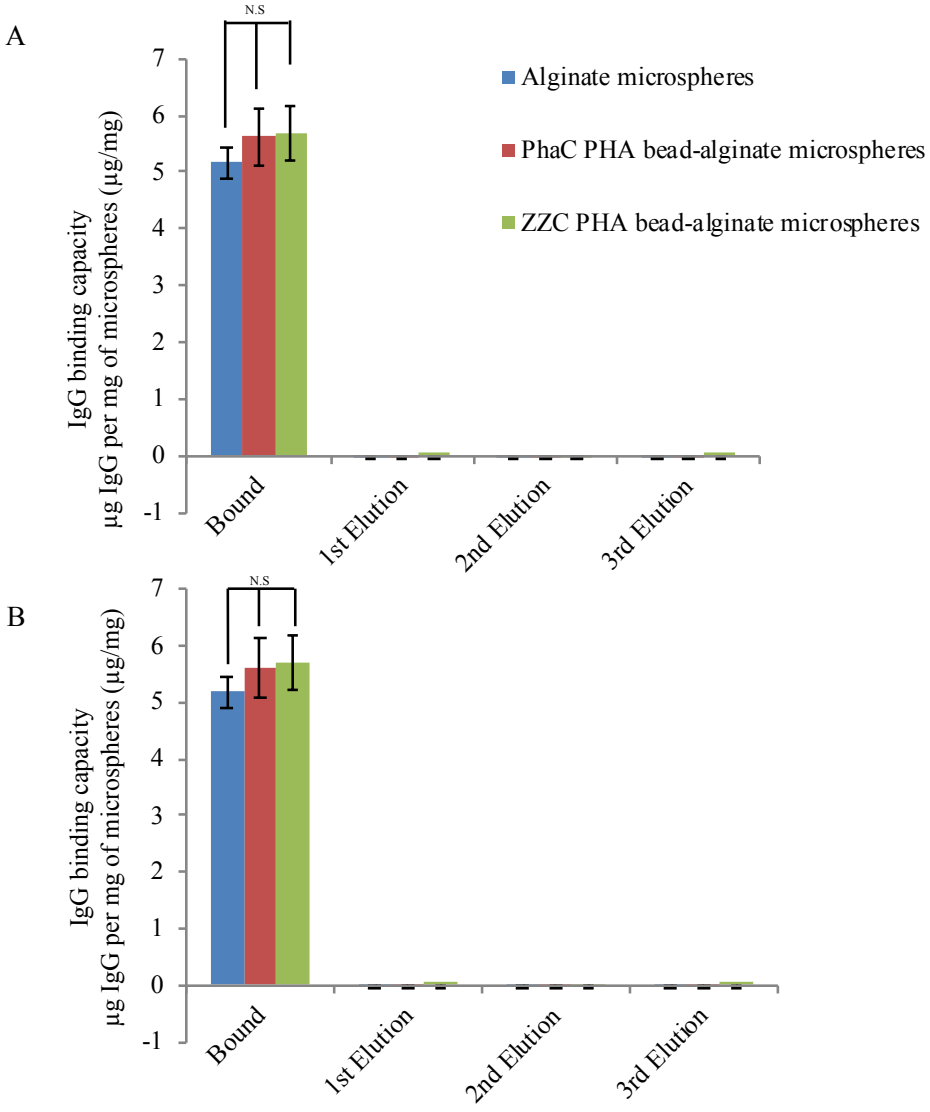

Figure 21: Comparative interaction of IgG with blank alginate and PHA bead-alginate microspheres in batch (A) and column (B) test. Microspheres were incubated in 3 mg/ml human IgG in TBS (pH7.4) for 30 minutes at 25°C with orbital rotational agitation. Elution was done three times and for 5 minutes each with 100mM Glycine (pH2.5). The test was done in triplicate and mean ± standard deviation is reported. N.S indicates no significant difference.

To confirm IgG had bound to the alginate microspheres in these tests, protein profiling of the alginate microspheres by SDS-PAGE after binding and elution phase was conducted (Section 2.14.1). Similar to the previous confirmation, the alginate microspheres were

washed until the residual IgG concentration in the supernatant in batch and flow through liquid from the column was reduced to negligible levels (1% of initial concentration) by Bradford assay (Section 2.14.2.2). After the confirmation, the microspheres were solubilised using the solubilising buffer, and SDS-PAGE was used to analyse the protein profile of the solubilised alginate gel matrix solutions and the extracted PHA bead suspensions (Figure 22).

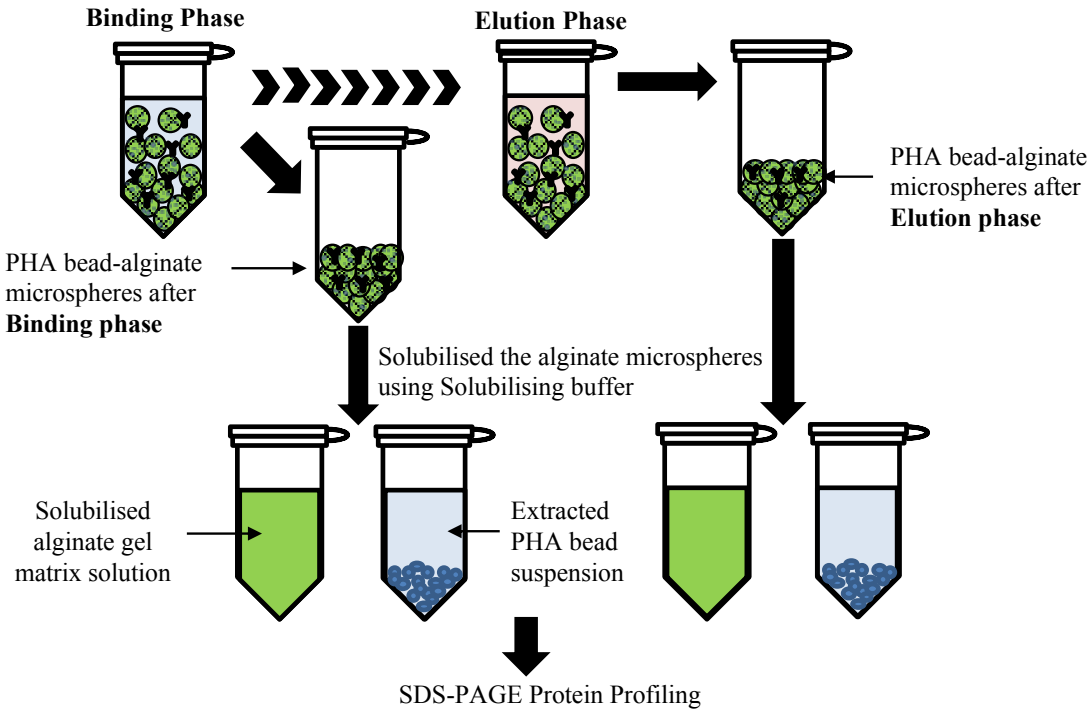

Figure 22: Schematic procedure of sampling of solubilised alginate microspheres and analysis for protein profiling.

After the binding phase, the blank alginate microspheres (negative control) showed the presence of IgG in the solution of solubilised alginate gel matrix (Figure 23, lane 4). The solubilised alginate gel matrix solutions of PHA bead-alginate microspheres also showed the presence of IgG (Figure 23, lane 5 for PhaC and lane 7 for ZZC) after the binding phase. The protein profile of the extracted PHA beads from the alginate microspheres showed that IgG was bound to the PhaC and ZZC proteins displayed on the surface of PHA beads (Figure 23 lanes 6 and 8, respectively), indicating IgG was capable of binding to the PhaC derived proteins of the encapsulated PHA beads in alginate microspheres. Similarly, IgG was observed in the alginate microspheres after the elution phase as shown on the SDS-PAGE gel after the elution phase (Figure 23, lanes 9-13). The presence of two protein bands of heavy and light chain of IgG indicated IgG was not eluted after the triplicate elution by 100 mM glycine (pH2.5).

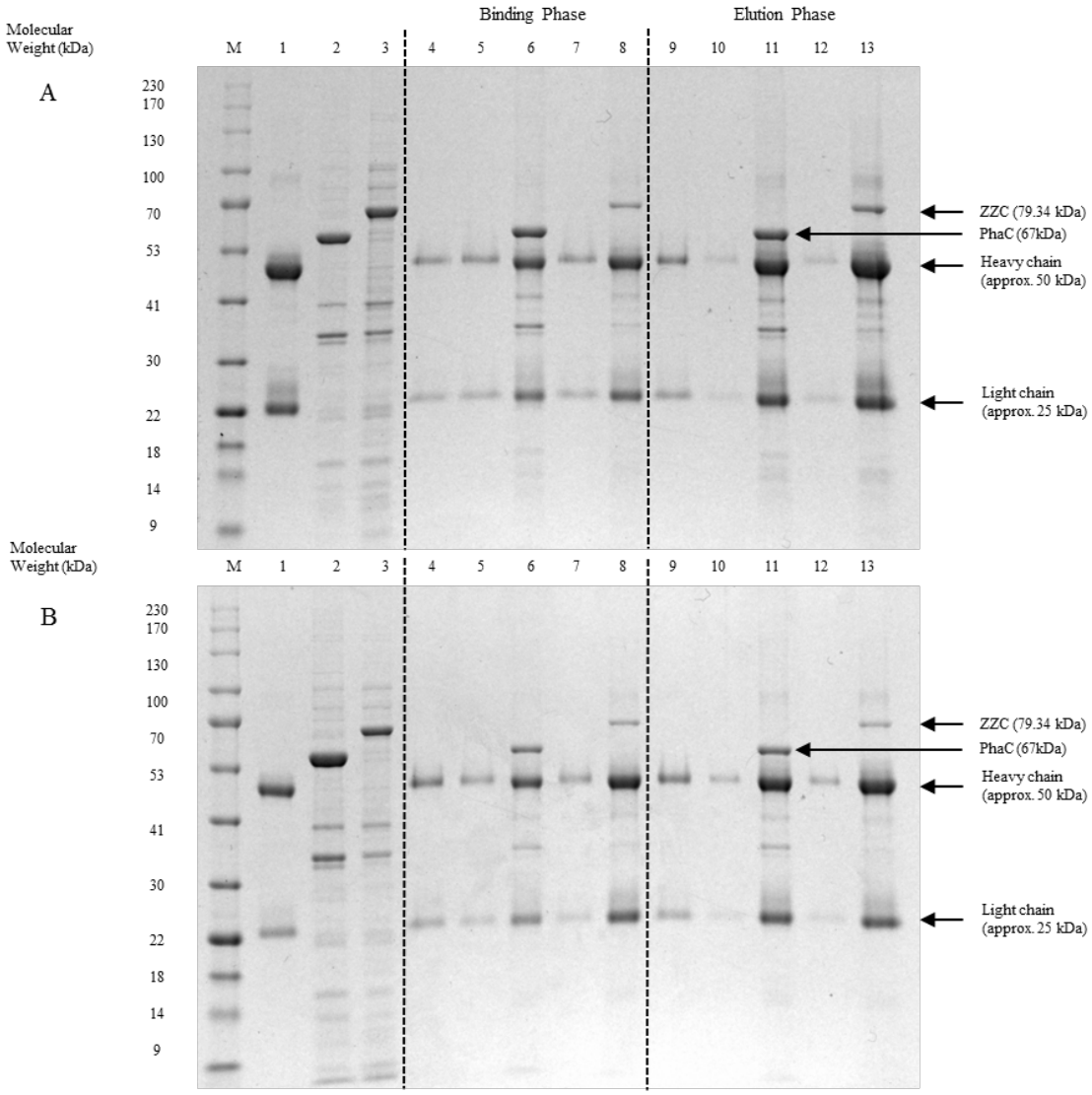

Figure 23: Protein profile of IgG bound to blank alginate and PHA bead-alginate microspheres in batch (A) and column (B) test. Blank alginate microspheres and PHA bead-alginate microspheres were incubated with 3 mg/ml human IgG in TBS, pH7.4, for 30 minutes at 25ºC. The blank alginate and PHA bead-alginate microspheres pellets were solubilised using a solubilising buffer (50 mM Tris-Cl, 150 mM NaCl, and 50 mM EDTA, pH7.4). Solubilised alginate gel matrix solutions and extracted PHA beads suspensions after binding and elution phase were analysed for the protein profile by SDS-PAGE. Lane M, molecular weight ladder (GangNam-STAIN prestained protein ladder); lane 1, IgG; lane 2, PhaC PHA beads; lane3, ZZC PHA beads; lanes 4-8 solubilised alginate gel matrix solutions and extracted PHA beads suspension (Binding Phase); lane 4, blank alginate microspheres; lane 5 alginate gel matrix solution of PhaC PHA bead-alginate microspheres; lane 6, extracted PhaC PHA beads with bound IgG; lane 7, alginate gel matrix solution of ZZC PHA bead-alginate microspheres; lane 8, extracted ZZC PHA beads with bound IgG; lane 9-13, solubilised alginate gel matrix solution and extracted PHA beads suspension (Elution Phase); lane 9, blank alginate microspheres; lane 10, algiante gel matrix solution of PhaC PHA bead-alginate microspheres; lane 11, extracted PhaC PHA beads with bound IgG; lane 12, alginate gel matrix solution of ZZC PHA bead-alginate microspheres; lane 13, extracted ZZC PHA beads with bound IgG.

The IgG binding capacity assay showed no significant differences between the types of alginate microspheres in both batch and column test conditions (Figure 21). Therefore, the effect of alginate encapsulation on the IgG binding performance of PhaC derived proteins (PhaC or ZZC) on PHA beads was determined by comparison of the amout of IgG bound to the PhaC derived proteins on free PHA beads and extracted PHA beads. Densitometry on the SDS-PAGE gel was used to quantify the amount of IgG bound to the PhaC derived proteins on the PHA beads (Section 2.14.2.1). The standard curve using BSA (50-500ng) and IgG (250-2,500 ng) produced an excellent correlation coefficient that allowed the quantification of proteins on the gel (Figure 43, Appendix III).

After incubation with the IgG solution (Binding phase), the encapsulated PHA beads in alginate microspheres were extracted and analysed for the amount of bound IgG on the PhaC derived proteins on PHA beads by SDS-PAGE densitometry (Section 2.14.2.1). The bound IgG on the PhaC derived proteins on PHA beads was shown to increase significantly in all the type of PHA bead-alginate microspheres in both batch and column test conditions when compared with the free PHA beads (Figure 24). The amount of IgG bound on PhaC protein on PhaC PHA bead-alginate microspheres was significantly higher than free PhaC PHA beads in batch and column test, increasing by 4.09 fold and 4.78 fold, respectively. The ZZC PHA bead-alginate microspheres also showed an increase in the amount of IgG bound to ZZC protein compared with the free ZZC PHA beads by 2.35 fold and 2.16 fold, in the batch and column tests respectively. Since ZZC PHA beads have IgG binding domains (ZZ), the amount of IgG bound to their PhaC derived protein was expected to be higher for ZZC PHA beads than PhaC PHA beads; it was 3.97 fold higher in the batch test and 3.11 fold higher in the column test. The comparison of the amount of IgG bound on the same type of PhaC derived proteins on PHA beads in alginate microspheres showed similar value ($p>0.05$) between batch and column test conditions.

After elution in 100 mM glycine (pH 2.5) three times, the encapsulated PHA beads in alginate microspheres were extracted and analysed by SDS-PAGE gel densitometry as previously conducted (Figure 22, Section 2.14.2.1). The amount of bound IgG on the free ZZC PHA beads showed a significant reduction ($p<0.05$) after the elution phase, indicating the bound IgG was eluted (Figure 24; ZZC). However, all the types of PHA bead-alginate microspheres resulted in significantly increased ($p<0.05$) in the amounts of bound IgG on the PhaC derived protein on PHA beads after the elution phase (Figure 24).

The amount of bound IgG in batch and column test conditions increased by 1.57 and 1.75 fold, respectively for the PhaC PHA bead-alginate microspheres, and by 1.25 and 1.43 fold, respectively for the ZZC PHA bead-alginate microspheres. There were no significant differences in the amount of bound IgG on the PhaC derived protein on PHA beads in alginate microspheres between the batch and column test after the elution phase ($p>0.05$).

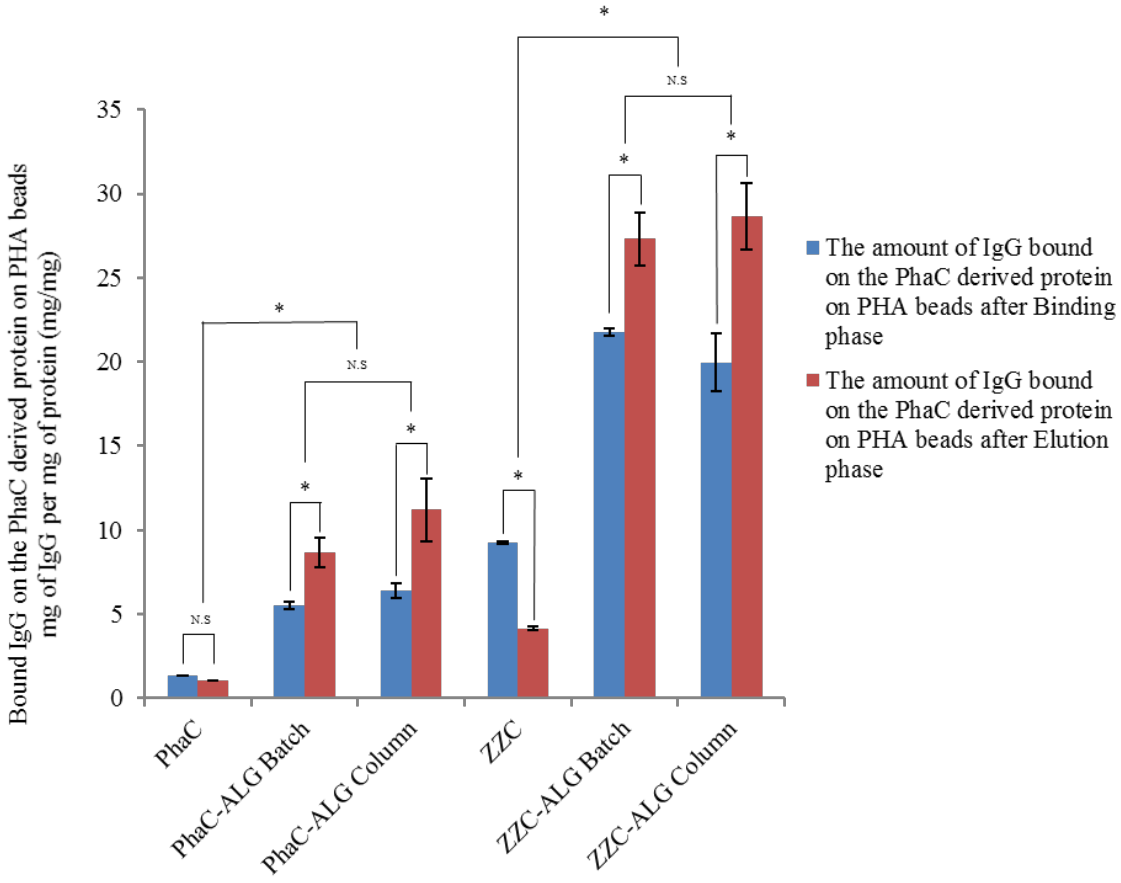

Figure 24: Comparative analysis of the amount of IgG bound to the PhaC derived proteins on free PHA beads and PHA bead-alginate microspheres in batch and column test. The IgG binding capacity was obtained by SDS-PAGE gel densitometry. PhaC and ZZC refer to PHA bead type, and PhaC-ALG and ZZC-ALG refer to their respective PHA beads encapsulated in alginate microspheres. The blue bar represents mg of IgG bound per mg of PhaC derived protein after incubation in 3 mg/ml in TBS (pH7.4) for 30 minutes at 25°C. The red bar represents mg of IgG bound per mg of PhaC derived protein after elution by 100 mM Glycine (pH2.5) for 5 minutes with agitation at 25°C. The elution results of PHA beads and PHA beads encapsulated in alginate microspheres were obtained after single and triple elution procedures, respectively. The test was done in triplicate and mean ± standard deviation is reported. * indicates a statistically significant difference ($p<0.05$). N.S indicates no significant difference.

3.2 PHA beads displaying OpdA encapsulated in alginate microspheres

3.2.1 PHA beads displaying OpdA

3.2.1.1 *In vivo* Production of PHA beads: PHA beads displaying OpdA

To produce alginate microspheres encapsulating PHA beads displaying an enzyme, the following previously constructed plasmids were selected: pPolyC (Hay *et al.*, 2017) and pET-14b PhaC-linker-OpdA (Blatchford *et al.*, 2012). pPolyC plasmid encodes PhaC with a linker fused to the C-terminus of PhaC, and pET-14b PhaC-linker-OpdA encodes OpdA fused to the C-terminus of PhaC via a linker. The pET14b expression vector was used as the negative control for the PHA beads production *in vivo*. The plasmids were confirmed by DNA sequencing (Section 2.10.3) and used to transform the production strain of BL21 (DE3) *E.coli* cells harbouring pMCS69 (Section 2.11). After the selection on LB agar containing ampicillin and chloramphenicol (Section 2.11), the transformants were cultivated under PHA bead accumulating conditions to produce PHA beads *in vivo* (Section 2.6.1).

As the routine for confirming PHA bead accumulation in the production *E. coli* strain, cells were stained with Nile red (Section 2.13.1.1) and visualised using fluorescence microscopy (Section 2.13.1.2). The fluorescence indicated the production of PHA beads *in vivo* and hence the activity of PHA synthase (Figure 25). Further confirmation was provided by TEM analysis (Section 2.13.2). In comparison to the PHA bead production negative control (pET14b), PHA beads were observed in the cytoplasm of *E. coli* cells transformed with pPolyC and pET-14b PhaC-linker-OpdA (Figure 26).

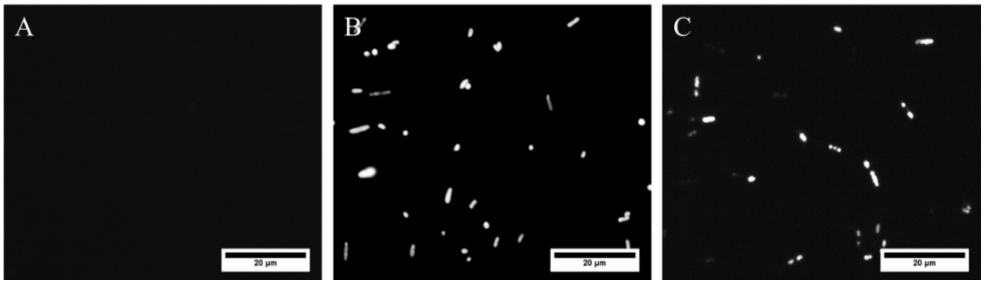

Figure 25: Fluorescence microscopy images of PHA beads produced in recombinant *E.coli* cells. A: BL21 (DE3) *E.coli*+pMCS69 (BL21_69) harbouring pET14b (negative control); B: BL21_69+pPolyC; C: BL21_69+pET-14b PhaC-OpdA.

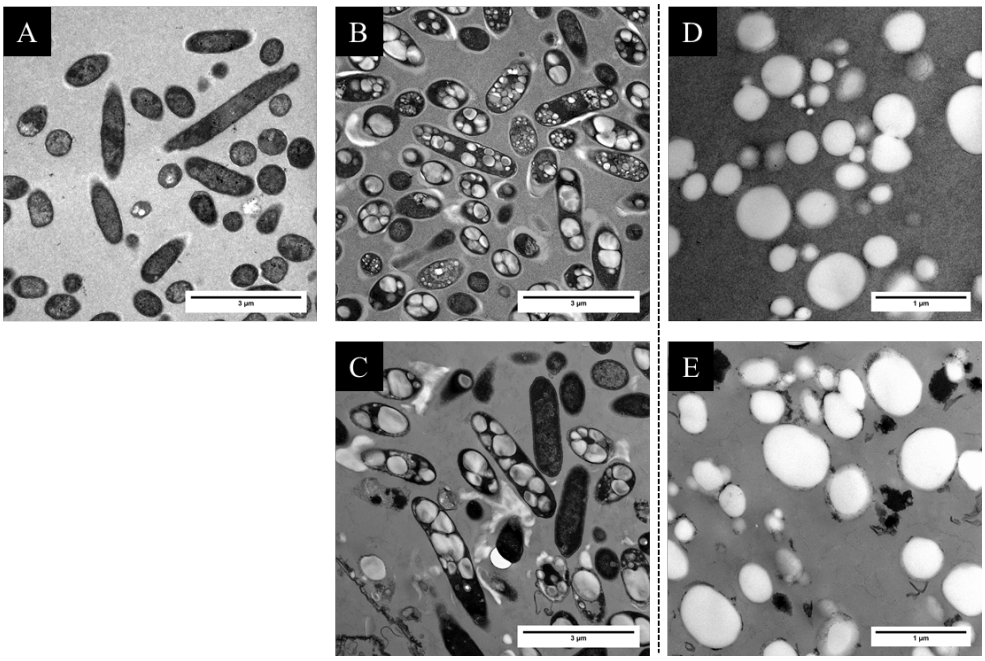

Figure 26: TEM analysis images of recombinant *E.coli* cells accumulating PHA beads, and isolated and purified PHA beads. A: BL21 (DE3) *E.coli*+pMCS69 (BL21_69) harbouring pET14b (negative control); B: BL21_69+pPolyC; C: BL21_69+pET-14b PhaC-OpdA; D: PhaC PHA beads; E: PhaC-OpdA PHA beads.

3.2.1.2 Characterisation of PHA beads displaying OpdA

PHA beads were isolated from *E. coli* cells by mechanical cell disruption (Section 2.12.2) and their characteristics were assessed. The morphology of the isolated PHA beads was observed by TEM and SEM analyses (Section 2.13.2). The TEM images showed the PHA beads were separate from the bacterial cells, indicating successful isolation from the *E.coli* cells (Figure 26). Further observation by SEM showed that the isolated PHA beads were spherical or slightly irregular shaped spheres (Figure 27).

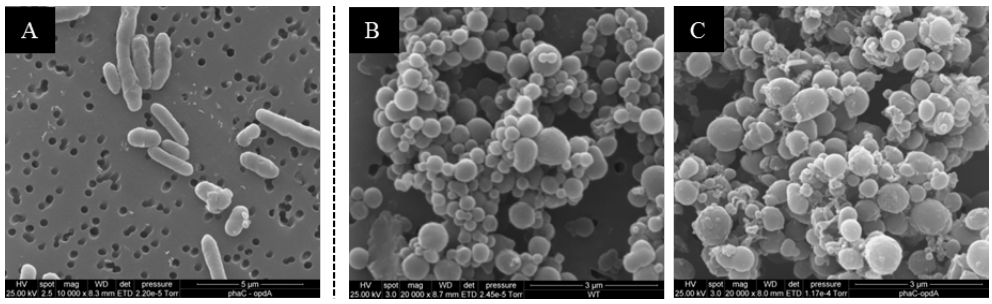

Figure 27: SEM analysis images of recombinant *E.coli* cells accumulating PHA beads, and isolated and purified PHA beads. A: BL21 (DE3) *E.coli*+pMCS69 harbouring pET-14b phaC-OpdA; B: PhaC PHA beads (WT); C: PhaC-OpdA PHA beads (phaC-opdA).

The particle size distribution of PHA beads in the stock suspension was analysed by laser diffraction (Section 2.13.3). Particle size distribution of PhaC and PhaC-OpdA PHA beads showed a maxima at 4.89 µm and 13.56 µm, respectively (Figure 28). The median particle size (D50) was 6.92 and 13.2 µm, respectively (Table 11, Appendix I). PhaC PHA beads demonstrated a broader distribution than PhaC-OpdA PHA beads, as shown by the higher SPAN factor value, however, these beads have approximately 1.8 times higher specific surface area than PhaC-OpdA PHA beads (as the majority of the beads were smaller). According to the TEM and SEM images (Figure 26 and Figure 27), the particle size could be estimated to be smaller than 1 µm. Therefore, the particle size distribution result demonstrated that these PHA beads were most likely aggregated in the stock suspension.

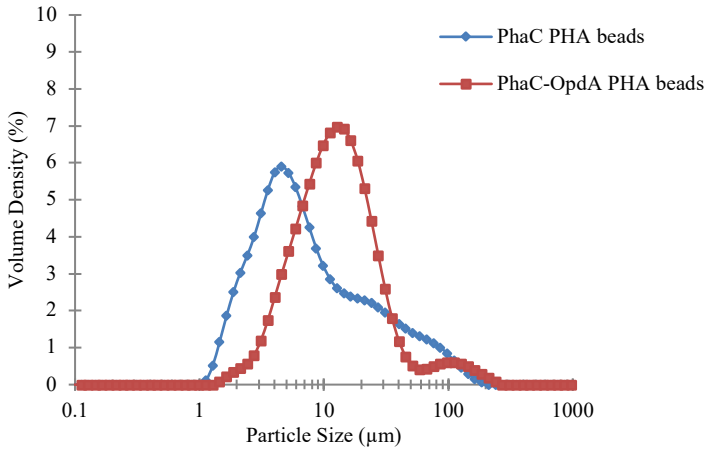

Figure 28: Particle size distribution of PhaC and PhaC-OpdA PHA beads in water.

The protein profile of fusion protein displayed on PHA beads was analysed by SDS-PAGE (Section 2.14.1.1) and the amount of the protein on the bead was quantified by densitometry on SDS-PAGE gel using BSA as the standard (Section 2.14.2.1). The protein profile of the whole cell lysate on the SDS-PAGE gel showed dominant protein bands in *E. coli* cells transformed with pPolyC and pET-14b PhaC-linker-OpdA. The protein bands corresponded to the theoretical molecular weight of 67 kDa for PhaC protein and 104 kDa for PhaC-OpdA protein (Figure 29). Therefore, the fusion protein was overproduced in these transformants. The purity of fusion protein in the isolated PHA bead suspensions (stock suspension) was analysed by densitometry (Section 2.14.1.1.4)

and showed that the PhaC derived protein accounted for 40.4% of the total protein in PhaC PHA bead fraction and 46.0% for PhaC-OpdA PHA bead fraction. The quantity of fusion protein on the PHA bead was 5.61±0.02 mg/g for PhaC PHA beads and 14.2±0.4 mg/g for PhaC-OpdA PHA beads based on wet weight (Table 11, Appendix I).

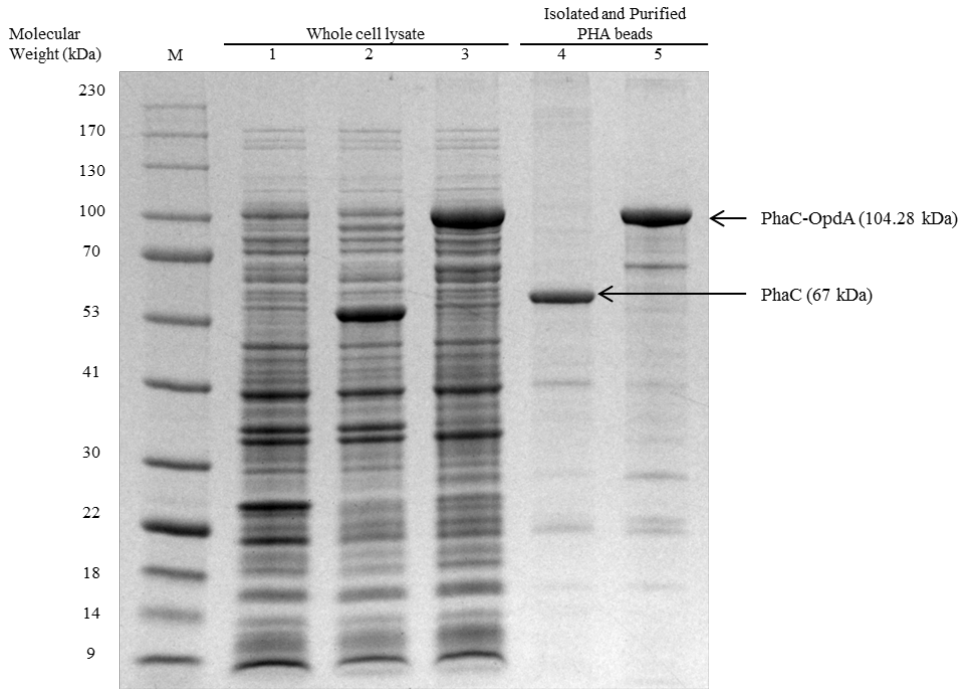

Figure 29: SDS-PAGE protein profile analysis of whole cell proteins from *E.coli* cells accumulating PHA beads, and isolated and purified PHA beads. Lane M, molecular weight ladder (GangNam-STAIN prestained protein ladder); lane 1, BL21 (DE3) *E.coli* strain+pMCS69 (BL21_69) harbouring pET14b (negative control); lane 2, BL21_69+pPolyC; lane 3, BL21_69+pET-14b PhaC-OpdA; lane 4, PhaC PHA beads; lane5, PhaC-OpdA PHA beads.

3.2.2 PHA beads displaying OpdA in encapsulated alginate microspheres

3.2.2.1 Characterisation of the microspheres

The PHA beads encapsulated in alginate microspheres (PHA bead-alginate microspheres) were prepared by a water-in-oil (w/o) emulsion with internal gelation (Section 2.16.2). The morphology of the alginate microspheres was assessed by phase contrast microscopy (Section 2.17.1.1). The PHA bead-alginate microspheres were observed as small particulates in the alginate microspheres while blank alginate microspheres were clear and transparent (Figure 30). The presence of PHA beads in the alginate microspheres was

confirmed by staining the microspheres with Nile red (Section 2.13.1.1) and visualised using phase contrast and fluorescence microscopy (Section 2.17.1.1). The fluorescence indicated the presence of PHA beads, and the position of the fluorescence corresponded to the position of alginate microspheres in the phase contrast images in both PhaC PHA beads (Figure 30B and D) and PhaC-OpdA PHA bead-alginate microspheres (Figure 30C and E). Therefore, PHA beads were successfully encapsulated in alginate microspheres by the w/o emulsion with internal gelation. In addition, the microspheres were well dispersed and spherical, and no aggregation of the spheres was observed. Additional morphological analysis by SEM demonstrated that the blank alginate microspheres were spherical in shape, however, the surface texture was different. The negative control (blank alginate microspheres) had a smooth surface while PHA bead-alginate microspheres had a rough surface (Figure 31).

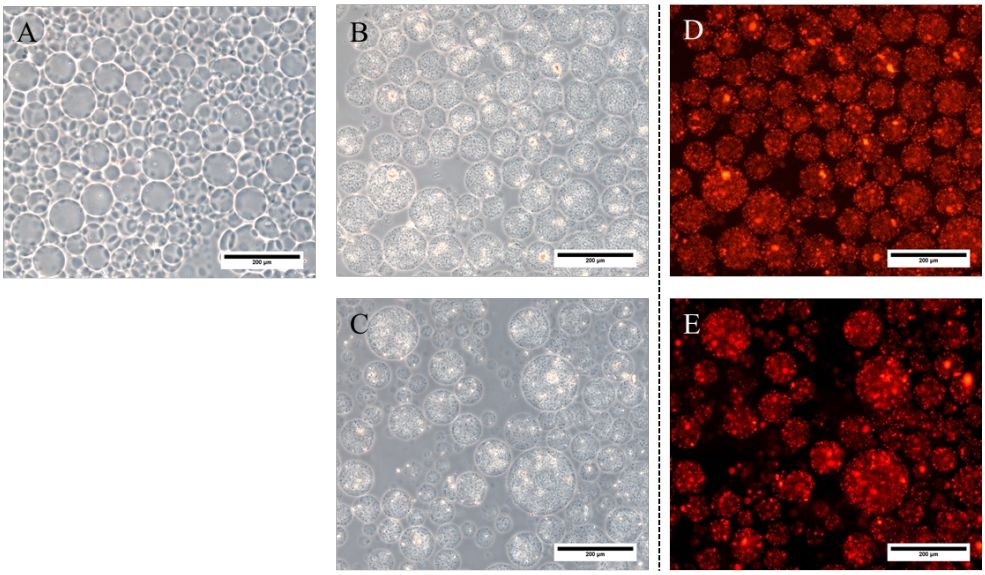

Figure 30: Microscopic images of alginate microspheres encapsulating PHA beads prepared with internal gelation. A-C: Phase contrast microscopic images; A: blank alginate microspheres; B: PhaC-alginate microspheres; C: PhaC-OpdA-alginate microspheres. D and E: fluorescence microscopic images of corresponded alginate microspheres encapsulating PHA beads; D: PhaC-alginate microspheres; E: PhaC-OpdA-alginate microspheres.

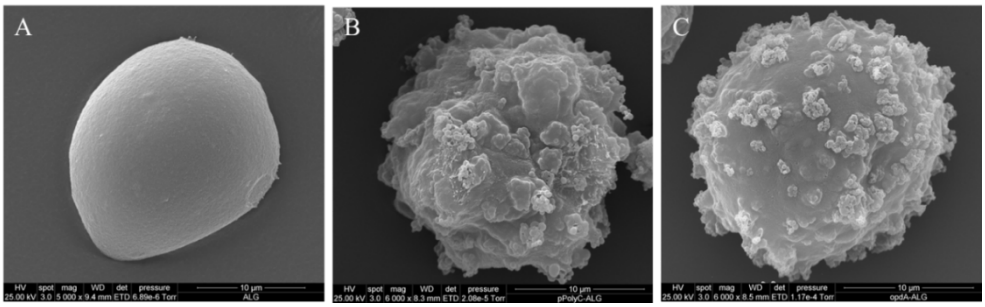

Figure 31: SEM analysis images of lyophilised blank alginate microspheres and PHA bead-alginate microspheres prepared with internal gelation. A, blank alginate microspheres; B, PhaC-alginate microspheres; C, PhaC-OpdA-alginate microspheres

The particle size distribution of the alginate microspheres in the stock solution was measured by laser diffraction (Section 2.17.1.3.1). The volume density graph showed that the peak of the blank alginate microspheres was 86.4 µm, PhaC PHA bead-alginate microspheres was 144 µm, and PhaC-OpdA PHA bead-alginate microspheres was 163 µm (Figure 32). These values were close to the median size of the particle size distribution (Table 13, Appendix II). The distribution of the microspheres was narrower for the blank alginate microspheres than alginate microspheres encapsulating PHA beads, indicating the blank alginate microspheres were prepared in a more uniform fashion than PHA bead-alginate microspheres.

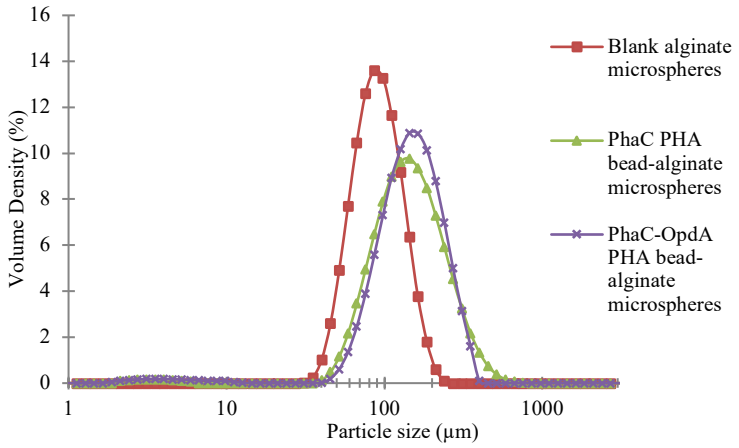

Figure 32: Particle size distribution analysis of blank alginate microspheres and PHA bead-alginate microspheres in water.

The encapsulation efficiency of PHA beads in alginate microspheres was determined using the combination of PHA beads extraction from alginate microspheres by solubilising the microspheres, the total protein quantification by the BCA assay, and the protein profiling of PhaC derived protein in the suspension by SDS-PAGE (Section 2.17.1.4). The encapsulation efficiency of PHA beads in alginate microspheres is summarised in Table 6. The encapsulation efficiency of PhaC and PhaC-OpdA PHA beads was 88.2±0.04% and 88.5±2.0%, respectively, after the w/o emulsion with internal gelation preparation. Interestingly, the proportion of PhaC derived protein (PhaC or PhaC-OpdA) on PHA beads was increased by 4.6% for PhaC PHA beads and 8.5% for PhaC-OpdA PHA beads in the bead fraction after extraction from microspheres.

Table 6: The encapsulation efficiency of PhaC and PhaC-OpdA PHA beads in alginate microspheres.

PHA bead types	Initial PhaC derived protein proportion (%)*	Final PhaC derived protein proportion (%)*	Encapsulation Efficiency (%)
PhaC	40.4	45.0	88.2±0.04
PhaC-OpdA	46.0	54.5	88.5±2.0

Note: * Protein proportion obtained from densitometry on SDS-PAGE gel

3.2.2.2 Functional assessment: Enzyme activity

The enzymatic activity of PHA beads displaying OdpA in the free and the encapsulated state was monitored by the increase in fluorescence intensity created by the liberation of the product by the enzyme activity (Section 2.17.2.2). Figure 33 shows the transition of fluorescence intensity over 4 hours. The enzyme negative controls, including free PhaC PHA beads, blank alginate microspheres, and PhaC PHA bead-alginate microspheres, showed no change in the level of fluorescence intensity throughout 4 hours monitoring. The enzyme positive control, the free PhaC-OpdA PHA beads, showed a gradual increase in the fluorescence intensity as soon as the PHA beads were added into the solution containing the substrate. It was observed that the rate of activity steadily increased from 0-2 hours, and then gradually decreased from 2 hours to the end of the measurement period. For PhaC-OpdA PHA bead-alginate microspheres, there was a significant reduction in the catalytic activity of OpdA when the PHA bead was encapsulated within alginate microspheres. The difference in fluorescence intensity level between the free and

the encapsulated state reached approximately 7.5 fold higher in the free PHA beads for approximately 1 hour then reached a maximum difference (8.19 fold) after 1.8 hours incubation. The difference gradually decreased from around 2 hours of incubation then reached 5.83 fold at the end of monitoring. The state of PHA bead-alginate microspheres in HEPES buffer (pH8.0) containing 20% v/v methanol during the monitoring process was observed by phase contrast microscopy and fluorescence microscopy (Section 2.17.1.1) over 6 hours. This showed that the structure of alginate microspheres was retained with PHA beads remaining enclosed within the alginate microspheres throughout the observation (Figure 34).

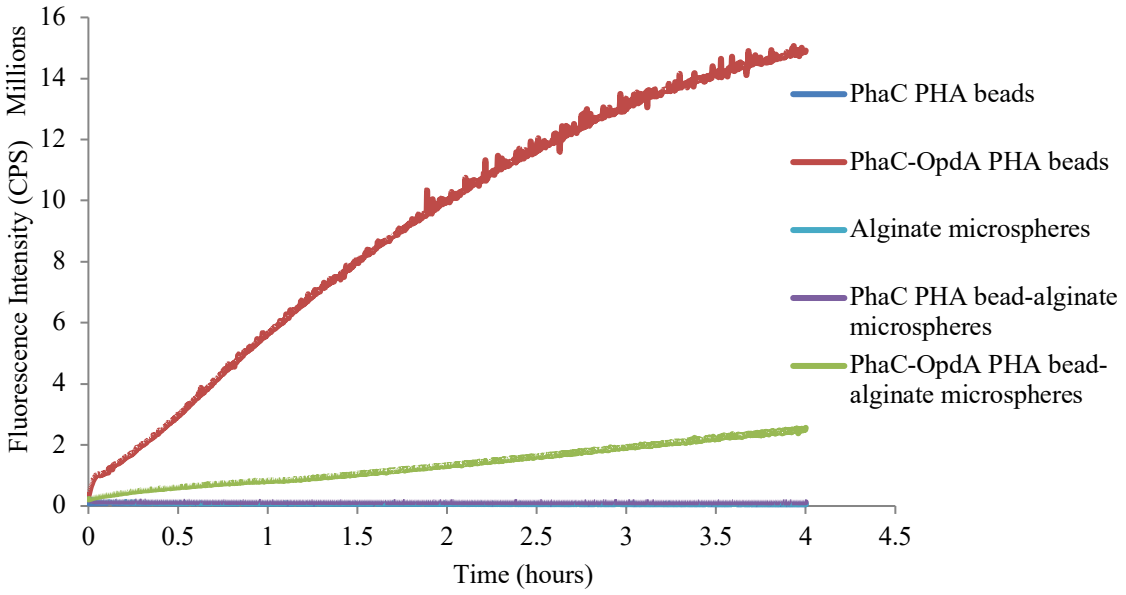

Figure 33: Enzyme kinetic curve of Coumaphos hydrolysis by free PHA beads and PHA bead-alginate microspheres. 100 µg of protein on the beads was used. Controls were PhaC PHA beads, blank alginate microspheres, and PhaC PHA bead-alginate microspheres as negative control and PhaC-OpdA PHA beads as positive control. Beads and microspheres were incubated in 50mM HEPES buffer (pH8.0) with 20% methanol containing 200µM Coumaphos. The sample was measured in a cuvette (3.5 mL) with a magnetic stirrer and monitored over 4 hours.

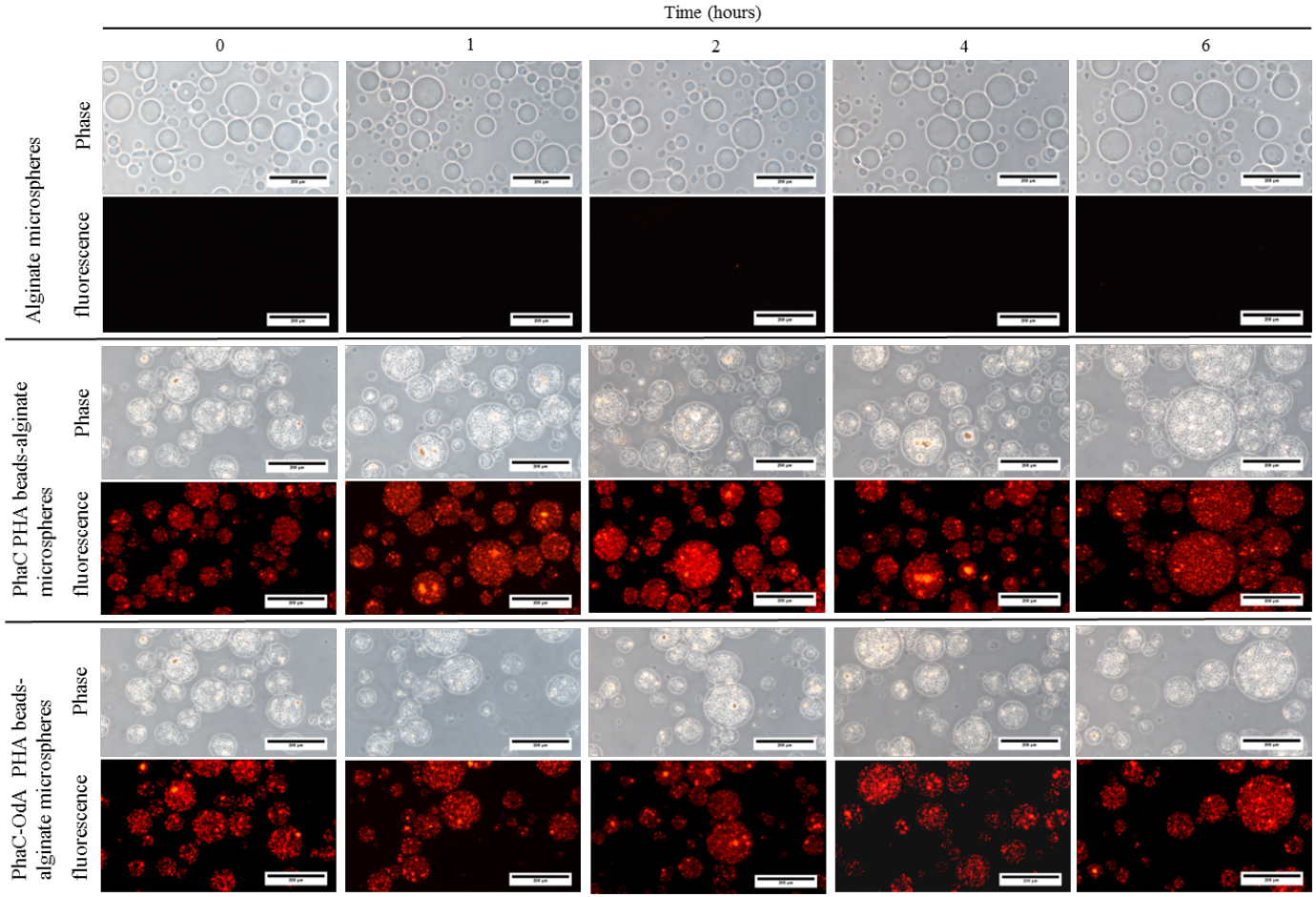

Figure 34: Phase contrast and fluorescence microscopy images of alginate microspheres in the testing condition over 6 hours. The microspheres were stained with Nile red. The testing condition was 50 mM HEPES buffer (pH 8.0) with 20% v/v methanol at 25ºC with stirring by a magnetic stirrer at 300 rpm. The black bar represents 200 µm.

3.3 PHA beads encapsulated in alginate millispheres for removal of a lipophilic substance removal from aqueous solution

3.3.1 PHA beads encapsulated in alginate millispheres

3.3.1.1 Characterisation of the millispheres

To produce PHA beads encapsulated in alginate millispheres (namely, PHA bead-alginate millispheres) for Nile red adsorption, a simple extrusion dropping method with external gelation was employed (Section 2.16.4). The method used $CaCl_2$ as the cross-linking solution. Alginate millispheres are shown in Figure 35. The blank alginate millispheres were pale grey and transparent whereas PHA bead-alginate millispheres were white and opaque. Further image analysis by SEM (Figure 36) showed that lyophilised PHA bead-alginate millispheres had a rough surface. The higher magnification image of the transection of a millisphere showed that the inner structure of the alginate matrix was rough, and tunnel-like structures could be observed. In the tunnel-like structures, PHA beads encapsulated in the alginate matrix can be seen, indicating successful immobilisation of the PHA beads in alginate millispheres. The millispheres were characterised by the diameter, wet weight, and PHA bead content. The characteristics of the millispheres are summarised in Table 7. The blank alginate millispheres were slightly smaller than PHA bead-alginate millispheres throughout all the parameters. The calcium concentration in the preparation influenced the particle size with increased particle size associated with lower concentration of calcium ion in the cross-linking solution. The alginate concentration also influenced the particle size as a lower concentration of alginate produced smaller millispheres. Meanwhile, the particle size showed no significant differences with the amount of PHA beads used in the preparation. The PHA bead amount per gram of alginate millispheres was measured by quantifying the amount of fusion protein on the PHA beads (Section 2.17.1.4). The PHA bead-alginate millispheres prepared with different concentrations of calcium ion (25-100 mM) showed a slight difference in the amount of PHA bead encapsulated however there was no significant difference among them. The concentration of PHA bead used in the preparation (0.5-1.5 %w/v PHA beads) directly correlated with the PHA bead amount per the weight of millispheres. The PHA bead-millispheres prepared with 1 %w/v alginate was a similar value to the millispheres prepared with 1.5 %w/v PHA beads due to smaller and lighter particles.

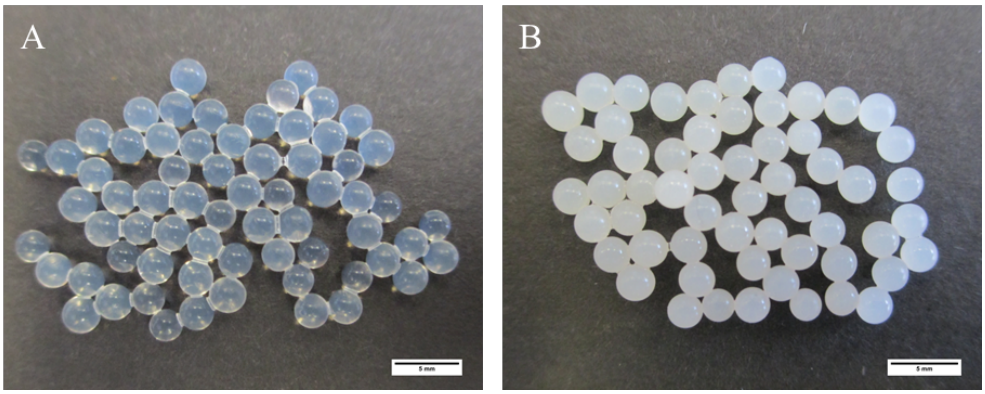

Figure 35: A representative image of blank alginate beads and PHA bead-alginate millispheres. A: Blank alginate millispheres; B: 1% w/v PHA bead-alginate millispheres. Both millispheres were formulated in 2% w/v alginate with 50mM $CaCl_2$ cross-linking solution.

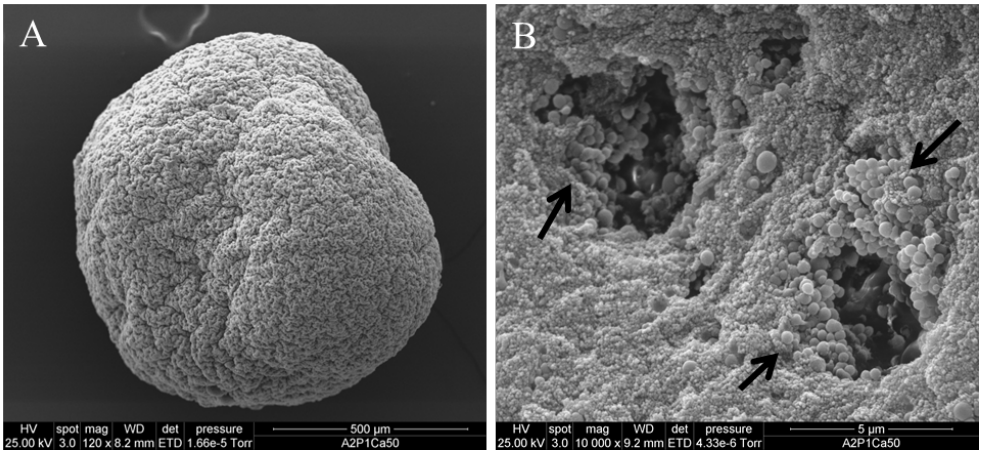

Figure 36: SEM analysis images of a lyophilised PHA bead-alginate millisphere. A: A whole view of a PHA bead-alginate millisphere (2% w/v alginate, 1% PHA beads, and 50 mM Ca^{2+}), B: High magnification image of inner structure of transection of the PHA bead-alginate millisphere. The arrow indicates the immobilised PHA beads inside the alginate matrix.

Table 7: Summary of blank alginate and PHA bead-alginate millisphere characteristics.

	Particle size in diameter±SD (mm)	Wet weight±SE (mg)	PHA beads per gram of millispheres±SD (mg per g)
Alginate millispheres			
Alginate 2%w/v; Ca^{2+} 25mM	2.7±0.1	8.2±0.1	-
Alginate 2%w/v; Ca^{2+} 50mM *	2.5±0.1	8.1±0.1	-
Alginate 2%w/v; Ca^{2+} 100mM	2.3±0.2	6.6±0.1	-
Alginate 1%w/v; Ca^{2+} 50mM	2.0±0.2	4.0±0.1	-
PHA beads encapsulated in alginate millispheres			
Alginate 2%w/v; PHA beads 1%w/v; Ca^{2+} 25mM	2.8±0.1	8.6±0.1	19.2±0.8
Alginate 2%w/v; PHA beads 1%w/v; Ca^{2+} 50mM*	2.8±0.2	8.0±0.1	17.4±0.5
Alginate 2%w/v; PHA beads 1%w/v; Ca^{2+} 100mM	2.5±0.1	6.1±0.03	18.6±0.5
Alginate 2%w/v; PHA beads 0.5%w/v; Ca^{2+} 50mM	2.7±0.2	7.5±0.02	9.1±0.9
Alginate 2%w/v; PHA beads 1.5%w/v; Ca^{2+} 50mM	2.7±0.1	7.5±0.1	27.0±1.0
Alginate 1%w/v; PHA beads 1%w/v; Ca^{2+} 50mM	2.2±0.1	4.2±0.1	27.4±1.9

Note: SD, standard deviation; SE, standard error of mean;*, the standard preparation

3.3.2 Functional assessment: Adsorption

3.3.2.1 Adsorption kinetics

To investigate the mechanism of adsorption of PHA bead-alginate millispheres, they were prepared with different parameters, and the difference in the adsorption kinetic performance among these parameters was analysed (Section 2.17.2.3.1). In this investigation, the parameters were calcium ion concentration ranging from 25-100 mM, the amount of PHA beads ranging from 0.5-1.5 % w/v, and alginate concentration ranging from 1-2 % w/v. The PHA bead-alginate millispheres prepared with 2% w/v alginate, 1% w/v PHA beads, and 50 mM calcium ion was used as the standard preparation. The interaction between Nile red and the glassware was measured at each selected sampling time in the 24 hours incubation. The Nile red concentration reduced in the first hour of incubation, however, the concentration was close to the initial concentration and stayed at a constant level during the incubation (Figure 44, Appendix IV).

The adsorption kinetics of PHA bead-alginate millispheres prepared with different concentrations of calcium ion in the cross-linking solution is shown in Figure 37. The

blank alginate millispheres prepared with 25-100 mM calcium ion showed no significant transition over the 24 hours incubation. The trend of increasing capacity to adsorb the dye was observed in all the type of PHA bead-alginate millispheres as soon as they were added to the Nile red solution. The rate of increase in adsorption capacity was higher in millispheres prepared with higher concentrations of calcium ion. The equilibrium adsorption capacity was at 3.10 ng/mg, 3.61 ng/mg (standard preparation), and 4.39 ng/mg for 25, 50, and 100 mM calcium ion, respectively, and the equilibrium point was observed after approximately 15-18 hours incubation. The adsorption kinetic of PHA bead-alginate millispheres prepared with different amounts of PHA beads is shown in Figure 38. The blank alginate beads showed no increase in adsorption capacity over the 24 hours incubation. The adsorption of Nile red was observed, and the rate of increase in adsorption capacity was higher in beads prepared using a higher amount of PHA beads. The equilibrium was observed at 2.7 ng/mg after 15 hours for 0.5%w/v PHA beads with a slight increasing trend for 1.5% w/v PHA beads after 24 hours incubation. However, this was within the standard deviation. Therefore, the beads prepared with 1.5%w/v PHA beads was assumed to reach the adsorption equilibrium at 18-24 hours incubation. The adsorption capacity was also calculated based on the amount of PHA beads used in the preparation between 0.5-1.5% w/v PHA beads instead of millisphere weight. The adsorption equilibrium point of 0.5, 1.0, and 1.5 % w/v PHA beads was 299, 207.5, and 159.3 ng/mg of PHA beads, respectively. The adsorption kinetic of PHA bead-alginate millispheres prepared with different concentrations of alginate is shown in Figure 39. The alginate concentration did not influence the adsorption capacity as shown by the negative controls. With the millispheres encapsulating PHA beads, the rate of increase was higher in millispheres prepared with the lower concentration of alginate. In addition, the adsorption equilibrium point of the millispheres prepared with 1% w/v alginate was 4.09 ng/mg after 12-15 hours incubation which was higher and faster than the standard preparation (3.61 ng/mg after 15-18 hours).

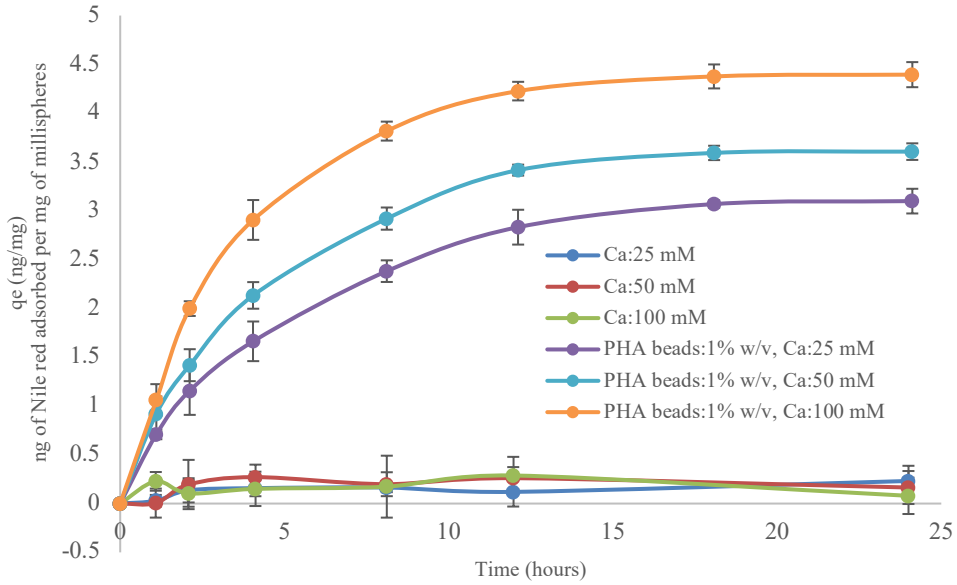

Figure 37: Equilibrium Nile red adsorbed as a function of time using different concentrations of calcium in the preparation of millispheres. The concentration of $CaCl_2$ used in the crosslinking solution: 25mM, 50mM or 100mM; Alginate: 2.0% w/v; PHA beads: 0%, as negative control and 1.0% w/v; initial concentration of Nile red solution containing 10% v/v DMSO: 70 ng/ml; incubation; 25°C with 100rpm shaking for 24 hours. The measurement was done in triplicate and mean ± standard deviation is reported.

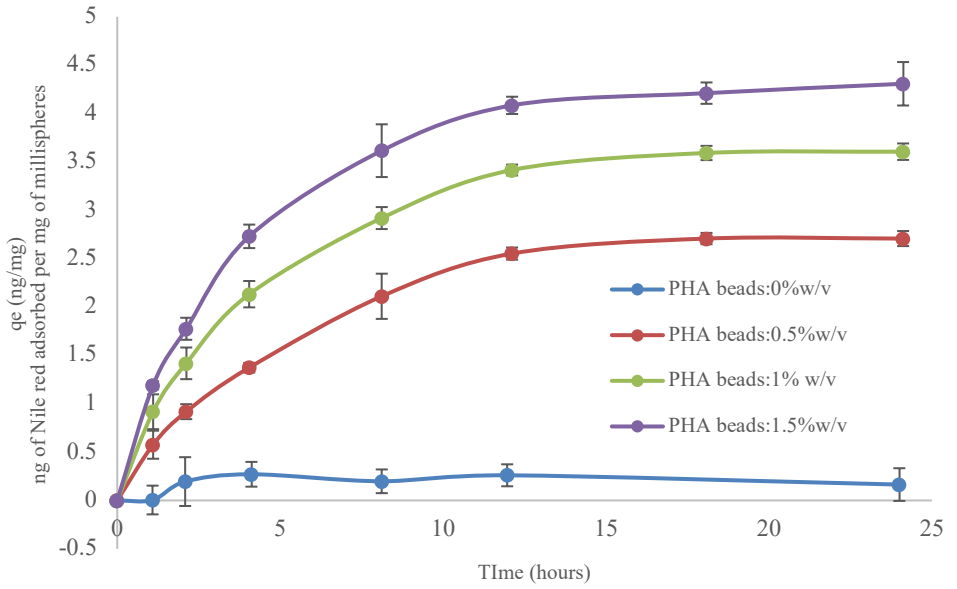

Figure 38: Equilibrium Nile red adsorbed as a function of time using different amount of PHA beads in the preparation of millispheres. The amount of PHA beads used: 0.5, 1.0 or 1.5% w/v; Alginate: 2.0% w/v; $CaCl_2$ concentration: 50 mM; initial concentration of Nile red solution containing 10% v/v DMSO: 70 $ngml^{-1}$; incubation: 25°C with 100rpm shaking for 24 hours. The measurement was done in triplicate and mean ± standard deviation is reported.

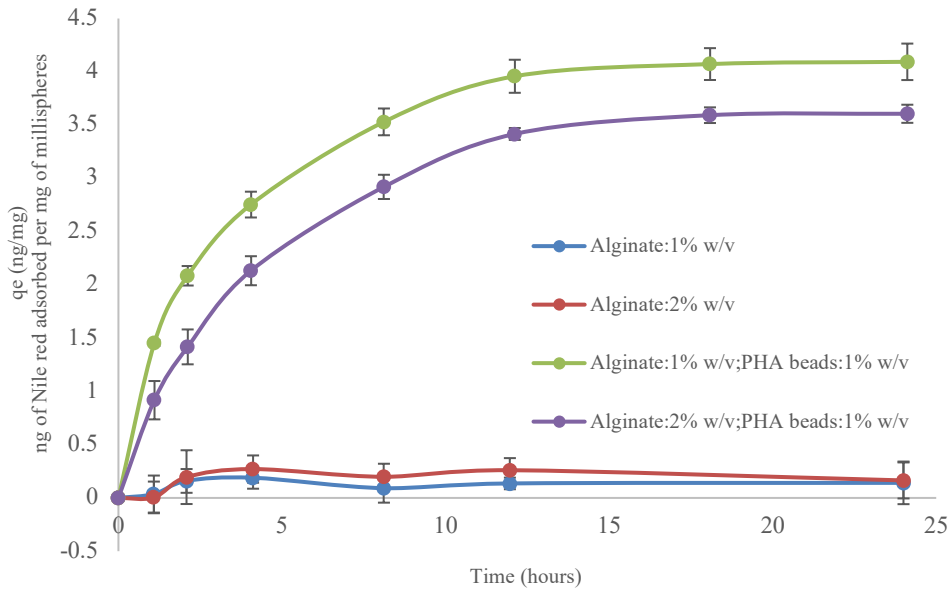

Figure 39: Equilibrium Nile red adsorbed as a function of time using different concentrations of alginate in the preparation of millispheres. Alginate concentration: 1.0 or 2.0%w/v; CaCl2 concentration: 50mM ; PHA beads: 0%, as negative control and 1.0% w/v; initial concentration of Nile red solution containing 10% v/v DMSO: 70ngml^{-1}; incubation: 25°C with 100rpm shaking for 24 hours. The measurement was done in triplicate and mean ± standard deviation is reported.

The process of Nile red removal from the aqueous solution was analysed by pseudo-first order and pseudo-second order kinetic models. The pseudo-first order model of Lagergren is expressed as:

$$log(q_e - q_t) = logq_e - \frac{k_1}{2.303}t$$

where q_e and q_t are the amount of Nile red adsorbed to the alginate bead at equilibrium and at time (t), respectively (ng/mg). k_1 is the rate of constant of first-order adsorption (h^{-1}). A straight line was plotted by log (q_e-q_t) versus t to determine the rate constant (k_1) and the correlation coefficient (R^2). The plotted straight line from the pseudo-first order kinetic model is shown in Figure 40.

The pseudo-second order kinetic model is expressed as:

$$\frac{t}{q_t} = \frac{1}{k_2 q_e{}^2} + \frac{1}{q_e}t$$

where k_2 is the rate constant of second order adsorption (ng/mgml), q_e and q_t are the maximum adsorption capacity and at time (t), respectively. A straight line was plotted by

t/q_t versus t to determine the rate constant (k_2) and correlation coefficient (R^2). The plotted line of the pseudo-second order kinetic model is shown in Figure 40. From the value obtained, the initial sorption rate (V_0, ng/mgh) was calculated by the following equation:

$$V_0 = k_2 q_e^2$$

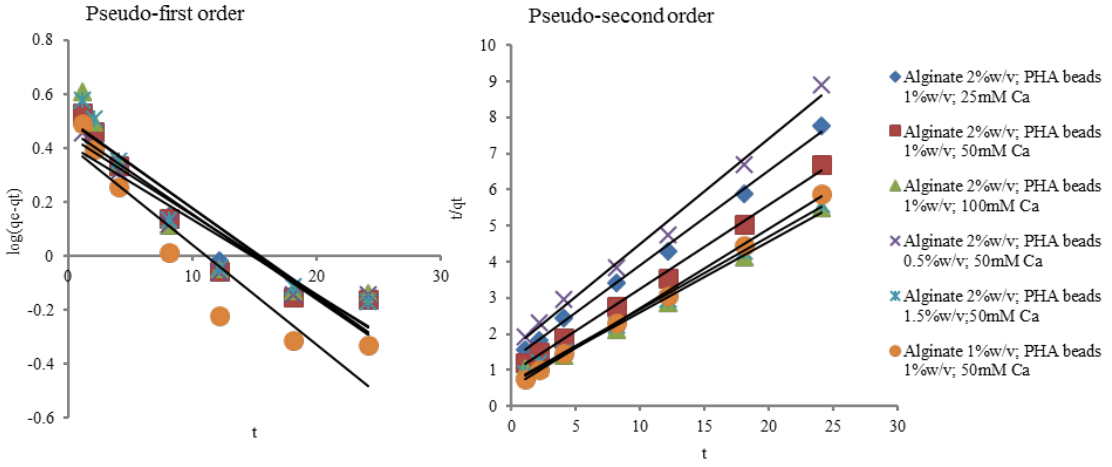

Figure 40: Adsorption kinetic data for PHA bead-alginate millispheres fitted to linear form of pseudo-first order and pseudo-second order kinetic models.

The summary of the calculated experimental data by pseudo-first and pseudo-second order kinetic models is summarised in Table 8. The calculations were also applied to the blank alginate millispheres. The results showed that the data did not match the pseudo-first order kinetic model, and poor correlation coefficient values in all the parameters in both order kinetic models, indicating the millispheres did not function for adsorbing Nile red. For the PHA bead-alginate millispheres, the values of adsorption capacity (q_e) calculated by the pseudo-first order was less than the values observed in experimental data by 0.1-1.5 ng/mg while more in the pseudo-second order by 0.5-0.7 ng/mg. The correlation coefficient (R^2) for the pseudo-first order was between 0.849-0.917 and was 0.992-0.999 for the pseudo-second order. The results of the pseudo-second order kinetic model clearly fitted the experimental data plotted in the adsorption kinetic tests. These results suggested that the adsorption system obeys the pseudo-second order kinetic model. As shown in the initial sorption rate (V_0) values obtained by the pseudo-second order kinetic model, the rate of adsorption was faster for higher concentrations of calcium ions,

more PHA beads, and lower concentrations of alginate used in the preparation of millispheres.

Table 8: Summary of pseudo-first and pseudo-second order kinetic model of blank alginate and PHA encapsulated in alginate millispheres.

	Pseudo-first order			Pseudo-second order			
	k_1 (h^{-1})	q_e (ng/mg)	R^2	V_0 (ng/mgh)	k_2 (ng/mgml)	q_e (ng/mg)	R^2
Blank alginate millispheres							
Alginate 2%w/v;25mM Ca^{2+}	0.0723	5.372	0.754	0.0449	0.671	0.259	0.771
Alginate 2%w/v;50mM Ca^{2+}	0.00346	2.014	0.026	0.0146	0.0324	0.671	0.021
Alginate 2%w/v;100mM Ca^{2+}	n/a*	n/a*	n/a*	-0.0322	-4.83	0.0816	0.864
Alginate 1%w/v;50mM Ca^{2+}	n/a*	n/a*	n/a*	0.0918	4.16	0.149	0.937
PHA beads encapsulated in alginate millispheres							
Alginate 2%w/v; PHA beads 1%w/v; 25mM Ca^{2+}	0.0682	2.799	0.917	0.798	0.0554	3.791	0.997
Alginate 2%w/v; PHA beads 1%w/v; 50mM Ca^{2+}	0.0725	2.949	0.886	1.091	0.0591	4.296	0.997
Alginate 2%w/v; PHA beads 1%w/v; 100mM Ca^{2+}	0.0751	3.179	0.849	1.562	0.0596	5.118	0.995
Alginate 2%w/v; PHA beads 0.5%w/v; 50mM Ca^{2+}	0.0643	2.583	0.884	0.637	0.0542	3.426	0.992
Alginate 2%w/v; PHA beads 1.5%w/v;50mM Ca^{2+}	0.076	3.215	0.882	1.483	0.0597	4.985	0.998
Alginate 1%w/v; PHA beads 1%w/v; 50mM Ca^{2+}	0.0854	2.579	0.877	1.916	0.0922	4.56	0.999

* Unable to calculate due to mathematical error

3.3.2.2 Adsorption isotherm

To analyse the interactive behaviour of PHA bead-alginate millispheres with Nile red in the aqueous solution, the adsorption isotherm test in Nile red solution ranging from 10-100 ng/ml Nile red concentration was conducted (Section 2.17.2.3.2). Initially, the interaction between glassware and Nile red in the solution was analysed in the blank flask containing the reagent solution after 24 hours incubation (Section 2.17.2.3.4). This confirmed that there was no interaction between the glassware and the Nile red (Figure 45, Appendix IV). In this test, the standard preparation which was prepared with 2% w/v alginate, 1% w/v PHA beads and gelated by 50 mM calcium ion, was compared with the blank alginate millispheres. Figure 41 shows the adsorption isotherm of blank alginate millispheres and PHA bead-alginate millispheres. It was observed that the adsorption of Nile red occurred in PHA bead-alginate millispheres, and the degree of adsorption increased as the initial concentration of Nile red in the solution increased. Meanwhile, there was no adsorption observed in the blank alginate millispheres.

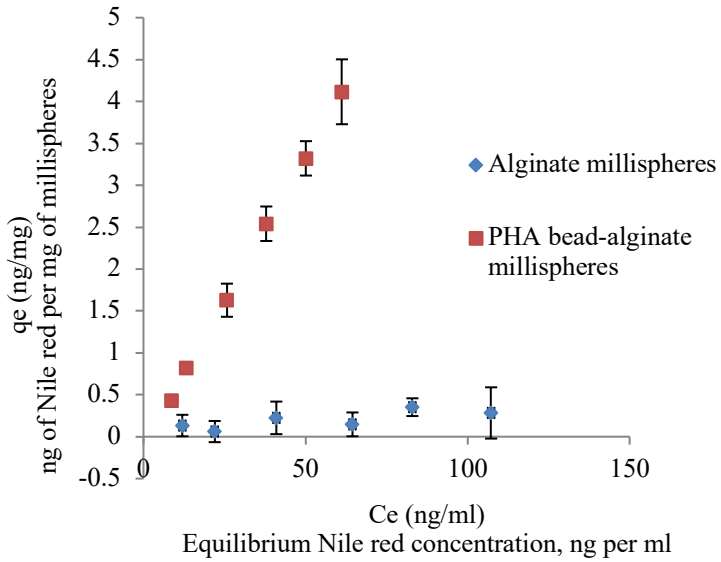

Figure 41: Adsorption isotherm of blank alginate millispheres and PHA bead-alginate millispheres. Millispheres: 0.2g; Nile red concentration: 10-100ngml^{-1}; pH: pH 6.7. The measurement was done in triplicate and means ± standard deviation is reported.

To quantify the adsorption capacity of blank alginate millispheres and PHA bead-alginate millispheres for Nile red adsorption from the aqueous solution, two most commonly used isotherm models were employed in this study, namely the Freundlich and Langmuir isotherm model. The Freundlich isotherm model can be represented by the following equation:

$$q_e = K_F C_e^{1/n}$$

Where q_e is the solid phase concentration at equilibrium (ng/mg), C_e is the aqueous phase concentration at equilibrium (ng/ml), K_F is an indicator of the adsorption capacity, and 1/n represents the adsorption intensity. The results obtained from the experiment were analysed by plotting linear line produced by q_e versus C_e. The following equation for the Freundlich isotherm formula was used:

$$\log q_e = \log K_F + \frac{1}{n} \log C_e$$

The Langmuir isotherm model can be represented by the following equation:

$$q_e = \frac{q_m b C_e}{1 + b C_e}$$

Where q_e is the equilibrium adsorption of solid phase (ng/mg), C_e is the equilibrium concentration of the aqueous phase (ng/ml), q_m is the maximum adsorption capacity (ng/mg), and b is the Langmuir isotherm constant (ml/ng). The linear equation of the above formula to plot q_e versus C_e was:

$$\frac{1}{q_e} = \left(\frac{1}{b q_m}\right)\frac{1}{C_e} + \frac{1}{q_m}$$

The linearised isotherm calculated by the Freundlich and Langmuir isotherm linear formulae are shown in Figure 42, and the resulting values were summarised in Table 9.

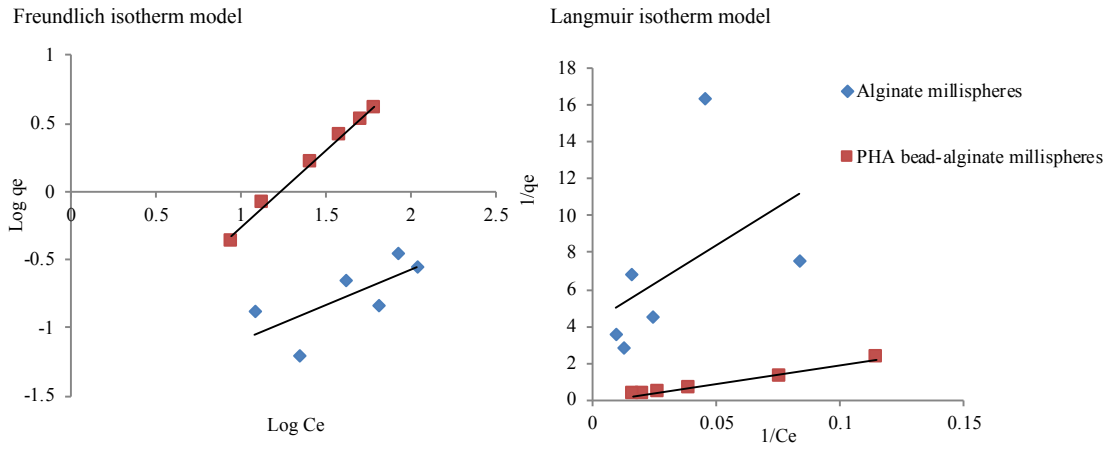

Figure 42: Adsorption isotherm data for blank alginate millispheres and PHA bead-alginate millispheres fitted to linear form of the Freundlich and Langmuir adsorption isotherm models.

Table 9: Summary of adsorption isotherm calculated by the Freundlich and Langmuir isotherm models.

	Frundlich			Langmuir		
	K_F (ng/mg(ng/ml)^n)	1/n	R^2	q_m (ng/mg)	b (ml/ng)	R^2
Alginate millispheres	0.023	1.874	0.501	0.234	0.052	0.227
PHA bead-alginate millispheres	0.040	0.882	0.995	-6.566	-0.007	0.984

According to the Freundlich isotherm result, the adsorption capacity of PHA bead-alginate millispheres was slightly higher than the blank alginate millispheres, however, the adsorption intensity value was lower than the negative control. In contrast, the Langmuir isotherm result showed that the adsorption capacity of the PHA bead-alginate millispheres exhibited much lower value in comparison with the negative control. However, it must be noted that the correlation coefficient of the blank alginate millispheres for both isotherm models showed poor correlations (R^2=0.501 for Freundlich and R^2=0.227 for Langmuir). This indicated that the blank alginate millispheres fitted neither isotherm model. Furthermore, based on the correlation coefficient, PHA bead-alginate millispheres showed a better fit to the Freundlich isotherm model than the Langmuir isotherm model (R^2=0.995 for Freundlich and R^2=0.984 for Langmuir). Moreover, the value obtained from the Langmuir isotherm model showed negative values. This indicated the isotherm model did not fit the adsorption performance of PHA bead-alginate millispheres.

Chapter 4: Discussion

4.1 Preparation of PHA beads for alginate encapsulation

Previous studies have demonstrated the successful production of genetically engineered PHA beads displaying a range of functionalised proteins on their surface (Grage *et al.*, 2009; Parlane *et al.*, 2017). This study aimed to produce alginate microspheres encapsulating the functionalised PHA beads and to evaluate the difference in functional activity of the protein on the PHA beads in the free and the encapsulated state. It was hypothesised that the fusion protein on PHA beads retains functional activity in the alginate microspheres, and the encapsulation within the alginate gel matrix will influence the level of the activity. In this study, PHA beads displaying ZZ domain (IgG binding domain) and OpdA (organophosphate hydrolase) were selected for encapsulating in alginate microspheres.

As shown in the fluorescence microscopy images (Figure 12 and Figure 25) and the TEM images (Figure 13 and Figure 26), *E. coli* cells transformed with the respective plasmids were shown to contain PHA beads, indicating the activation of PHA synthase (PhaC) that catalyses the synthesis of the PHA to mediate the bead formation (Rehm, 2007). Furthermore, SDS-PAGE gel confirmed the overproduction of the fusion protein displayed on the PHA bead, and the predominant band corresponded to the expected theoretical molecular weight (Figure 16 and Figure 29). Other protein bands were still present after PHA bead isolation and purification procedures, and these may be a part of commonly found co-purified proteins such as ATPase, Elongation factor-Tu and outer membrane proteins (OmpF and OmpA) (Bäckström *et al.*, 2007). The particle size of the PHA beads measured using laser diffraction showed that particle size was larger than the general particle size of a single PHA bead (50-500 nm in diameter) (Grage *et al.*, 2009). Therefore, the particle size distribution results in this study of 1-100 μm in diameter indicated that PHA beads were aggregated. This observation was also seen in a previous study (Reyes *et al.*, 2016). The aggregation was probably due to non-specific intermolecular and hydrophobic interactions. In addition, due to the small particle size of the PHA beads, material factors (size, shape, and surface charge) and environmental factors (temperature, gravity force, pH and ionic strength of solution) may cause the formation of the aggregates (Zhang, 2014). As shown in Figure 17 and Figure 33, the

functional activity of the fusion proteins on the surface of PHA beads was confirmed before producing PHA beads encapsulated in alginate microspheres.

4.2 PHA beads encapsulated in alginate microspheres

4.2.1 Internal gelation

The PHA beads displaying the ZZ domain (an IgG binding domain) or OpdA were encapsulated in alginate microspheres using a water-in-oil (w/o) emulsion with internal gelation in which calcium crosslinking is induced by the calcium ion release from insoluble calcium ($CaCO_3$) by pH reduction (Poncelet, 2001). This method produces micron-sized alginate spheres (Fundueanu *et al.*, 1999). This is considered the most favourable particle size for the functional tests in this study because small particle sizes give higher specific surface area and reduce the distance between the functional proteins displayed on PHA beads and its substrate (Doherty Speirs *et al.*, 1995; Hussain *et al.*, 2015). For the IgG binding test using alginate microspheres encapsulating ZZC PHA beads, the microspheres were subjected to an additional gelation (double gelation) (Section 4.2.2). The alginate microspheres encapsulating OpdA PHA beads were prepared with internal gelation only.

4.2.1.1 Morphology of PHA beads encapsulated in alginate microspheres

The alginate microspheres prepared by the w/o emulsion with internal gelation produced micron-sized and spherical-shaped microspheres as expected. The morphology was easily distinguishable between blank and PHA bead-alginate microspheres using a phase contrast microscope, as there were particulates enclosed in the alginate microspheres, while blank alginate microspheres were transparent (Figure 30). The presence of PHA beads in the alginate microspheres was readily confirmed by Nile red staining (Spiekermann *et al.*, 1999). SEM image analysis showed both blank and PHA bead-microspheres were spherical, discrete, and distinct with a solid dense structure (Figure 31). For the PHA bead-alginate microspheres, the surface texture was seen as very rough, and PHA beads were seen exposed on the outer surface of the microsphere. There were no apparent morphological differences between microspheres prepared with internal gelation only and double gelation (Figure 19 and Figure 36). The rough surface morphology in SEM images may be due to the sample preparation method, which used

ethanol to dehydrate the alginate microspheres, and the intrinsic structure of the PHA bead polymer core resisted further shrinkage of the microspheres during lyophilisation.

4.2.1.2 Particle size distribution of alginate microspheres: Internal gelation

As expected, the particle size distribution of alginate microspheres prepared by the w/o emulsion with internal gelation was relatively uniform (a unimodal distribution with no secondary peaks) (Figure 32). This observation was commonly observed in previous studies using this method (Silva *et al.*, 2006; Wang *et al.*, 2011; Lupo *et al.*, 2014). The diameter distribution of alginate microspheres prepared by this method depends on the droplet size in the dispersed phase of the emulsion. The size of the droplet is determined by a balance between dispersive force and the surface tension force that emulsify the mixture and cause merging of droplets, respectively (Reis *et al.*, 2006; Ching *et al.*, 2017). In the present study, a lipophilic surfactant, Span80, was used to reduce the interfacial tension between the dispersed (water) phase droplets and paraffin oil in the continuous (oil) phase, promoting an increase in stability of the w/o emulsion (Ching *et al.*, 2017). Therefore, the particle size distribution in this study generated relatively uniform particle sizes of microspheres when prepared using the same parameters.

A change in the stirring speed, hence dispersive force, influenced the particle size distribution of the alginate microspheres prepared at 250, 350, and 450 rpm (Table 12, Appendix II). This observation agrees with previous studies (Perumal, 2001; Silva *et al.*, 2006) that demonstrated higher stirring speed decreased the particle size. However, it has also been reported that using higher stirring speed increased particle size distribution, causing higher heterogeneity of the batch (Silva *et al.*, 2005; Mokhtari *et al.*, 2017). In the w/o emulsion, shear stress is higher at the tip of the propeller than at the centre, creating a difference in energy distribution. The higher stirring speed modifies the random droplet coalescence, and consequently gives rise to an increase in particle size distribution (Silva *et al.*, 2006). However, in this study, the particle size distribution of microspheres prepared with different stirring speeds gave no significant difference in SPAN factor (which represents the spread of the particle size distribution). The broader size distribution has been observed at higher stirring speeds (higher than 600 rpm) than used in the present study (Silva *et al.*, 2005). Therefore, the lack of heterogeneity may be due to the stirring speeds selected (250, 350, and 450 rpm). Simultaneously, the interfacial tension reduction induced by emulsifiers (Reis *et al.*, 2006) as well as physical properties

of materials, such as viscosity of water phase and oil phase (Hudson *et al.*, 2003; De Bruyn *et al.*, 2014), might have contributed to the stability of the emulsion and helped to avoid the coalescence of the droplets.

4.2.1.3 Encapsulation efficiency

The encapsulation efficiency of PHA beads in alginate microspheres was determined by quantifying the amount of fusion protein on the PHA beads in combination with protein profiling by SDS-PAGE. The results showed the microspheres prepared with w/o emulsion with internal gelation had a high encapsulation efficiency. The microspheres prepared for an IgG binding test (PhaC and ZZC PHA beads) had an encapsulation efficiency of more than 92 % meanwhile microspheres prepared for the enzyme test (PhaC and PhaC-OpdA PHA beads) demonstrated more than 88 % encapsulation efficiency. The loss of encapsulated material, leading to a reduced encapsulation efficiency, is often due to the diffusion of encapsulated materials out through the porous gel structure created by the release of CO_2 during the solubilisation of $CaCO_3$ in the internal gelation reaction (Silva *et al.*, 2005; Lee & Mooney, 2012). The high encapsulation efficiency in this study might be attributed to the particle size of the PHA beads. The bead particle size could be larger than the pore size of the alginate gel matrix, preventing leakage of the PHA beads out from the microspheres. Moreover, this may also explain the increase in the proportion of PhaC derived protein on the PHA beads observed after the PHA beads were extracted from the microspheres (Table 5 and Table 6). The non-immobilised proteins, such as bacterial membrane proteins, diffused out of the microspheres while the PHA beads remained within the alginate microspheres. Therefore, this highlights the advantage of protein immobilisation on PHA beads as they can retain protein at relatively high levels within alginate microspheres.

In this study, the high encapsulation efficiency of proteins on PHA beads was obtained using an acidic acetate buffer as the recovery medium from the emulsion in the washing cycle as previously reported (Silva *et al.*, 2005). The reduction in pH influences the degree of ionisation of proteins that promote interactions between proteins and the alginate polymer of opposite charge (Dumitriu & Chornet, 1998). The acetate buffer was pH 5.5 so alginate remained in a polyanionic state (pKa of M and G residual are 3.38 and 3.65, respectively) (Ching *et al.*, 2017). The theoretical isoelectric point (p*I*) of PhaC, ZZC, and PhaC-opdA proteins given by ExPASy pI/Mw tool is 6.09, 5.75, and 6.47

respectively, therefore, the proteins were considered to be positively charged in the acidic conditions. The positively charged proteins may contribute to the high encapsulation efficiency by forming an electrostatic interaction with the alginate polymer throughout the washing procedure. Moreover, microsphere recovery using an acetate buffer was considered to maintain the solubilisation of the remaining $CaCO_3$ in microspheres, thus contributing to the gel strength of the microspheres (Silva *et al.*, 2005).

4.2.2 Double gelation: Microsphere preparation with internal gelation followed by additional gelation

The original design of preparing the ZZ domain-displaying PHA beads encapsulated in alginate microspheres aimed to use only internal gelation and to analyse the IgG binding capacity of this in packed bed column utilising the porous structure of the resulting alginate microspheres. However, the microspheres showed not enough mechanical strength to be retained in the column even at a low centrifugation, had low PHA bead density per unit volume, and showed very poor mass transport (Data not shown). Therefore, the additional gelation step was conducted to provide higher mechanical strength by creating more interaction between calcium ions and alginate (Donati & Paoletti, 2009), and to increase the PHA bead density per unit volume by condensing the microsphere. However, increased alginate gel network leads to a greater resistance to liquid mass transport (Amsden & Turner, 1999). Therefore, a conventional affinity chromatography protocol was employed in the column test instead of the packed bed column chromatography in this study.

4.2.2.1 Morphology and particle size distribution: Double gelation

There were no distinctive differences in the morphology between microspheres prepared with double gelation and internal gelation only. Instead, the fluorescence images suggested the PHA beads within alginate microspheres prepared with double gelation were more dense (Figure 18D, E and Figure 30D, E), indicating the additional gelation influenced the structural characteristic of microspheres. The result from laser diffraction supports this as it showed the additional gelation resulted in a reduction in particle size of 50-70%. It was observed that the percentage reduction in diameter of alginate microspheres was higher for microspheres prepared at lower stirring speed in the internal gelation step (Table 12, Appendix II). This was probably due to the addition of extra calcium ions inducing gel shrinkage by increasing the degree of cross-linkage between

the free G residual of alginate polymer and calcium ion (Martinsen *et al.*, 1989). Also, the larger microspheres produced by a slower stirring speed provide more interior space for calcium ion to react the free G residual and therefore capable of a higher degree of shrinkage than smaller microspheres. Surprisingly, in contrast to the previous study that used $CaCl_2$ solution for the microsphere recovery medium from w/o emulsion (Poncelet *et al.*, 1992), the median particle size decreased, and the particle size distribution remained unimodal in this study (Figure 20). Previous studies reported $CaCl_2$ washing causes the loss of water molecules from microspheres that induces gel shrinkage, but also induces adhesion between microspheres results in their aggregation by forming a new hydrogen bond between hydroxyl groups of alginate polymers. As a result, there will be an increase in median size (Poncelet *et al.*, 1995; Fundueanu *et al.*, 1999; Chai *et al.*, 2004). However, in this study, increase in median particle size was not observed. Therefore, the results suggest additional gelation after a full recovery process from the emulsion allows the alginate microspheres to remain discrete with a unimodal particle distribution.

4.2.2.2 Encapsulation efficiency after additional gelation (double gelation)

The encapsulation efficiency of microspheres prepared with double gelation was reduced by 34 % for PhaC PHA beads and 26.1 % for ZZC PHA beads compared with internal gelation only. The significant loss of encapsulated material by the additional gelation has also been demonstrated in the microsphere recovery from a w/o emulsion and may be due to the release of encapsulated PHA beads into the $CaCl_2$ solution (Ostberg *et al.*, 1993; Silva *et al.*, 2005). However, as expected, the double gelation microspheres produced denser PHA beads within the microspheres than microspheres prepared with only internal gelation as suggested by the fluorescent microscopy results (Figure 18 and Figure 30). Although this is qualitative data, it could indicate that external pressure created by the addition of calcium ion and alginate polymer interaction (Donati & Paoletti, 2009), and the relatively large pore size created by internal gelation (Liu *et al.*, 2002), released PHA beads into the cross-linking solution, resulting in lowering the encapsulation efficiency.

4.2.2.3 Effect of different solutions

The particle size distribution of alginate microspheres prepared for the IgG binding test was measured in water, TBS (50 mM Tris, 50 mM NaCl, pH7.4) and 100 mM glycine (pH2.5) solutions. The results confirmed that there was a change in particle size in the

buffer solution tested (Figure 20 and Table 12, Appendix II). As expected, the degree of swelling was higher in TBS than glycine buffer because of its ionic strength and neutral pH (Matyash *et al.*, 2014). Unexpectedly, the alginate microspheres in glycine (pH 2.5) showed larger particle sizes than in water even though the microsphere size is known to decrease at low pH (Lee *et al.*, 1997; Darrabie *et al.*, 2006; Soni *et al.*, 2010). Therefore, it indicated that glycine buffer induced swelling of microspheres even at low pH. The smaller particle sizes observed in water could be due to the loss of water molecules from the microspheres, which accompanied ion diffusion to the external solution in low osmolarity (Martinsen *et al.*, 1989).

The laser diffraction results showed alginate microspheres prepared with double gelation at 250-450 rpm produced particle sizes >10 µm in all of the preparations. This is bigger than the pore size of the porous support of the test column (Pierce™ Spin Cups Paper Filter column (Section 2.17.2.1.2)). The particle size is an important factor as smaller particles provides higher specific surface area and more efficient exchange of components in and out of the microsphere (Paques, 2015). In this study, there were two reasons to choose the alginate microspheres prepared at 350 rpm to use for the following IgG binding capacity test. These are: (1) to avoid the potential leakage through the porous support of the column by small alginate microspheres with particle sizes prepared at 450 rpm and (2) to give high efficiency of substrate exchange due to generating the smallest diameter particle possible.

4.2.3 IgG binding test

4.2.3.1 IgG binding assay to PHA bead-alginate microspheres

IgG binding capacity of PHA bead-alginate microspheres was assessed by an IgG binding assay in batch and column test conditions using purified human IgG. It was found that there was no significant difference in the IgG binding capacity between blank alginate microspheres, PhaC PHA bead-alginate microspheres, and ZZC PHA bead-alginate microspheres (Figure 21). These results indicated that IgG binds non-specifically to the alginate microspheres. In addition, the elution fraction analysis showed almost no IgG, indicating the bound IgG was not eluted from the microspheres. SDS-PAGE confirmed IgG was present in the microspheres before and after the elution phase. Also, the extracted PHA beads still contained bound IgG to the PhaC derived proteins after elution showing that the pH reduction by 100 mM glycine (pH 2.5) did not cause elution of IgG in the

microspheres (Figure 23). A previous study has shown that IgG can diffuse into alginate microspheres (Mørch *et al.*, 2006), and another study has demonstrated the immobilisation of IgG in alginate microspheres in a pH neutral solution via electrostatic interaction with calcium ions (Chen *et al.*, 2013). Therefore, these studies may help explain the results in this study that no significant difference in the level of IgG binding capacity found between all the types of alginate microspheres. Alginate microspheres have been reported to be responsive to external stimuli such as the pH and ionic strength of the buffer solution (Lee *et al.*, 1997; Ching *et al.*, 2017). Previous studies demonstrated encapsulation of protein in alginate microspheres for oral delivery purposes and showed that the cumulative release of the encapsulated material was limited in low pH medium (Martins *et al.*, 2007; Isiklan *et al.*, 2011; Zhang *et al.*, 2011). This is attributed to shrinkage of the alginate microspheres and the reduction of pore size of the alginate gel matrix (Gombotz & Wee, 2012). In the present study, particle size reduction was also observed (Figure 20). Therefore, the low pH of 100 mM glycine (pH 2.5) may have caused the particle size and pore size reduction, which in turn inhibited the movement of IgG out from the alginate microspheres. A difference in IgG binding capacity between batch and column test condition was found, however, this was due to the degree of liquid removal before the microspheres were weighed.

4.2.3.2 IgG binding test to the PhaC derived proteins on PHA beads in alginate microspheres

As discussed above, the IgG binding capacity assay in batch and column conditions did not show a significant difference between blank alginate microspheres and PHA bead-alginate microspheres (Figure 21). However, SDS-PAGE confirmed the presence of IgG in the alginate microspheres and the IgG was bound to both PhaC derived proteins (PhaC or ZZC) on PHA beads in alginate microspheres (Figure 23). Therefore, the effect of alginate encapsulation on the amount of IgG bound to the PhaC derived proteins on PHA beads was investigated by quantifying bound IgG on the protein of the extracted PHA beads from alginate microspheres using SDS-PAGE gel densitometry (Figure 43, Appendix III). In comparison with IgG binding capacity value obtained from a previously described IgG binding assay (Jahns *et al.*, 2013), the SDS-PAGE gel densitometry of free PHA beads resulted in similar values (Figure 17 and Figure 24), indicating the feasibility of testing the IgG binding capacity using this method. The amount of IgG bound to the PhaC derived protein on the PHA beads encapsulated in alginate microspheres was

significantly higher than on the corresponding free bead state in both test conditions (batch and column). However, there was very little difference in the amount of IgG bound to the PhaC derived proteins in the different test conditions ($p>0.05$). Since ZZ domain-displaying PHA beads have IgG binding sites (ZZ), the amount of bound IgG was much higher than that of PhaC PHA beads, even after alginate encapsulation. These results indicate that the IgG binding domain displayed on PHA beads within an alginate hydrogel matrix was capable of binding IgG, and the alginate encapsulation enhanced the binding ability of the PhaC derived protein on PHA beads with IgG. Further studies are needed to investigate why the amount of bound IgG to the PhaC derived protein on PHA beads in alginate microspheres was enhanced, however, the protocol in the IgG binding assay might explain the difference in the binding performance. According to the conventional protocol for analysing IgG binding capacity of PHA beads as described in Jahns *et al.* (2013), free PHA beads were collected by centrifugation and were re-suspended by pipetting. At each step, PHA beads in the test may form aggregates, which significantly reduce the specific surface area of the functionalised PHA beads. In contrast, the encapsulated PHA beads are entrapped and immobilised in the alginate gel matrix of microspheres, which effectively prevented aggregation of PHA beads. Therefore, it could be considered that the specific surface area of PHA beads was more easily retained than with the free PHA beads.

As expected, the free PHA beads showed a reduction in bound IgG after elution indicating the IgG was eluted successfully (Figure 24, ZZC). Interestingly, the amount of IgG bound on the PhaC derived proteins of the encapsulated PHA beads of both encapsulated PhaC and ZZC PHA beads was significantly higher after the elution phase than after the binding phase (Figure 24). This indicates that the bound IgG after the binding phase was not eluted, however, IgG binding to the protein on PHA beads was enhanced. From the observation of particle size reduction in low pH (Figure 20) and lack of IgG elution after triplicate elution phase (Figure 21), the following explanations for this are suggested. The alginate microspheres were dispersed in the low pH medium, reducing particle size and pore size of microspheres, thus inhibiting movement of IgG out from the microspheres and leading to entrapment of IgG within the microspheres. Subsequently, the physical distance between IgG and the protein displayed on the PHA beads was decreased and the reduction in particle size possibly increased the inner pressure of the alginate microsphere, assisting binding of IgG towards the protein on PHA beads. Alternatively, it may simply be that

the PhaC derived proteins on the encapsulated PHA beads were exposed to IgG for a longer time in the microspheres. Further studies are needed to investigate these possibilities.

4.2.4 Enzyme activity

The fluorescence intensity created by the liberated chlorferon from Coumaphos was used as a measure of the catalytic activity of the encapsulated OpdA displayed on the PHA beads in alginate microspheres. The result showed there was no change in the level of fluorescence intensity for the negative controls, including free PhaC PHA beads, blank alginate microspheres, and PhaC PHA bead-alginate microspheres. These results confirmed that the alginate gel matrix and PHA beads lacking the OpdA do not possess functionality in the catalytic reaction of the substrate. As expected, the free PhaC-OdpA PHA beads showed a gradual increase in the fluorescence intensity as soon as the PHA beads were introduced in the solution containing the substrate. This indicates the OpdA on the PHA beads functioned. The PhaC-OdpA PHA bead-alginate microspheres also showed an increase in fluorescence intensity, thus the catalytic activity of the encapsulated PHA beads displaying OpdA in the alginate microsphere gel matrix was confirmed. However, the rate of the activity of the encapsulated PhaC-OdpA PHA beads was significantly reduced compared to the free PhaC-OdpA PHA beads. Therefore, the catalytic activity of OpdA on the PHA beads was restricted by the alginate encapsulation. In previous studies, this phenomenon has also been reported, and they suggested that there might be limitations in mass transfer of substrate into the microspheres in order to reach the active site of the enzyme (Blandino *et al.*, 2003; Rehman *et al.*, 2013; Nawaz *et al.*, 2015). In addition to this, the substrate in this study, Coumaphos, is a hydrophobic compound (Sanchez-Bayo & Goka, 2014) while its hydrolysis products, chlorferon and diethylthiophosphate (DETP), have higher water solubility and have been shown to diffuse into alginate hydrogel (Ha *et al.*, 2008). Therefore, these chemical properties might also influence the rate of diffusion into the hydrophilic microenvironment inside the alginate microspheres, and limit the exchange of substrate into the alginate microspheres.

The catalytic activity observed in this test could be attributed to PHA beads released from the microspheres. To exclude this possibility, the Nile red-stained PHA bead-alginate microspheres were monitored by phase contrast and fluorescence microscopy to observe

the microspheres structure and the position of PHA beads in the test conditions (Figure 34). The images showed that the microspheres structure was maintained and the PHA beads remained enclosed in the microspheres throughout the incubation. This qualitative data suggests a catalytic reaction occurred as a result of PHA beads encapsulated in alginate microspheres, and highlighted the advantage of immobilising the enzyme on a solid material (in this case, PHA beads) to prevent the spontaneous leakage of the enzyme through the porous structure of alginate microspheres, similar to that demonstrated by Zhao *et al.* (2015).

4.3 PHA beads encapsulated in alginate millisphere for lipophilic substance removal from aqueous solution

The core of the PHA beads is composed of hydrophobic polymers (Grage *et al.*, 2009). Using this property, a lipophilic fluorescent dye, Nile red, has been used to confirm the presence of hydrophobic polymers in the cytoplasm of bacterial cells (Spiekermann *et al.*, 1999). In addition, a biomimetic adsorbent produced from PHB has been shown to adsorb lipophilic organic pollutants from an aqueous solution (Zhang *et al.*, 2010b). Therefore, the hydrophobic polymer core of PHA beads has the potential to function as the reservoir for lipophilic substances. In this study, the aim was to produce PHA beads encapsulated in alginate millispheres and to assess their ability to remove a lipophilic substance from an aqueous solution, using Nile red as a model lipophilic substance. It was hypothesised that PHA beads encapsulated in alginate millispheres are capable of adsorbing lipophilic substances from aqueous solutions and that the preparation parameters would influence the degree of adsorption.

4.3.1 Morphology of PHA bead-alginate millispheres

A simple extrusion dripping method was employed to add PHA beads and alginate mixtures into a $CaCl_2$ cross-linking solution to produce PHA beads encapsulated in alginate millispheres (PHA bead-alginate millispheres) by external gelation. The PHA bead-alginate millispheres were produced using different concentrations of alginate, PHA beads, and calcium ions, and evaluated for their adsorption performance. The blank alginate millispheres and PHA bead-alginate millispheres have a smooth surface, and the difference between them was distinguished easily by the white colour of the PHA beads within the alginate millispheres (Figure 35). In addition, the lyophilised PHA bead-alginate particle showed the core of a millisphere forms a tunnel-like structure, and PHA

beads were observed being immobilised on the wall of the tunnel (Figure 36). These observations suggested successful encapsulation of the PHA beads into alginate millispheres by the external gelation method.

4.3.2 Effect of calcium ion concentration

The particle size of the alginate millispheres was influenced significantly by the concentration of calcium ion used in the cross-linking solution, indicating calcium ion is critical in particle preparation (Daemi & Barikani, 2012). The adsorption kinetics of the blank alginate millispheres showed no adsorption capacity over the 24 hours incubation, indicating calcium ion is not the factor responsible for adsorption of Nile red from the solution. In contrast, PHA bead-alginate millispheres showed a gradual increase in the adsorption capacity, indicating the adsorption of Nile red from the solution occurred in the millisphere encapsulating PHA beads. Moreover, the adsorption rate was higher in the millisphere prepared with a higher concentration of calcium ions, thus the calcium ion concentration in the millisphere preparation contributes to the degree of adsorption performance. The alginate gel produced by external gelation causes a heterogeneous gelling profile with a denser gel network on the surface of the millisphere (Ching *et al.*, 2017). Moreover, the concentration of calcium ion influences the degree of the gel network with less diffusion of solute to the core of the particle in high concentration of calcium ion due to the denser peripheral gel matrix (Radovich, 1985). Therefore, the higher adsorption capacity observed in higher concentration of calcium ion was considered to be due to smaller particle size which provides more specific surface area (Wang & Shadman, 2013).

4.3.3 Effect of alginate concentration

The diameter of alginate millispheres, prepared with lower alginate concentration (1% w/v alginate) was smaller than those prepared with a higher concentration (2% w/v alginate) (Table 7), as observed in previous studies (Chan *et al.*, 2009; Bhujbal *et al.*, 2014; Davarcı *et al.*, 2017). This was attributed to a higher alginate concentration as higher viscosity requires a higher flow rate, thus pressure, to cut the droplet (Bhujbal *et al.*, 2014). Therefore, under a constant flow rate in this study, a droplet formed on the end of a needle will be larger in a more viscous solution, which in turn leads to an increase in resultant particle size. In addition to this, it has been shown that a droplet formed from a lower concentration of alginate is prone to shrink more than higher concentration of

alginate upon gelation (Chan *et al.*, 2009). Nile red was not adsorbed by the blank alginate microspheres. Meanwhile, the PHA bead-alginate millispheres did show adsorption of Nile red from the solution, and the rate of adsorption was higher in millispheres prepared from a lower alginate concentration. This showed that millispheres generated from a different alginate concentrations influence Nile red adsorption from the solution. As previous studies have reported, lower concentrations of alginate produced less dense and smaller alginate particle size (Klemenz *et al.*, 2003; Salsac *et al.*, 2009; Stewart *et al.*, 2009). The higher specific surface area and lower polymer density of the gel matrix in smaller alginate millispheres could account for the higher adsorption capacity in the PHA bead-alginate millispheres prepared with 1% w/v alginate.

4.3.4 Effect of PHA bead concentration

The concentration of PHA beads used in the preparation influenced the extent of Nile red adsorption. As expected, higher concentrations of PHA beads in the millispheres increased the rate and amount of Nile red adsorption owing to more adsorption sites (Zulfikar *et al.*, 2016). However, the adsorption capacity of PHA beads for Nile red was inversely correlated to the concentration of PHA beads used in the preparation when the adsorption capacity was calculated based on the amount of PHA beads weight instead of millisphere weight. This may be due to the distribution of PHA beads within the alginate millispheres. At high concentration of PHA beads, PHA beads were distributed at high density within alginate millispheres, providing more adsorption sites for Nile red. However, adsorption predominately occurred at the peripheral area of the millispheres, thus the adsorption sites of PHA beads at the centre of millispheres were not saturated. Meanwhile, lower concentrations of PHA beads would have space to allow Nile red to penetrate through the alginate gel matrix and reach the adsorption sites of PHA beads at the centre of the millisphere. In addition to this, the lower adsorption in higher concentration of PHA beads may have been due to steric hindrance of Nile red molecule that hindered full penetration of the molecule into the core of millispheres (Aljeboree *et al.*, 2017).

4.3.5 Adsorption Kinetics

The adsorption of Nile red from the aqueous solution was time dependent. Based on the adsorption kinetic data obtained from different parameters in the preparation of alginate millispheres, the data was modelled to determine if it followed pseudo-first or pseudo-

second order kinetics (Zhou *et al.*, 2015; Li *et al.*, 2017). Based on the correlation coefficient (R^2) value, the pseudo-second order kinetic model fitted better than pseudo-first order kinetic model. In addition, the theoretical adsorption capacity (q_e) from pseudo-second order kinetic model was closer to the experimental adsorption capacity value, confirming the validity of the model. Furthermore, the initial adsorption rate (V_0) seemed to follow the rate of adsorption capacity curve. Therefore, the model suggests the adsorption rate depends on the availability of active sites of PHA bead-alginate millisphere rather than the concentration of Nile red in the solution. Moreover, the adsorption mechanism suggested was chemisorption that relates to valent forces through sharing or exchanging electrons between the adsorbent (PHA bead-alginate millisphere) and adsorbate (Nile red) (Rudzinski & Plazinski, 2009). However, it is known that Nile red interacts with polymers by hydrophobic interaction (Riahi *et al.*, 2017), which is considered as a physisorption mechanism (Holzer *et al.*, 2017). Therefore, further study is needed to elucidate the exact mechanism of the adsorption.

4.3.6 Adsorption Isotherm

The adsorption isotherm of Nile red in water containing 10% v/v DMSO at 25°C, and pH 6.7 showed that as the initial concentration of Nile red increased, the amount of Nile red adsorbed on PHA bead-alginate millisphere also increased. This may be attributed to an increase in contact between the active site of PHA beads in the alginate millisphere and Nile red in the solution (Hu *et al.*, 2017; Riahi *et al.*, 2017). However, no maximum adsorption value for PHA bead-alginate millispheres was obtained in the isotherm experiment (Figure 41). This could be attributed to the low concentration of Nile red in the solution (due to its poor water solubility), thus adsorption saturation did not occur (Greenspan & Fowler, 1985; Kurniasih *et al.*, 2015); this was also seen in other studies for the adsorption of lipophilic substances from aqueous solutions (Ru *et al.*, 2007; Liu *et al.*, 2009). The adsorption capacity of blank alginate millispheres and PHA bead-alginate millispheres was evaluated using Freundlich and Langmuir isotherm model. The former assumes that the adsorption occurs on a heterogeneous surface by multilayer adsorption and the latter assumes that adsorption occurs on a homogeneous surface by monolayer adsorption (Ngah & Fatinathan, 2008; Peretz *et al.*, 2015; Zhou *et al.*, 2015). Based on the coefficient correlation value for blank alginate millispheres, both models showed poor correlation (Table 9). Therefore, the blank alginate millispheres fit neither isotherm model, indicating the gel matrix of alginate millisphere do not adsorb Nile red from the

solution in any way, and this is consistent with the observation above (Figure 41). For the PHA bead-alginate millispheres, the adsorption was better evaluated by the Freundlich than the Langmuir isotherm model, based on the higher coefficient correlation (Freundlich R^2=0.995, Langmuir R^2=0.984). Therefore, this indicated that the adsorption behaviour of PHA bead-alginate millispheres occurs on a heterogeneous surface by multilayer adsorption. A Freundlich isotherm parameter "n" shows the adsorption intensity, thus the favourability of the adsorption (Ngah & Fatinathan, 2008). If the value is $n<1$, it indicates that the adsorption intensity was favourable over the range of concentrations in the study, while $n>1$ indicates adsorption is favourable in higher adsorbate concentrations than lower concentrations (Nomanbhay & Palanisamy, 2005). The results showed the n-value is $n>1$, therefore, it indicated that the adsorption of PHA bead-alginate millisphere is favourable in a high concentration of Nile red in the solution.

4.4 Summary

This study aimed to encapsulate PHA beads within an alginate hydrogel matrix by ionotropic gelation methods and assess the functionality of the hybrid material.

PHA beads displaying IgG binding domain (ZZ) were encapsulated in alginate microspheres prepared by w/o emulsion with internal gelation. The microspheres were subjected to subsequent additional gelation to give higher mechanical strength. The additional gelation caused significant reduction of the encapsulation efficiency (approximately 30%) compared to internal gelation alone. IgG binding capacity of the microspheres was tested. Due to non-specific binding of IgG to the alginate microspheres, there was no difference found between negative controls (blank and PhaC PHA bead-alginate microspheres) and ZZC PHA bead-alginate microspheres. Also, no IgG could be obtained after elution. However, the amount of IgG bound on the PhaC derived proteins (PhaC or ZZC) on PHA beads analysed by SDS-PAGE gel densitometry showed that alginate encapsulation enhanced binding of IgG to the PhaC derived protein on the encapsulated PHA beads.

PHA beads displaying OpdA were encapsulated in alginate microspheres by w/o emulsion with internal gelation. The encapsulation efficiency of PHA beads was high at over 90 %. The enzymatic activity of OpdA on the encapsulated PHA beads was measured by the increase in fluorescence intensity caused by the liberation of enzymatic product. The results showed that alginate encapsulation significantly reduced the activity

of the enzyme displayed on the PHA beads. This was probably due to the alginate limiting mass transfer of the substrate to the active site of the enzyme. However, this system had an advantage that leakage of the enzyme through the porous structure of the alginate hydrogel matrix was inhibited by the particle size of the PHA beads.

Alginate millispheres encapsulating PHA beads were produced by a simple extrusion dripping method with external gelation in a $CaCl_2$ cross-linking solution. PHA bead-alginate millispheres were prepared with different concentrations of alginate, calcium ion, and PHA beads. The former two parameters directly influenced the particle size of the millispheres. Lower alginate concentration and higher calcium ion concentration produced smaller millispheres, which provided higher specific surface area, resulting in higher adsorption capacity. More PHA beads in the preparation of millispheres adsorbed more Nile red. However, when adsorption was calculated based on the PHA bead weight, fewer PHA beads used in the preparation adsorbed more Nile red. This was presumably because the adsorption sites at the peripheral region of the millisphere were quickly saturated with the higher concentrations of PHA beads, while Nile red had easier access to the core of the millisphere with fewer PHA beads. The adsorption kinetic and isotherm were evaluated. According to the coefficient correlation (R^2) values, PHA bead-alginate millispheres fit a pseudo-second order kinetic model and the Freundlich isotherm model.

4.5 Future directions

4.5.1 ZZC PHA bead-alginate microspheres

In this study, the amount of IgG binding to the protein displayed on the surface of PHA beads was enhanced by encapsulation within alginate microspheres. However, from the materials point of view, it is strongly recommended to use an alternative polymer to encapsulate the PHA beads displaying the IgG binding domain for an IgG purification application. This is because alginate microspheres are prone to change their structure due to changes in external stimuli, such as pH and ionic strength in the solution (Matyash *et al.*, 2014). Moreover, the elution buffer (100 mM glycine (pH2.5)) is prone to cause proton hydrolysis of alginate polymer (Haug *et al.*, 1963). Then, the subsequent dispersion of the alginate microspheres in a neutral pH solution causes the alginate to dissolve, destroying the microsphere's structure (Mørch *et al.*, 2007), thus reducing the reusability of the microspheres. Furthermore, alginate microspheres resulted in non-specific interaction with IgG in the present study, and previous studies have used alginate

for several protein purifications based on its direct interactions with proteins (Jain *et al.*, 2006). Based on these results, alginate is not recommended for encapsulating material for application in protein purification utilising the protein displayed on PHA beads. Therefore, the PHA beads displaying IgG binding domain should be encapsulated with a physiologically inert hydrogel with a high mechanical strength. Also, it is important to consider the porosity of the scaffold to ensure sufficient mass transfer of solute through the matrix, which would, in turn, result in higher IgG binding. This would also ensure higher efficiency in eluting bound IgG from the protein immobilised on the encapsulated PHA beads. However, the pore size has to be small enough to hold the bead within the hydrogel matrix.

4.5.2 PhaC-OpdA PHA bead-alginate microspheres

In this study, the enzymatic activity of PhaC-OpdA PHA beads encapsulated in alginate microspheres was only shown by the increase in fluorescence intensity due to the liberation of enzymatic product. The enzyme kinetic data should be quantitatively estimated using an equation. For instance, use a Lineweaver-Burk plot to analyse the Michaelis-Menten equation to obtain the catalytic constant (k_{cat}), Michaelis-Menten constant (K_M) and second order rate constant (k_{cat}/K_M) (Al-Mayah, 2012). In addition, this study only tested one condition. As previous studies have shown, the main advantage of alginate encapsulation is an enhancement of enzyme stability (Zhu *et al.*, 2005). Therefore, a future experiment should examine the stability of the enzyme activity in a wide range of different conditions (pH or temperature).

The limited exchange of solute (mass transfer) into alginate microspheres could be improved by blending alginate with other polymers to alter the structural properties of alginate hydrogel. For instance, a previous study has shown that that blending poly(vinyl-alcohol) in alginate formed porous microspheres that enhanced mass transfer of solute. Moreover, the microspheres encapsulating lipase enhanced its activity in the hydrolysis of olive oil in comparison to free lipase (De Queiroz *et al.*, 2006). In addition, a study has shown that density of encapsulated material within alginate hydrogel influences the effective diffusion of substrate (Ha *et al.*, 2008). Therefore, increasing enzyme activity by optimisation of PHA bead load in alginate microspheres should be investigated in future studies.

This study has provided qualitative data suggesting protein immobilised on PHA beads may inhibit spontaneous leakage of the functional protein owing to the particle size of PHA beads. Therefore, another possible application for the enzyme-displaying PHA beads encapsulated in alginate hydrogel, is in a fixed-bed reactor. As a previous study showed, alginate encapsulation of enzyme immobilised on chemically reduced graphene oxide greatly inhibited leakage of enzyme while it retained its activity within a broad range of conditions (pH and temperature) (Zhao *et al.*, 2015). As shown in the present study, the particle size of PHA beads may inhibit the potential leakage of the enzyme immobilised on the PHA beads from the alginate matrix. This may be similar to the study mentioned above, therefore, it would be interesting to test the potential application in a column to model a continuous fixed-bed enzyme catalytic reaction.

4.5.3 PHA bead-alginate millispheres for lipophilic substance removal

To gain an in-depth understand of the adsorption mechanisms of the alginate encapsulated PHA beads, further studies are required. In this study, it was demonstrated that different parameters in the preparation of the PHA bead-alginate millispheres resulted in different adsorption performances. However, the effects of the various conditions, such as temperature, pH, initial concentration of adsorbate (in the case of this study, Nile red), and initial dose of adsorbent should be investigated to elucidate the dynamic behaviour of adsorption. Furthermore, Brunauer–Emmett–Teller (BET) analysis should be applied to determine the surface area and pore size using nitrogen adsorption test (Park *et al.*, 2007).

The present study has concluded that adsorption was chemisorption due to higher correlation coefficient in pseudo-second order kinetics. To confirm this, the data should be further analysed using the intra-particle diffusion equation and investigated using Fourier transform infrared spectroscopy (FT-IR) to read the spectra of interaction between adsorbent and adsorbate before and after the adsorption test (Vijayakumar *et al.*, 2012).

In this study, two commonly used isotherm models, the Freundlich and Langmuir isotherm models, were used to analyse the adsorption isotherm. This concluded that the date in this study fits better to the Freundlich isotherm model than the Langmuir isotherm model according to the correlation coefficient obtained from plotting of linear equations of both models. In addition to this, several isotherm models have been used in this

particular topic. For example, a linear isotherm model has been used in a study which had a similar adsorption curve pattern to the present study (linear adsorption curve) due to the solubility of adsorbate in their study (Liu *et al.*, 2009). Thus, the model may suggest other adsorption mechanisms based on the data in this study.

Due to the hydrophobic nature of the lipophilic substance, the diffusion behaviour of the lipophilic substance across the hydrophilic alginate inner microenvironment is of particular interest. This is because the diffusion behaviour may influence the degree of adsorption to the PHA beads in alginate millispheres.

In this study, the adsorption capacity of free PHA beads was not characterised. Therefore, the effect of alginate encapsulation on the adsorption performance could not be determined. This was due to difficulties in controlling the rate of adsorption by the free PHA beads, and the interaction of the adsorbate (Nile red) with plastic wares used in this study. High performance liquid chromatography (HPLC) could be used to analyse the concentration of residual adsorbate as described in Zhang *et al.* (2010b).

Nile red was used as the model adsorbate in this study. This lipophilic substance has been shown to be a promising substance for testing interactions with the polymer core of PHA beads (Peters *et al.*, 2007). The next stage of utilising the hydrophobic nature of the inner core is testing with other lipophilic substances. This may include organic pollutants as well as lipophilic substances used for medical or pharmaceutical applications. Therefore, this has the potential to widen the application of PHA beads as a carrier in drug delivery systems.

Alginate has been used for water treatment applications utilising the property of chelating with heavy metal ions (Pandey *et al.*, 2007). In addition to this, previous studies showed that alginate encapsulation of activated carbon had the property of dual adsorption of heavy metal ions and organic pollutants (Park *et al.*, 2007). Therefore, PHA bead-alginate millispheres should be applicable for dual adsorption ability as well and future studies could investigate this.

4.5.4 PHA bead-alginate hybrid material fabrication

Future work also involves optimisation of hybrid material fabrication methods. This is because the properties of alginate hydrogel are highly variable depending on the source of alginate, which has varying chemical compositions and monomer sequences, and the

type of cross-linker used. For example, alginate with higher G-block content would produce hydrogels with stronger mechanical properties with high porosity. Divalent cations with higher affinity for alginate polymers, such as barium ions, would also enhance the mechanical properties.

The structure of alginate microspheres prepared with internal gelation could also be improved by using calcium carbonate nanoparticles (15-40 nm) instead of ultrafine calcium carbonate particle (micron-size) (Paques *et al.*, 2014a). Calcium carbonate nanoparticles would reduce the spatial variations of calcium concentrations within an alginate droplet, and the smaller particle size would give a faster reaction when the gelling agent is added. Therefore, the hydrogel prepared with calcium carbonate nanoparticle would produce a more homogeneous gel network than that produced with ultrafine calcium carbonate particles.

An alternative preparation method of alginate microspheres is the use of devices for modified extrusion techniques, such as electrostatic atomization and impinging aerosol method (Ching *et al.*, 2017). These techniques produce alginate microspheres with a uniform particle size and eliminate the extensive washing procedures required in w/o emulsion microsphere production. In addition, they avoid exposure of encapsulated materials in alginate microspheres to acid during the process of dissolving calcium carbonate in the internal gelation method.

A study has demonstrated coating alginate microspheres by poly(L-histidine) through electrostatic interaction between the negatively charged alginate polymer and the positively charged poly-histidine (Wang *et al.*, 2005). Previously, poly-histidine tag fused at N-terminus of PhaC was constructed, and PHA beads displaying poly-histidine tag were produced (Lee, 2011). During the preparation of alginate microspheres, the charge differences may give a positive effect, especially in encapsulation efficiency.

4.5.5 Applications

Potential applications of the hybrid material of PHA beads and alginate are mainly in the biomedical and pharmaceutical fields. For instance, oral administration of drugs and vaccine delivery are of particular interest. Alginates have been employed as an encapsulating carrier material in drug delivery system owing to its favourable properties. They can provide the controlled release of drugs at specific destinations (Lee & Mooney,

2012). Also, oral administration of vaccines encapsulated in alginate microspheres has elicited protective immune responses (Bowersock *et al.*, 1996). PHA beads have also been demonstrated as carriers of drugs, enzymes, and vaccines. Therefore, alginate encapsulation of functionalised PHA beads could be used as a novel formulation for drug delivery systems. Future studies could aim to include animal and human trials of hybrid materials designed to control the release of encapsulated drugs or enzymes on PHA beads.

4.6 Conclusion

This study has developed novel hybrid materials of PHA beads with alginate and assessed their functionality. The results demonstrated that the functional proteins displayed on PHA beads retained their function within the alginate hydrogel matrix. In comparison to their free state PHA beads, alginate encapsulation enhanced the binding capacity of an IgG binding domain (ZZ), but reduced the activity of OpdA. Therefore, the effect of alginate encapsulation depended on the function of the proteins on the surface of the PHA beads, and its substrate. The hydrophobic core of PHA beads within alginate millispheres acted as an adsorbent for Nile red in aqueous solution. The preparation parameters influenced the adsorption capacity of the millispheres. Alginate concentration and calcium concentration directly influenced the particle size of resultant PHA bead-millispheres, thus generating differences in the specific surface area. Although a higher concentration of PHA bead provide more adsorption sites, the adsorption capacity was higher when fewer PHA beads were used in the preparation, when it was based on the weight of PHA beads. The rate of adsorption was found to obey pseudo-second order kinetics and the equilibrium data were fitted to the Freundlich isotherm model. This study has shown the effect of alginate encapsulation on the functionality of PHA beads within the hydrogel matrix, however, further studies on optimisation of fabrication methods and formulations and characterisation of the hybrid material are required. PHA beads have been shown to be a versatile platform to display various functional proteins on their surface, and the number of functional proteins that can be immobilised on PHA beads is likely to increase. In addition to this, the hydrophobic core of PHA beads also has a vast potential as a reservoir for lipophilic substances. Therefore, further studies on the production of hybrid materials of PHA beads with polymer materials including alginate should be conducted to maximise the function of PHA beads and widen their applications.

Chapter 5: References

Al-Mayah, A. M. R. (2012). Simulation of enzyme catalysis in calcium alginate beads. *Enzyme research* **2012**.

Aljeboree, A. M., Alshirifi, A. N. & Alkaim, A. F. (2017). Kinetics and equilibrium study for the adsorption of textile dyes on coconut shell activated carbon. *Arabian Journal of Chemistry* **10**: S3381-S3393.

Amara, A. A. & Rehm, B. H. A. (2003). Replacement of the catalytic nucleophile cysteine-296 by serine in class II polyhydroxyalkanoate synthase from *Pseudomonas aeruginosa*-mediated synthesis of a new polyester: identification of catalytic residues. *Biochemical Journal* **374**(2): 413-421.

Amsden, B. & Turner, N. (1999). Diffusion characteristics of calcium alginate gels. *Biotechnology and Bioengineering* **65**(5): 605-610.

Andersen, T., Auk-Emblem, P. & Dornish, M. (2015). 3D cell culture in alginate hydrogels. *Microarrays (Basel)* **4**(2): 133-161.

Arnau, J., Lauritzen, C., Petersen, G. E. & Pedersen, J. (2006). Current strategies for the use of affinity tags and tag removal for the purification of recombinant proteins. *Protein Expression and Purification* **48**(1): 1-13.

Asthana, A., Verma, R., Singh, A. K., Susan, M. A. & Adhikari, R. (2016). Silver nanoparticle entrapped calcium-alginate beads for Fe(II) removal via adsorption. *Macromolecular Symposia* **366**(1): 42-51.

Augst, A. D., Kong, H. J. & Mooney, D. J. (2006). Alginate hydrogels as biomaterials. *Macromolecular Bioscience* **6**(8): 623-633.

Bäckström, B. T., Brockelbank, J. A. & Rehm, B. H. A. (2007). Recombinant *Escherichia coli* produces tailor-made biopolyester granules for applications in fluorescence activated cell sorting: functional display of the mouse interleukin-2 and myelin oligodendrocyte glycoprotein. *BMC Biotechnology* **7**(1): 3.

Banki, M. R., Gerngross, T. U. & Wood, D. W. (2005). Novel and economical purification of recombinant proteins: Intein-mediated protein purification using in vivo polyhydroxybutyrate (PHB) matrix association. *Protein Science* **14**(6): 1387-1395.

Barnard, G. C., McCool, J. D., Wood, D. W. & Gerngross, T. U. (2005). Integrated recombinant protein expression and purification platform based on *Ralstonia eutropha*. *Applied and environmental microbiology* **71**(10): 5735-5742.

Beeby, M., Cho, M., Stubbe, J. & Jensen, G. J. (2012). Growth and localization of polyhydroxybutyrate granules in *Ralstonia eutropha*. *Journal of Bacteriology* **194**(5): 1092-1099.

Bhujbal, S. V., Paredes-Juarez, G. A., Niclou, S. P. & de Vos, P. (2014). Factors influencing the mechanical stability of alginate beads applicable for immunoisolation of mammalian cells. *Journal of the Mechanical Behavior of Biomedical Materials* **37**: 196-208.

Blandino, A., Macias, A. & Cantero, D. (2003). Calcium alginate gel as encapsulation matrix for coimmobilized enzyme systems. *Applied Biochemistry and Biotechnology* **110**(1): 53-60.

Blandino, A., Macias, M. & Cantero, D. (2001). Immobilization of glucose oxidase within calcium alginate gel capsules. *Process Biochemistry* **36**(7): 601-606.

Blatchford, P. A., Scott, C., French, N. & Rehm, B. H. A. (2012). Immobilization of organophosphohydrolase OpdA from *Agrobacterium radiobacter* by

overproduction at the surface of polyester inclusions inside engineered *Escherichia coli*. *Biotechnology and Bioengineering* **109**(5): 1101-1108.
Boatman, E. S. (1964). Observations on the fine structure of spheroplasts of *Rhodospirillum rubrum*. *The Journal of cell biology* **20**: 297-311.
Bowersock, T. L., Hogenesch, H., Suckow, M., Porter, R. E., Jackson, R., Park, H. & Park, K. (1996). Oral vaccination with alginate microsphere systems. *Journal of Controlled Release* **39**(2): 209-220.
Bresan, S., Sznajder, A., Hauf, W., Forchhammer, K., Pfeiffer, D. & Jendrossek, D. (2016). Polyhydroxyalkanoate (PHA) granules have no phospholipids. *Scientific Reports* **6**.
Brockelbank, J. A., Peters, V. & Rehm, B. H. A. (2006). Recombinant *Escherichia coli* strain produces a ZZ domain displaying biopolyester granules suitable for immunoglobulin G purification. *Applied and environmental microbiology* **72**(11): 7394-7397.
Bryant, S. J. & Vernerey, F. J. (2018). Programmable hydrogels for cell encapsulation and neo-tissue growth to enable personalized tissue engineering. *Advanced Healthcare Materials* **7**(1).
Cataldo, S., Gianguzza, A., Milea, D., Muratore, N. & Pettignano, A. (2016). Pb(II) adsorption by a novel activated carbon - alginate composite material. A kinetic and equilibrium study. *International Journal of Biological Macromolecules* **92**: 769-778.
Celem, E. B., Bolle, S. S. & Onal, S. (2009). Efficient and rapid purification of lentil alpha-galactosidase by affinity precipitation with alginate. *Indian Journal of Biochemistry & Biophysics* **46**(5): 366-370.
Chai, Y., Mei, L. H., Wu, G. L., Lin, D. Q. & Yao, S. J. (2004). Gelation conditions and transport properties of hollow calcium alginate capsules. *Biotechnology and Bioengineering* **87**(2): 228-233.
Chan, E.-S., Lee, B.-B., Ravindra, P. & Poncelet, D. (2009). Prediction models for shape and size of ca-alginate macrobeads produced through extrusion–dripping method. *Journal of Colloid and Interface Science* **338**(1): 63-72.
Chan, L. W., Lee, H. Y. & Heng, P. W. S. (2006). Mechanisms of external and internal gelation and their impact on the functions of alginate as a coat and delivery system. *Carbohydrate Polymers* **63**(2): 176-187.
Chan, L. W., Lim, L. T. & Heng, P. W. (2000). Microencapsulation of oils using sodium alginate. *Journal of Microencapsulation* **17**(6): 757-766.
Chen, G. Q. (2009). A microbial polyhydroxyalkanoates (PHA) based bio- and materials industry. *Chemical Society Reviews* **38**(8): 2434-2446.
Chen, G. Q., Hajnal, I., Wu, H., Lv, L. & Ye, J. W. (2015). Engineering biosynthesis mechanisms for diversifying polyhydroxyalkanoates. *Trends in Biotechnology* **33**(10): 565-574.
Chen, G. Q. & Wu, Q. (2005). The application of polyhydroxyalkanoates as tissue engineering materials. *Biomaterials* **26**(33): 6565-6578.
Chen, W. Y., Kim, J. H., Zhang, D., Lee, K. H., Cangelosi, G. A., Soelberg, S. D., Furlong, C. E., Chung, J. H. & Shen, A. Q. (2013). Microfluidic one-step synthesis of alginate microspheres immobilized with antibodies. *Journal of the Royal Society Interface* **10**(88): 8.
Ching, S. H., Bansal, N. & Bhandari, B. (2017). Alginate gel particles-A review of production techniques and physical properties. *Critical Reviews in Food Science and Nutrition* **57**(6): 1133-1152.

Daemi, H. & Barikani, M. (2012). Synthesis and characterization of calcium alginate nanoparticles, sodium homopolymannuronate salt and its calcium nanoparticles. *Scientia Iranica* **19**(6): 2023-2028.

Darrabie, M. D., Kendall, W. F. & Opara, E. C. (2006). Effect of alginate composition and gelling cation on microbead swelling. *Journal of Microencapsulation* **23**(6): 613-621.

Davarcı, F., Turan, D., Ozcelik, B. & Poncelet, D. (2017). The influence of solution viscosities and surface tension on calcium-alginate microbead formation using dripping technique. *Food Hydrocolloids* **62**: 119-127.

De Bruyn, P., Chen, D., Moldenaers, P. & Cardinaels, R. (2014). The effects of geometrical confinement and viscosity ratio on the coalescence of droplet pairs in shear flow. *Journal of Rheology* **58**(6): 1955-1980.

De Queiroz, A. A. A., Passos, E. D., Alves, S. D., Silva, G. S., Higa, O. Z. & Vitolo, M. (2006). Alginate-poly(vinyl alcohol) core-shell microspheres for lipase immobilization. *Journal of Applied Polymer Science* **102**(2): 1553-1560.

Desai, K. G. H. & Park, H. J. (2005). Recent developments in microencapsulation of food ingredients. *Drying Technology* **23**(7): 1361-1394.

Deze, E. G., Papageorgiou, S. K., Favvas, E. P. & Katsaros, F. K. (2012). Porous alginate aerogel beads for effective and rapid heavy metal sorption from aqueous solutions: Effect of porosity in Cu2+ and Cd2+ ion sorption. *Chemical Engineering Journal* **209**: 537-546.

Doherty Speirs, E., Halling, P. J. & McNeil, B. (1995). The importance of bead size measurement in mass-transfer modelling with immobilised cells. *Applied Microbiology and Biotechnology* **43**(3): 440-444.

Donati, I., Holtan, S., Mørch, Y. A., Borgogna, M., Dentini, M. & Skja˚k-Bræk, G. (2005). New hypothesis on the role of alternating sequences in calcium-alginate gels. *Biomacromolecules* **6**(2): 1031-1040.

Donati, I. & Paoletti, S. (2009). Material properties of alginates. Alginates: Biology and Applications. B. H. A. Rehm. Berlin, Heidelberg, Springer Berlin Heidelberg**:** 1-53.

Draget, K., I., Gåserød, O., Aune, I., Andersen, P. O., Storbakken, B., Stokke, B. T. & Smidsrød, O. (2001). Effects of molecular weight and elastic segment flexibility on syneresis in Ca-alginate gels. *Food Hydrocolloids* **15**(4): 485-490.

Draget, K. I., Simensen, M. K., Onsoyen, E. & Smidsrød, O. (1993). Gel strength of Ca-limited alginate gels mage *in-situ*. *Hydrobiologia* **261**: 563-569.

Draget, K. I. & Skja˚k-Bræk, G. (2011). Chapter 7 Alginates: existing and potential biotechnological and medical applications. Renewable Resources for Functional Polymers and Biomaterials: Polysaccharides, Proteins and Polyesters, The Royal Society of Chemistry**:** 186-209.

Draget, K. I., Smidsrød, O. & Skjåk-Bræk, G. (2005). Alginates fromalgae. Biopolymers Online, Wiley-VCH Verlag GmbH & Co. KGaA.

Dragostin, I., Dragostin, O., Pelin, A. M., Grigore, C. & Zamfir, C. L. (2017). The importance of polymers for encapsulation process and for enhanced cellular functions. *Journal of Macromolecular Science Part a-Pure and Applied Chemistry* **54**(7): 489-493.

Draper, J. L. & Rehm, B. H. (2012). Engineering bacteria to manufacture functionalized polyester beads. *Bioengineered* **3**(4): 203-208.

Du, J. & Rehm, B. H. A. (2017a). Purification of target proteins from intracellular inclusions mediated by intein cleavable polyhydroxyalkanoate synthase fusions. *Microbial Cell Factories* **16**(184).

Du, J. & Rehm, B. H. A. (2017b). Purification of therapeutic proteins mediated by *in vivo* polyester immobilized sortase. *Biotechnology Letters* **40**(2): 369-373.

Dumitriu, S. & Chornet, E. (1998). Inclusion and release of proteins from polysaccharide-based polyion complexes. *Advanced Drug Delivery Reviews* **31**(3): 223-246.

Dunlop, W. F. & Robards, A. W. (1973). Ultrastructural study of polyhydroxybutyrate granules from *Bacillus cereus*. *Journal of Bacteriology* **114**(3): 1271-1280.

Elabd, C., Silva, F., Grinstein, V., Vargas, V. & Patel, A. (2016). *In vitro* evaluation of an encapsulation system for the transplantation of a human stem cell-derived tissue engineered brown fat. *Cytotherapy* **18**(6): S7-S7.

Esposito, D. & Chatterjee, D. K. (2006). Enhancement of soluble protein expression through the use of fusion tags. *Current Opinion in Biotechnology* **17**(4): 353-358.

Feng, J. J., Ding, H., Yang, G., Wang, R. T., Li, S. G., Liao, J. N., Li, Z. Y. & Chen, D. M. (2017). Preparation of black-pearl reduced graphene oxide-sodium alginate hydrogel microspheres for adsorbing organic pollutants. *Journal of Colloid and Interface Science* **508**: 387-395.

Francis, L., Meng, D. C., Knowles, J., Keshavarz, T., Boccaccini, A. R. & Roy, I. (2011). Controlled delivery of gentamicin using poly(3-hydroxybutyrate) microspheres. *International Journal of Molecular Sciences* **12**(7): 4294-4314.

Fundueanu, G., Nastruzzi, C., Carpov, A., Desbrieres, J. & Rinaudo, M. (1999). Physico-chemical characterization of Ca-alginate microparticles produced with different methods. *Biomaterials* **20**(15): 1427-1435.

Gan, L., Li, H., Chen, L. W., Xu, L. J., Liu, J., Geng, A. B., Mei, C. T. & Shang, S. M. (2018). Graphene oxide incorporated alginate hydrogel beads for the removal of various organic dyes and bisphenol A in water. *Colloid and Polymer Science* **296**(3): 607-615.

Gao, C., Liu, M., Chen, J. & Zhang, X. (2009). Preparation and controlled degradation of oxidized sodium alginate hydrogel. *Polymer Degradation and Stability* **94**(9): 1405-1410.

Gasperini, L., Mano, J. F. & Reis, R. L. (2014). Natural polymers for the microencapsulation of cells. *Journal of the Royal Society Interface* **11**(100).

Gautier, A., Carpentier, B., Dufresne, M., Vu Dinh, Q., Paullier, P. & Legallais, C. (2011). Impact of alginate type and bead diameter on mass transfers and the metabolic activities of encapsulated C3A cells in bioartificial liver applications. *Eur Cell Mater* **21**: 94-106.

Gerngross, T. U. & Martin, D. P. (1995). Enzyme-catalyzed synthesis of poly[(R)-(-)-3-hydroxybutyrate]: formation of macroscopic granules *in vitro*. *Proceedings of the National Academy of Sciences of the United States of America* **92**(14): 6279-6283.

Gerngross, T. U., Reilly, P., Stubbe, J., Sinskey, A. J. & Peoples, O. P. (1993). Immunocytochemical analysis of poly-beta-hydroxybutyrate (PHB) synthase in *Alcaligenes eutrophus* H16: localization of the synthase enzyme at the surface of PHB granules. *Journal of Bacteriology* **175**(16): 5289-5293.

Gill, I. & Ballesteros, A. (2000). Bioencapsulation within synthetic polymers (Part 1): sol-gel encapsulated biologicals. *Trends in Biotechnology* **18**(7): 282-296.

Gombotz, W. R. & Wee, S. F. (2012). Protein release from alginate matrices. *Advanced Drug Delivery Reviews* **64**: 194-205.

Grage, K., Jahns, A. C., Parlane, N., Palanisamy, R., Rasiah, I. A., Atwood, J. A. & Rehm, B. H. A. (2009). Bacterial polyhydroxyalkanoate granules: biogenesis, structure, and potential use as nano-/micro-beads in biotechnological and biomedical applications. *Biomacromolecules* **10**(4): 660-669.

Grage, K., McDermott, P. & Rehm, B. H. A. (2017). Engineering *Bacillus megaterium* for production of functional intracellular materials. *Microbial Cell Factories* **16**: 12.

Grage, K., Peters, V. & Rehm, B. H. A. (2011). Recombinant protein production by *in vivo* polymer inclusion display. *Applied and environmental microbiology* **77**(18): 6706-6709.

Greenspan, P. & Fowler, S. D. (1985). Spectrofluorometric studies of the lupid probe, Nile red. *Journal of Lipid Research* **26**(7): 781-789.

Gupta, M. N., Dong, G. Q. & Mattiasson, B. (1993). Purification of endo-polygalacturonase by affinity precipitation using alginate. *Biotechnology and Applied Biochemistry* **18**: 321-327.

Gupta, M. N., Jain, S. & Roy, I. (2002). Immobilized metal affinity chromatography without chelating ligands: Purification of soybean trypsin inhibitor on zinc alginate beads. *Biotechnology Progress* **18**(1): 78-81.

Ha, J., Engler, C. R. & Lee, S. J. (2008). Determination of diffusion coefficients and diffusion characteristics for chlorferon and diethylthiophosphate in Ca-alginate gel beads. *Biotechnology and Bioengineering* **100**(4): 698-706.

Han, M. R., Kwon, M. C., Lee, H. Y., Kim, J. C., Kim, J. D., Yoo, S. K., Sin, I. S. & Kim, S. M. (2007). pH-dependent release property of alginate beads containing calcium carbonate particles. *Journal of Microencapsulation* **24**(8): 787-796.

Hanahan, D. (1983). Studies on transformation of Escherichia coli with plasmids. *Journal of Molecular Biology* **166**(4): 557-580.

Handrick, R., Reinhardt, S. & Jendrossek, D. (2000). Mobilization of poly(3-hydroxybutyrate) in *Ralstonia eutropha*. *Journal of Bacteriology* **182**(20): 5916-5918.

Hanefeld, U., Cao, L. Q. & Magner, E. (2013). Enzyme immobilisation: fundamentals and application. *Chemical Society Reviews* **42**(15): 6211-6212.

Hanefeld, U., Gardossi, L. & Magner, E. (2009). Understanding enzyme immobilisation. *Chemical Society Reviews* **38**(2): 453-468.

Hanley, S. Z., Pappin, D. J. C., Rahman, D., White, A. J., Elborough, K. M. & Slabas, A. R. (1999). Re-evaluation of the primary structure of *Ralstonia eutropha* phasin and implications for polyhydroxyalkanoic acid granule binding. *Febs Letters* **447**(1): 99-105.

Hariyadi, D. M., Lin, S. C. Y., Wang, Y. W., Bostrom, T., Turner, M. S., Bhandari, B. & Coombes, A. G. A. (2010). Diffusion loading and drug delivery characteristics of alginate gel microparticles produced by a novel impinging aerosols method. *Journal of Drug Targeting* **18**(10): 831-841.

Haug, A., Bjorn, L. & Smidsrod, O. (1963). The degradation of alginates at different pH values. *Acta Chemica Scandinavia* **17**(5): 1466-1468.

Hay, I. D., Du, J., Reyes, P. R. & Rehm, B. H. A. (2015). *In vivo* polyester immobilized sortase for tagless protein purification. *Microbial Cell Factories* **14**(190).

Hay, I. D., Hooks, D. O. & Rehm, B. H. A. (2017). Use of bacterial polyhydroxyalkanoates in protein display technologies. Hydrocarbon and Lipid Microbiology Protocols: Bioproducts, Biofuels, Biocatalysts and Facilitating Tools. T. J. McGenity, K. N. Timmis & B. Nogales. Berlin, Heidelberg, Springer Berlin Heidelberg**:** 71-86.

Helgerud, T., Gåserød, O., Fjæreide, T., Andersen, P. O. & Larsen, C. K. (2009). Alginates. Food stabilisers, thickeners and gelling agents. A. Imeson. Oxford, Wiley-Blackwell**:** 50-72.

Hiraishi, A. & Khan, S. T. (2003). Application of polyhydroxyalkanoates for denitrification in water and wastewater treatment. *Applied Microbiology and Biotechnology* **61**(2): 103-109.

Hiraishi, T., Kikkawa, Y., Fujita, M., Normi, Y. M., Kanesato, M., Tsuge, T., Sudesh, K., Maeda, M. & Doi, Y. (2005). Atomic force microscopic observation of in vitro polymerized poly (R)-3-hydroxybutyrate : Insight into possible mechanism of granule formation. *Biomacromolecules* **6**(5): 2671-2677.

Holte, O., Tønnesen, H. H. & Karlsen, J. (2006). Measurement of diffusion through calcium alginate gel matrices. *Pharmazie* **61**(1): 30-34.

Holzer, B., Manoli, K., Ditaranto, N., Macchia, E., Tiwari, A., Di Franco, C., Scamarcio, G., Palazzo, G. & Torsi, L. (2017). Characterization of covalently bound anti-human immunoglobulins on self-assembled monolayer modified gold electrodes. *Advanced Biosystems* **1**(11): n/a-n/a.

Hooks, D. O., Blatchford, P. A. & Rehm, B. H. A. (2013). Bioengineering of bacterial polymer inclusions catalyzing the synthesis of N-acetylneuraminic acid. *Applied and environmental microbiology* **79**(9): 3116-3121.

Hu, S., Lin, X., Zhang, Y., Shi, M. & Luo, X. (2017). Preparation of Ca-alginate coated nZVI core shell beads for uranium (VI) removal from aqueous solution. *Journal of Radioanalytical and Nuclear Chemistry* **314**(3): 2405-2416.

Huang, K. S., Yang, C. H., Lin, Y. S., Wang, C. Y., Lu, K., Chang, Y. F. & Wang, Y. L. (2011). Electrostatic droplets assisted synthesis of alginate microcapsules. *Drug Delivery and Translational Research* **1**(4): 289-298.

Huang, Y. & Wang, Z. (2018). Preparation of composite aerogels based on sodium alginate, and its application in removal of Pb2+and Cu2+from water. *International Journal of Biological Macromolecules* **107**: 741-747.

Hudson, S. D., Jamieson, A. M. & Burkhart, B. E. (2003). The effect of surfactant on the efficiency of shear-induced drop coalescence. *Journal of Colloid and Interface Science* **265**(2): 409-421.

Hussain, A., Kangwa, M., Yumnam, N. & Fernandez-Lahore, M. (2015). Operational parameters and their influence on particle-side mass transfer resistance in a packed bed bioreactor. *AMB Express* **5**: 51.

Isiklan, N., Inal, M., Kursun, F. & Ercan, G. (2011). pH responsive itaconic acid grafted alginate microspheres for the controlled release of nifedipine. *Carbohydrate Polymers* **84**(3): 933-943.

Jahns, A. C., Maspolim, Y., Chen, S. X., Guthrie, J. M., Blackwell, L. F. & Rehm, B. H. A. (2013). *In vivo* self-assembly of fluorescent protein microparticles displaying specific binding domains. *Bioconjugate Chemistry* **24**(8): 1314-1323.

Jahns, A. C. & Rehm, B. H. A. (2015). Immobilization of active lipase B from *Candida antarctica* on the surface of polyhydroxyalkanoate inclusions. *Biotechnology Letters* **37**(4): 831-835.

Jain, S. & Gupta, M. N. (2004). Purification of goat immunoglobulin G by immobilized metal-ion affinity using cross-linked alginate beads. *Biotechnology and Applied Biochemistry* **39**: 319-322.

Jain, S., Mondal, K. & Gupta, M. N. (2006). Applications of alginate in bioseparation of proteins. *Artificial Cells Blood Substitutes and Biotechnology* **34**(2): 127-144.

Jendrossek, D. (2005). Fluorescence microscopical investigation of poly(3-hydroxybutyrate) granule formation in bacteria. *Biomacromolecules* **6**(2): 598-603.

Jendrossek, D. & Handrick, R. (2002). Microbial degradation of polyhydroxyalkanoates. *Annual Review of Microbiology* **56**: 403-432.

Jendrossek, D., Schirmer, A. & Schlegel, H. G. (1996). Biodegradation polyhydroxyalkanoic acids. *Applied Microbiology and Biotechnology* **46**(5-6): 451-463.

Jendrossek, D., Selchow, O. & Hoppert, M. (2007). Poly(3-hydroxybutyrate) granules at the early stages of formation are localized close to the cytoplasmic membrane in *Caryophanon latum*. *Applied and environmental microbiology* **73**(2): 586-593.

Jia, K. M., Cao, R. K., Hua, D. H. & Li, P. (2016). Study of class I and class III polyhydroxyalkanoate (PHA) synthases with substrates containing a modified side chain. *Biomacromolecules* **17**(4): 1477-1485.

Jiao, C. L., Xiong, P. G., Tao, J., Xu, S. J., Zhang, D. S., Lin, H. & Chen, Y. Y. (2016). Sodium alginate/graphene oxide aerogel with enhanced strength-toughness and its heavy metal adsorption study. *International Journal of Biological Macromolecules* **83**: 133-141.

Jung, K. W., Jeong, T. U., Choi, J. W., Ahn, K. H. & Lee, S. H. (2017). Adsorption of phosphate from aqueous solution using electrochemically modified biochar calcium-alginate beads: Batch and fixed-bed column performance. *Bioresource Technology* **244**: 23-32.

Keshavarz, T. & Roy, I. (2010). Polyhydroxyalkanoates: bioplastics with a green agenda. *Current Opinion in Microbiology* **13**(3): 321-326.

Keskin, G., Kizil, G., Bechelany, M., Pochat-Bohatier, C. & Oner, M. (2017). Potential of polyhydroxyalkanoate (PHA) polymers family as substitutes of petroleum based polymers for packaging applications and solutions brought by their composites to form barrier materials. *Pure and Applied Chemistry* **89**(12): 1841-1848.

Klein, J., Stock, J. & Vorlop, K.-D. (1983). Pore size and properties of spherical Ca-alginate biocatalysts. *European journal of applied microbiology and biotechnology* **18**(2): 86-91.

Klemenz, A., Schwinger, C., Brandt, J. & Kressler, J. (2003). Investigation of elasto-mechanical properties of alginate microcapsules by scanning acoustic microscopy. *Journal of Biomedical Materials Research Part A* **65A**(2): 237-243.

Kuo, C. K. & Ma, P. X. (2001). Ionically crosslinked alginate hydrogels as scaffolds for tissue engineering: Part 1. Structure, gelation rate and mechanical properties. *Biomaterials* **22**(6): 511-521.

Kurniasih, I. N., Liang, H., Mohr, P. C., Khot, G., Rabe, J. P. & Mohr, A. (2015). Nile red dye in aqueous surfactant and micellar solution. *Langmuir* **31**(9): 2639-2648.

Lee, B.-B., Ravindra, P. & Chan, E.-S. (2013). Size and shape of calcium alginate beads produced by extrusion dripping. *Chemical Engineering & Technology* **36**(10): 1627-1642.

Lee, J. W. (2011). Molecular characterisation of PHA synthase and the *in vivo* synthesis of functionalised PHA beads with surface immobilised proteins. Palmerston North, New Zealand, Massey Unversity. **Master of Science**.

Lee, J. W., Parlane, N. A., Rehm, B. H. A., Buddle, B. M. & Heiser, A. (2017a). Engineering mycobacteria for the production of self-assembling biopolyesters displaying mycobacterial antigens for use as a tuberculosis vaccine. *Applied and environmental microbiology* **83**(5).

Lee, J. W., Parlane, N. A., Wedlock, D. N. & Rehm, B. H. A. (2017b). Bioengineering a bacterial pathogen to assemble its own particulate vaccine capable of inducing cellular immunity. *Scientific Reports* **7**.

Lee, K. Y. & Mooney, D. J. (2012). Alginate: Properties and biomedical applications. *Progress in Polymer Science* **37**(1): 106-126.

Lee, O. S., Ha, B. J., Park, S. N. & Lee, Y. S. (1997). Studies on the pH-dependent swelling properties and morphologies of chitosan/calcium-alginate complexed beads. *Macromolecular Chemistry and Physics* **198**(9): 2971-2976.

Leong, J. Y., Lam, W. H., Ho, K. W., Voo, W. P., Lee, M. F. X., Lim, H. P., Lim, S. L., Tey, B. T., Poncelet, D. & Chan, E. S. (2016). Advances in fabricating spherical alginate hydrogels with controlled particle designs by ionotropic gelation as encapsulation systems. *Particuology* **24**: 44-60.

Levine, A. C., Heberlig, G. W. & Nomura, C. T. (2016). Use of thiol-ene click chemistry to modify mechanical and thermal properties of polyhydroxyalkanoates (PHAs). *International Journal of Biological Macromolecules* **83**: 358-365.

Li, C. D., Lu, J. J., Li, S. M., Tong, Y. B. & Ye, B. (2017). Synthesis of magnetic microspheres with sodium alginate and activated carbon for removal of methylene blue. *Materials* **10**(1).

Lim, J., You, M. L., Li, J. & Li, Z. B. (2017). Emerging bone tissue engineering via Polyhydroxyalkanoate (PHA)-based scaffolds. *Materials Science & Engineering C-Materials for Biological Applications* **79**: 917-929.

Lim, S. F. & Chen, J. P. (2007). Synthesis of an innovative calcium-alginate magnetic sorbent for removal of multiple contaminants. *Applied Surface Science* **253**(13): 5772-5775.

Lin, Y., Fugetsu, B., Terui, N. & Tanaka, S. (2005). Removal of organic compounds by alginate gel beads with entrapped activated carbon. *Journal of Hazardous Materials* **120**(1): 237-241.

Liu, H., Ru, J., Qu, J., Dai, R., Wang, Z. & Hu, C. (2009). Removal of persistent organic pollutants from micro-polluted drinking water by triolein embedded absorbent. *Bioresource Technology* **100**(12): 2995-3002.

Liu, X. D., Yu, W. Y., Zhang, Y., Xue, W. M., Tu, W. T., Xiong, Y., Ma, X. J., Chen, Y. & Yuan, Q. (2002). Characterization of structure and diffusion behaviour of Ca-alginate beads prepared with external or internal calcium sources. *Journal of Microencapsulation* **19**(6): 775-782.

Lundgren, D. G., Merrick, J. M. & Pfister, R. M. (1964). Structure of poly-beta-hydroxybutyric acid granules. *Journal of General Microbiology* **34**(3): 441-&.

Lupo, B., Maestro, A., Porras, M., Gutierrez, J. M. & Gonzalez, C. (2014). Preparation of alginate microspheres by emulsification/internal gelation to encapsulate cocoa polyphenols. *Food Hydrocolloids* **38**: 56-65.

Madison, L. L. & Huisman, G. W. (1999). Metabolic engineering of poly(3-hydroxyalkanoates): From DNA to plastic. *Microbiology and Molecular Biology Reviews* **63**(1): 21-53.

Maestro, B. & Sanz, J. M. (2017). Polyhydroxyalkanoate-associated phasins as phylogenetically heterogeneous, multipurpose proteins. *Microbial Biotechnology* **10**(6): 1323-1337.

Manavitehrani, I., Fathi, A., Badr, H., Daly, S., Shirazi, A. N. & Dehghani, F. (2016). Biomedical Applications of Biodegradable Polyesters. *Polymers* **8**(1).

Martinez-Abad, A., Gonzalez-Ausejo, J., Lagaron, J. M. & Cabedo, L. (2016). Biodegradable poly(3-hydroxybutyrate-co-3-hydroxyvalerate)/thermoplastic polyurethane blends with improved mechanical and barrier performance. *Polymer Degradation and Stability* **132**: 52-61.

Martinez-Donato, G., Piniella, B., Aguilar, D., Olivera, S., Perez, A., Castanedo, Y., Alvarez-Lajonchere, L., Duenas-Carrera, S., Lee, J. W., Burr, N., Gonzalez-Miro, M. & Rehm, B. H. A. (2016). Protective T cell and antibody immune responses

against hepatitis C virus achieved using a bipolyester-bead-based vaccine delivery system. *Clinical and Vaccine Immunology* **23**(4): 370-378.

Martins, S., Sarmento, B., Souto, E. B. & Ferreira, D. C. (2007). Insulin-loaded alginate microspheres for oral delivery - Effect of polysaccharide reinforcement on physicochemical properties and release profile. *Carbohydrate Polymers* **69**(4): 725-731.

Martinsen, A., Skjåk-Bræk, G., Smidsrød, O., Zanetti, F. & Paoletti, S. (1991). Comparison of different methods for determination of molecular weight and molecular weight distribution of alginates. *Carbohydrate Polymers* **15**(2): 171-193.

Martinsen, A., Skjakbraek, G. & Smidsrod, O. (1989). Alginate as immobilisation material. 1. Correlation between chemical and physical properties of alginate gel beads. *Biotechnology and Bioengineering* **33**(1): 79-89.

Matyash, M., Despang, F., Ikonomidou, C. & Gelinsky, M. (2014). Swelling and mechanical properties of alginate hydrogels with respect to promotion of neural growth. *Tissue Eng Part C Methods* **20**(5): 401-411.

Mayer, F., Madkour, M. H., PieperFurst, U., Wieczorek, R., Gesell, M. L. & Steinbuchel, A. (1996). Electron microscopic observations on the macromolecular organization of the boundary layer of bacterial PHA inclusion bodies. *Journal of General and Applied Microbiology* **42**(6): 445-455.

Mergaert, J. & Swings, J. (1996). Biodiversity of microorganisms that degrade bacterial and synthetic polyesters. *Journal of Industrial Microbiology & Biotechnology* **17**(5-6): 463-469.

Mifune, J., Grage, K. & Rehm, B. H. A. (2009). Production of functionalized biopolyester granules by recombinant *Lactococcus lactis*. *Applied and environmental microbiology* **75**(14): 4668-4675.

Mohamad, N. R., Marzuki, N. H. C., Buang, N. A., Huyop, F. & Wahab, R. A. (2015). An overview of technologies for immobilization of enzymes and surface analysis techniques for immobilized enzymes. *Biotechnology & Biotechnological Equipment* **29**(2): 205-220.

Mokhtari, S., Jafari, S. M. & Assadpour, E. (2017). Development of a nutraceutical nano-delivery system through emulsification/internal gelation of alginate. *Food Chemistry* **229**: 286-295.

Mondal, K., Mehta, P. & Gupta, M. N. (2004). Affinity precipitation of Aspergillus niger pectinase by microwave-treated alginate. *Protein Expression and Purification* **33**(1): 104-109.

Mørch, Ý. A., Donati, I., Strand, B. L. & Skjåk-Bræk, G. (2006). Effect of Ca2+, Ba2+, and Sr2+ on alginate microbeads. *Biomacromolecules* **7**(5): 1471-1480.

Mørch, Ý. A., Donati, I., Strand, B. L. & Skjåk-Bræk, G. (2007). Molecular engineering as an approach to design new functional properties of alginate. *Biomacromolecules* **8**(9): 2809-2814.

Muhammadi, Shabina, Afzal, M. & Hameed, S. (2015). Bacterial polyhydroxyalkanoates-eco-friendly next generation plastic: Production, biocompatibility, biodegradation, physical properties and applications. *Green Chemistry Letters and Reviews* **8**(3-4): 56-77.

Nagata, R., Koga, K., Gondo, S., Uemura, Y. & Hatate, Y. (2001). Preparation of calcium alginate micro-gel beads using a rotating nozzle. *Kagaku Kogaku Ronbunshu* **27**(5): 648-651.

Nagpal, M., Maheshwari, D. K., Rakha, P., Dureja, H., Goyal, S. & Dhingra, G. (2012). Formulation development and evaluation of alginate microspheres of ibuprofen. *Journal of Young Pharmacists : JYP* **4**(1): 13-16.

Nawaz, M. A., Rehman, H. U., Bibi, Z., Aman, A. & Ul Qader, S. A. (2015). Continuous degradation of maltose by enzyme entrapment technology using calcium alginate beads as a matrix. *Biochemistry and biophysics reports* **4**: 250-256.

Ngah, W. S. W. & Fatinathan, S. (2008). Adsorption of Cu(II) ions in aqueous solution using chitosan beads, chitosan-GLA beads and chitosan-alginate beads. *Chemical Engineering Journal* **143**(1-3): 62-72.

Nicodemus, G. D. & Bryant, S. J. (2008). Cell encapsulation in biodegradable hydrogels for tissue engineering applications. *Tissue Engineering Part B-Reviews* **14**(2): 149-165.

Nomanbhay, S. M. & Palanisamy, K. (2005). Removal of heavy metal from industrial wastewater using chitosan coated oil palm shell charcoal. *Electronic Journal of Biotechnology* **8**(1): 43-53.

Olabisi, R. M. (2015). Cell microencapsulation with synthetic polymers. *Journal of Biomedical Materials Research Part A* **103**(2): 846-859.

Ollis, D. L., Cheah, E., Cygler, M., Dijkstra, B., Frolow, F., Franken, S. M., Harel, M., Remington, S. J., Silman, I., Schrag, J., Sussman, J. L., Verschueren, K. H. G. & Goldman, A. (1992). The α/β hydrolase fold. *Protein Engineering* **5**(3): 197-211.

Ostberg, T., Vesterhus, L. & Graffner, C. (1993). Calcium alginate matrices for oral multiple-unit administration. 2. Effect of process and formulation factors on matrix properties. *International Journal of Pharmaceutics* **97**(1-3): 183-193.

Palmer, I. & Wingfield, P. T. (2012). Preparation and extraction of insoluble (inclusion-body) proteins from *Escherichia coli*. *Current protocols in protein science* **Chapter 6**.

Pandey, A., Bera, D., Shukla, A. & Ray, L. (2007). Studies on Cr(VI), Pb(II) and Cu(II) adsorption-desorption using calcium alginate as biopolymer. *Chemical Speciation and Bioavailability* **19**(1): 17-24.

Paques, J. P. (2015). Chapter 3 - Alginate nanospheres prepared by internal or external gelation with nanoparticles. Microencapsulation and Microspheres for Food Applications. San Diego, Academic Press**:** 39-55.

Paques, J. P., Sagis, L. M. C., van Rijn, C. J. M. & van der Linden, E. (2014a). Nanospheres of alginate prepared through w/o emulsification and internal gelation with nanoparticles of CaCO3. *Food Hydrocolloids* **40**: 182-188.

Paques, J. P., van der Linden, E., van Rijn, C. J. M. & Sagis, L. M. C. (2013). Alginate submicron beads prepared through w/o emulsification and gelation with CaCl2 nanoparticles. *Food Hydrocolloids* **31**(2): 428-434.

Paques, J. P., van der Linden, E., van Rijn, C. J. M. & Sagis, L. M. C. (2014b). Preparation methods of alginate nanoparticles. *Advances in Colloid and Interface Science* **209**: 163-171.

Park, H. G., Kim, T. W., Chae, M. Y. & Yoo, I.-K. (2007). Activated carbon-containing alginate adsorbent for the simultaneous removal of heavy metals and toxic organics. *Process Biochemistry* **42**(10): 1371-1377.

Park, J. P., Lee, K. B., Lee, S. J., Park, T. J., Kim, M. G., Chung, B. H., Lee, Z. W., Choi, I. S. & Lee, S. Y. (2005). Micropatterning proteins on polyhydroxyalkanoate substrates by using the substrate binding domain as a fusion partner. *Biotechnology and Bioengineering* **92**(2): 160-165.

Park, S. J., Kim, T. W., Kim, M. K., Lee, S. Y. & Lim, S. C. (2012). Advanced bacterial polyhydroxyalkanoates: Towards a versatile and sustainable platform for unnatural tailor-made polyesters. *Biotechnology Advances* **30**(6): 1196-1206.

Parlane, N. A., Grage, K., Lee, J. W., Buddle, B. M., Denis, M. & Rehm, B. H. A. (2011). Production of a particulate hepatitis C vaccine candidate by an engineered *Lactococcus lactis* strain. *Applied and environmental microbiology* **77**(24): 8516-8522.

Parlane, N. A., Grage, K., Mifune, J., Basaraba, R. J., Wedlock, D. N., Rehm, B. H. A. & Buddle, B. M. (2012). Vaccines displaying mycobacterial proteins on biopolyester beads stimulate cellular immunity and induce protection against Tuberculosis. *Clinical and Vaccine Immunology* **19**(1): 37-44.

Parlane, N. A., Gupta, S. K., Rubio-Reyes, P., Chen, S. X., Gonzalez-Miro, M., Wedlock, D. N. & Rehm, B. H. A. (2017). Self-assembled protein-coated polyhydroxyalkanoate beads: properties and biomedical applications. *Acs Biomaterials Science & Engineering* **3**(12): 3043-3057.

Parlane, N. A., Wedlock, D. N., Buddle, B. M. & Rehm, B. H. A. (2009). Bacterial polyester inclusions engineered to display vaccine candidate antigens for use as a novel class of safe and efficient vaccine delivery agents. *Applied and environmental microbiology* **75**(24): 7739-7744.

Paulo, B. B., Ramos, F. D. & Prata, A. S. (2017). An investigation of operational parameters of jet cutting method on the size of Ca-alginate beads. *Journal of Food Process Engineering* **40**(6).

Peretz, S., Anghel, D. F., Vasilescu, E., Florea-Spiroiu, M., Stoian, C. & Zgherea, G. (2015). Synthesis, characterization and adsorption properties of alginate porous beads. *Polymer Bulletin* **72**(12): 3169-3182.

Perumal, D. (2001). Microencapsulation of ibuprofen and Eudragit (R) RS 100 by the emulsion solvent diffusion technique. *International Journal of Pharmaceutics* **218**(1-2): 1-11.

Peters, V., Becher, D. & Rehm, B. H. A. (2007). The inherent property of polyhydroxyalkanoate synthase to form spherical PHA granules at the cell poles: The core region is required for polar localization. *Journal of Biotechnology* **132**(3): 238-245.

Peters, V. & Rehm, B. H. A. (2005). *In vivo* monitoring of PHA granule formation using GFP-labeled PHA synthases. *Fems Microbiology Letters* **248**(1): 93-100.

Peters, V. & Rehm, B. H. A. (2006). In vivo enzyme immobilization by use of engineered polyhydroxyalkanoate synthase. *Applied and environmental microbiology* **72**(3): 1777-1783.

Peters, V. & Rehm, B. H. A. (2008). Protein engineering of streptavidin for *in vivo* assembly of streptavidin beads. *Journal of Biotechnology* **134**(3-4): 266-274.

Pfeiffer, D. & Jendrossek, D. (2012). Localization of poly(3-Hydroxybutyrate) (PHB) granule-associated proteins during PHB granule formation and identification of two new phasins, PhaP6 and PhaP7, in *Ralstonia eutropha* H16. *Journal of Bacteriology* **194**(21): 5909-5921.

Pfeiffer, D., Wahl, A. & Jendrossek, D. (2011). Identification of a multifunctional protein, PhaM, that determines number, surface to volume ratio, subcellular localization and distribution to daughter cells of poly(3-hydroxybutyrate), PHB, granules in *Ralstonia eutropha* H16. *Molecular Microbiology* **82**(4): 936-951.

Philip, S., Keshavarz, T. & Roy, I. (2007). Polyhydroxyalkanoates: biodegradable polymers with a range of applications. *Journal of Chemical Technology and Biotechnology* **82**(3): 233-247.

Poirier, Y., Dennis, D. E., Klomparens, K. & Somerville, C. (1992). Polyhydroxybutyrate, abiodegradable thermoplastic, produced in transgenic plants. *Science* **256**(5056): 520-523.

Poncelet, D. (2001). Production of alginate beads by emulsification/internal gelation. Bioartificial Organs Iii: Tissue Sourcing, Immunoisolation, and Clinical Trials. D. Hunkeler, A. Cherrington, A. Prokop & R. Rajotte. New York, New York Acad Sciences. **944:** 74-82.

Poncelet, D., Desmet, B. P., Beaulieu, C., Huguet, M. L., Fournier, A. & Neufeld, R. J. (1995). Production of alginate beads by emulsification/internal gelation. 2. Physichochemistry. *Applied Microbiology and Biotechnology* **43**(4): 644-650.

Poncelet, D., Lencki, R., Beaulieu, C., Halle, J. P., Neufeld, R. J. & Fournier, A. (1992). Production of alginate beads by emulsification/internal gelation. 1. Methodology. *Applied Microbiology and Biotechnology* **38**(1): 39-45.

Pötter, M., Madkour, M. H., Mayer, F. & Steinbüchel, A. (2002). Regulation of phasin expression and polyhydroxyalkanoate (PHA) granule formation in *Ralstonia eutropha* H16. *Microbiology-Sgm* **148**: 2413-2426.

Prieto, M. A., Buhler, B., Jung, K., Witholt, B. & Kessler, B. (1999). PhaF, a polyhydroxyalkanoate-granule-associated protein of *Pseudomonas oleovorans* GPo1 involved in the regulatory expression system for pha genes. *Journal of Bacteriology* **181**(3): 858-868.

Priji, P., Sajith, S., Sreedevi, S., Unni, K. N., Kumar, S. & Benjamin, S. (2016). *Candida tropicalis* BPU1 produces polyhydroxybutyrate on raw starchy substrates. *Starch-Starke* **68**(1-2): 57-66.

Qi, Q., Steinbuchel, A. & Rehm, B. H. A. (2000). *In vitro* synthesis of poly(3-hydroxydecanoate): purification and enzymatic characterization of type II polyhydroxyalkanoate synthases PhaC1 and PhaC2 from *Pseudomonas aeruginosa*. *Applied Microbiology and Biotechnology* **54**(1): 37-43.

Qi, Q. S. & Rehm, B. H. A. (2001). Polyhydroxybutyrate biosynthesis in *Caulobacter crescentus*: molecular characterization of the polyhydroxybutyrate synthase. *Microbiology-Sgm* **147**: 3353-3358.

Qiu, Y., Hamilton, S. K. & Temenoff, J. (2011). 4 - Improving mechanical properties of injectable polymers and composites A2 - Vernon, Brent. Injectable Biomaterials, Woodhead Publishing**:** 61-91.

Radovich, J. M. (1985). Mass transfer effects in fermentations using immobilised whole cells. *Enzyme and Microbial Technology* **7**(1): 2-10.

Raj, N. K. & Sharma, C. P. (2003). Oral insulin-a perspective. *J Biomater Appl* **17**(3): 183-196.

Rasiah, I. A. & Rehm, B. H. A. (2009). One-Step Production of Immobilized alpha-Amylase in Recombinant *Escherichia coli*. *Applied and environmental microbiology* **75**(7): 2012-2016.

Reddy, C. S. K., Ghai, R., Rashmi & Kalia, V. C. (2003). Polyhydroxyalkanoates: an overview. *Bioresource Technology* **87**(2): 137-146.

Rehm, B. H. A. (2003). Polyester synthases: natural catalysts for plastics. *Biochemical Journal* **376**: 15-33.

Rehm, B. H. A. (2007). Biogenesis of microbial polyhydroxyalkanoate granules: a platform technology for the production of tailor-made bioparticles. *Current Issues in Molecular Biology* **9**: 41-62.

Rehm, B. H. A. (2010). Bacterial polymers: biosynthesis, modifications and applications. *Nature Reviews Microbiology* **8**(8): 578-592.

Rehm, B. H. A., Antonio, R. V., Spiekermann, P., Amara, A. A. & Steinbuchel, A. (2002). Molecular characterization of the poly(3-hydroxybutyrate) (PHB) synthase from *Ralstonia eutropha*: *in vitro* evolution, site-specific mutagenesis and development of PHB synthase protein model. *Biochimica Et Biophysica Acta-Proteins and Proteomics* **1598**(1-2): 195-195.

Rehm, F. B. H., Chen, S. X. & Rehm, B. H. A. (2016). Enzyme engineering for *in situ* immobilization. *Molecules* **21**(10).

Rehman, H. U., Arnan, A., Silipo, A., Ul Qader, S. A., Molinaro, A. & Ansari, A. (2013). Degradation of complex carbohydrate: Immobilization of pectinase from *Bacillus licheniformis* KIBGE-IB21 using calcium alginate as a support. *Food Chemistry* **139**(1-4): 1081-1086.

Reis, C. P., Neufeld, R. J., Vilela, S., Ribeiro, A. J. & Veiga, F. (2006). Review and current status of emulsion/dispersion technology using an internal gelation process for the design of alginate particles. *Journal of Microencapsulation* **23**(3): 245-257.

Remminghorst, U. & Rehm, B. H. A. (2006). Bacterial alginates: from biosynthesis to applications. *Biotechnology Letters* **28**(21): 1701-1712.

Reusch, R. N. (2000). Transmembrane ion transport by polyphosphate/poly-(R)-3-hydroxybutyrate complexes. *Biochemistry-Moscow* **65**(3): 280-295.

Reyes, P. R., Parlane, N. A., Wedlock, D. N. & Rehm, B. H. A. (2016). Immunogencity of antigens from *Mycobacterium tuberculosis* self-assembled as particulate vaccines. *International Journal of Medical Microbiology* **306**(8): 624-632.

Riahi, K., Chaabane, S. & Ben Thayer, B. (2017). A kinetic modeling study of phosphate adsorption onto Phoenix dactylifera L. date palm fibers in batch mode. *Journal of Saudi Chemical Society* **21**: S143-S152.

Rinaudo, M. (2014). Biomaterials based on a natural polysaccharide: alginate. *TIP* **17**(1): 92-96.

Robins, K. J., Hooks, D. O., Rehm, B. H. A. & Ackerley, D. F. (2013). *Escherichia coli* NemA Is an efficient chromate reductase that can be biologically immobilized to provide a cell free system for remediation of hexavalent chromium. *Plos One* **8**(3).

Roy, I. & Gupta, M. N. (2000). Current trends in affinity-based separations of proteins/enzymes. *Current Science* **78**(5): 587-591.

Roy, I., Jain, S., Teotia, S. & Gupta, M. N. (2004). Evaluation of microbeads of calcium alginate as a fluidized bed medium for affinity chromatography of *Aspergillus niger* pectinase. *Biotechnology Progress* **20**(5): 1490-1495.

Ru, J., Liu, H. J., Qu, J. H., Wang, A. M., Dai, R. H. & Wang, Z. J. (2007). Selective removal of organochlorine pesticides (OCPs) from aqueous solution by triolein-embedded composite adsorbent. *Journal of Environmental Science and Health, Part. B* **42**(1): 53-61.

Rudzinski, W. & Plazinski, W. (2009). On the applicability of the pseudo-second order equation to represent the kinetics of adsorption at solid/solution interfaces: a theoretical analysis based on the statistical rate theory. *Adsorption-Journal of the International Adsorption Society* **15**(2): 181-192.

Salsac, A., Liguo, Z. & Gherbezza, J. (2009). Measurement of mechanical properties of alginate beads using ultrasound. 19ème Congrès Français de Mécanique.

Sanchez-Bayo, F. & Goka, K. (2014). Pesticide residues and bees - A risk assessment. *Plos One* **9**(4): 16.

Sharma, A., Sharma, S. & Gupta, M. N. (2000a). Purification of wheat germ amylase by precipitation. *Protein Expression and Purification* **18**(1): 111-114.

Sharma, R. & Ray, A. R. (1995). Polyhydroxybutyrate, its copolymers and blends. *Journal of Macromolecular Science-Reviews in Macromolecular Chemistry and Physics* **C35**(2): 327-359.

Sharma, S. & Gupta, M. N. (2001). Alginate as a macroaffinity ligand and an additive for enhanced activity and thermostability of lipases. *Biotechnology and Applied Biochemistry* **33**: 161-165.

Sharma, S., Sharma, A. & Gupta, M. N. (2000b). One step purification of peanut phospholipase D by precipitation with alginate. *Bioseparation* **9**(2): 93-98.

Shelke, N. B., James, R., Laurencin, C. T. & Kumbar, S. G. (2014). Polysaccharide biomaterials for drug delivery and regenerative engineering. *Polymers for Advanced Technologies* **25**(5): 448-460.

Shishatskaya, E. I., Volova, T. G., Puzyr, A. P., Mogilnaya, O. A. & Efremov, S. N. (2004). Tissue response to the implantation of biodegradable polyhydroxyalkanoate sutures. *Journal of Materials Science-Materials in Medicine* **15**(6): 719-728.

Silva, C. M., Ribeiro, A. J., Figueiredo, I. V., Goncalves, A. R. & Veiga, F. (2006). Alginate microspheres prepared by internal gelation: Development and effect on insulin stability. *International Journal of Pharmaceutics* **311**(1-2): 1-10.

Silva, C. M., Ribeiro, A. J., Figueiredo, M., Ferreira, D. & Veiga, F. (2005). Microencapsulation of hemoglobin in chitosan-coated alginate microspheres prepared by emulsification/internal gelation. *Aaps Journal* **7**(4): E903-E913.

Simpliciano, C., Clark, L., Asi, B., Chu, N., Mercado, M., Diaz, S., Goedert, M. & Mobed-Miremadi, M. (2013). Cross-linked alginate film pore size determination using atomic force microscopy and validation using diffusivity determinations. *Journal of Surface Engineered Materials and Advanced Technology* **3**: 1-12.

Singh, M. N., Hemant, K. S., Ram, M. & Shivakumar, H. G. (2010). Microencapsulation: A promising technique for controlled drug delivery. *Res Pharm Sci* **5**(2): 65-77.

Skjåk-Bræk, G., Grasdalen, H. & Smidsrød, O. (1989). Inhomogeneous polysaccharide ionic gels. *Carbohydrate Polymers* **10**(1): 31-54.

Skjermo, J., Defoort, T., Dehasque, M., Espevik, T., Olsen, Y., Skjåk-Bræk, G., Sorgeloos, P. & Vadstein, O. (1995). Immunostimulation of juvenile turbot (*Scophthalmusmaximus L.*) using an alginate with high mannuronic acid content administered via the live food organism Artemia. *Fish & Shellfish Immunology* **5**(7): 531-534.

Smidsrød, O. (1974). Molecular basis for some physical properties of alginates in the gel state. *Faraday Discussions of the Chemical Society* **57**(0): 263-274.

Smidsrød, O. & Skja˚k-Bræk, G. (1990). Alginate as immobilization matrix for cells. *Trends in Biotechnology* **8**: 71-78.

Somers, W., Vantreit, K., Rozie, H., Rombouts, F. M. & Visser, J. (1989). Isolation and purification of endo-polycalacturonase by affinity-chromatography in a fluidized-bed reactor. *Chemical Engineering Journal and the Biochemical Engineering Journal* **40**(1): B7-B19.

Soni, M. L., Kumar, M. & Namdeo, K. P. (2010). Sodium alginate microspheres for extending drug release: formulation and in vitro evaluation. *International Journal of Drug Delivery* **2**(1): 64-68.

Spiekermann, P., Rehm, B. H. A., Kalscheuer, R., Baumeister, D. & Steinbuchel, A. (1999). A sensitive, viable-colony staining method using Nile red for direct screening of bacteria that accumulate polyhydroxyalkanoic acids and other lipid storage compounds. *Arch Microbiol* **171**(2): 73-80.

Steinbüchel, A., Hustede, E., Liebergesell, M., Pieper, U., Timm, A. & Valentin, H. (1992). Molecular basis for biosynthesis and accumulation of polyhydroxyalkanoic acids in bacteria. *Fems Microbiology Letters* **103**(2-4): 217-230.

Steinbüchel, A. & Valentin, H. E. (1995). Diversity of bacterial polyhydroxyalkanoic acids. *Fems Microbiology Letters* **128**(3): 219-228.

Steinmann, B., Christmann, A., Heiseler, T., Fritz, J. & Kolmar, H. (2010). *In vivo* enzyme immobilization by inclusion body display. *Applied and environmental microbiology* **76**(16): 5563-5569.

Stewart, T. J., Yau, J. H., Allen, M. M., Brabander, D. J. & Flynn, N. T. (2009). Impacts of calcium-alginate density on equilibrium and kinetics of lead(II) sorption onto hydrogel beads. *Colloid and Polymer Science* **287**(9): 1033-1040.

Stewart, W. W. & Swaisgood, H. E. (1993). Characterization of calcium alginate pore diameter by size-exclusion chromatography using protein standards. *Enzyme and Microbial Technology* **15**(11): 922-927.

Sudesh, K., Loo, C. Y., Goh, L. K., Iwata, T. & Maeda, M. (2007). The oil-absorbing property of polyhydroxyalkanoate films and its practical application: A refreshing new outlook for an old degrading material. *Macromolecular Bioscience* **7**(11): 1199-1205.

Sun, J. C. & Tan, H. P. (2013). Alginate-based biomaterials for regenerative mdicine aplications. *Materials* **6**(4): 1285-1309.

Tan, G. Y. A., Chen, C. L., Li, L., Ge, L., Wang, L., Razaad, I. M. N., Li, Y., Zhao, L., Mo, Y. & Wang, J. Y. (2014). Start a research on biopolymer polyhydroxyalkanoate (PHA): A Review. *Polymers* **6**(3): 706-754.

Tanaka, H., Matsumura, M. & Veliky, I. A. (1984). Diffusion characteristics of substrates in Ca‐alginate gel beads. *Biotechnology and Bioengineering* **26**(1): 53-58.

Teotia, S., Khare, S. K. & Gupta, M. N. (2001a). An efficient purification process for sweet potato beta-amylase by affinity precipitation with alginate. *Enzyme and Microbial Technology* **28**(9-10): 792-795.

Teotia, S., Lata, R., Khare, S. K. & Gupta, M. N. (2001b). One-step purification of glucoamylase by affinity precipitation with alginate. *Journal of Molecular Recognition* **14**(5): 295-299.

Thomson, N., Summers, D. & Sivaniah, E. (2010). Synthesis, properties and uses of bacterial storage lipid granules as naturally occurring nanoparticles. *Soft Matter* **6**(17): 4045-4057.

Thu, B., Smidsrød, O. & Skjåk-Bræk, G. (1996). Alginate gels-some structure-function correlations relevant to their use as immobilization matrix for cells. *Immobilized cells: basics and applications* **11**: 19.

Tian, J. M., He, A. M., Lawrence, A. G., Liu, P. H., Watson, N., Sinskey, A. J. & Stubbe, J. (2005). Analysis of transient polyhydroxybutyrate production in *Wautersia eutropha* H16 by quantitative western analysis and transmission electron microscopy. *Journal of Bacteriology* **187**(11): 3825-3832.

Timm, A. & Steinbüchel, A. (1992). Cloning and molecular analysis of the poly (3‐hydroxyalkanoic acid) gene locus of *Pseudomonas aeruginosa* PAO1. *European Journal of Biochemistry* **209**(1): 15-30.

Tritz, J., Rahouadj, R., de Isla, N., Charif, N., Pinzano, A., Mainard, D., Bensoussan, D., Netter, P., Stoltz, J. F., Benkirane-Jessel, N. & Huselstein, C. (2010). Designing a three-dimensional alginate hydrogel by spraying method for cartilage tissue engineering. *Soft Matter* **6**(20): 5165-5174.

Tsuge, T., Hyakutake, M. & Mizuno, K. (2015). Class IV polyhydroxyalkanoate (PHA) synthases and PHA-producing *Bacillus*. *Applied Microbiology and Biotechnology* **99**(15): 6231-6240.

Tsuge, T., Taguchi, K., Taguchi, S. & Doi, Y. (2003). Molecular characterization and properties of (R)-specific enoyl-CoA hydratases from *Pseudomonas aeruginosa*: Metabolic tools for synthesis of polyhydroxyalkanoates via fatty acid beta-oxidation. *International Journal of Biological Macromolecules* **31**(4-5): 195-205.

Vijayakumar, G., Tamilarasan, R. & Dharmendirakumar, M. (2012). Adsorption, kinetic, equilibrium and thermodynamic studies on the removal of basic dye rhodamine-B from aqueous solution by the use of natural adsorbent perlite. *Journal of Material and Environmental Science* **3**(1): 157-170.

Vu, H. C., Dwivedi, A. D., Le, T. T., Seo, S. H., Kim, E. J. & Chang, Y. S. (2017). Magnetite graphene oxide encapsulated in alginate beads for enhanced adsorption of Cr(VI) and As(V) from aqueous solutions: Role of crosslinking metal cations in pH control. *Chemical Engineering Journal* **307**: 220-229.

Wahl, A., Schuth, N., Pfeiffer, D., Nussberger, S. & Jendrossek, D. (2012). PHB granules are attached to the nucleoid via PhaM in *Ralstonia eutropha*. *Bmc Microbiology* **12**.

Wang, H. & Shadman, F. (2013). Effect of particle size on the adsorption and desorption properties of oxide nanoparticles. *Aiche Journal* **59**(5): 1502-1510.

Wang, J. G. & Bakken, L. R. (1998). Screening of soil bacteria for poly-beta-hydroxybutyric acid production and its role in the survival of starvation. *Microbial Ecology* **35**(1): 94-101.

Wang, S. B., Xu, F. H., He, H. S. & Weng, L. J. (2005). Novel alginate-poly(L-histidine) microcapsules as drug carriers: in vitro protein release and short term stability. *Macromolecular Bioscience* **5**(5): 408-414.

Wang, S. C., Chen, W., Xiang, H. X., Yang, J. J., Zhou, Z. & Zhu, M. F. (2016). Modification and potential application of short-chain-length polyhydroxyalkanoate (SCL-PHA). *Polymers* **8**(8): 28.

Wang, T., Ye, L. & Song, Y. R. (1999). Progress of PHA production in transgenic plants. *Chinese Science Bulletin* **44**(19): 1729-1736.

Wang, X., Zhu, K. X. & Zhou, H. M. (2011). Immobilization of glucose oxidase in alginate-chitosan microcapsules. *International Journal of Molecular Sciences* **12**(5): 3042-3054.

Wang, Z., Wu, H., Chen, J., Zhang, J., Yao, Y. & Chen, G. (2008). A novel self-cleaving phasin tag for purification of recombinant proteins based on hydrophobic polyhydroxyalkanoate nanoparticles. *Lab on a Chip* **8**(11): 1957-1962.

Waugh, D. S. (2005). Making the most of affinity tags. *Trends in Biotechnology* **23**(6): 316-320.

Wu, C., Zhu, Y., Chang, J., Zhang, Y. & Xiao, Y. (2010). Bioactive inorganic-materials/alginate composite microspheres with controllable drug-delivery ability. *J Biomed Mater Res B Appl Biomater* **94**(1): 32-43.

Wu, Z., Zhong, H., Yuan, X., Wang, L., Chen, X., Zeng, G. & Wu, Y. (2014). Adsorptive removal of methylene blue by rhamnolipid-functionalized graphene oxide from wastewater. *Water Research* **67**: 330-344.

Yamashita, N., Saitou, K., Takagi, A. & Maruyama, A. (2009). Preparation and characterization of gelatin sponge millispheres injectable through microcatheters. *Medical Devices (Auckland, N.Z.)* **2**: 19-25.

York, G. M., Stubbe, J. & Sinskey, A. J. (2002). The *Ralstonia eutropha* PhaR protein couples synthesis of the PhaP phasin to the presence of polyhydroxybutyrate in

cells and promotes polyhydroxybutyrate production. *Journal of Bacteriology* **184**(1): 59-66.

Yotsuyanagi, T., Yoshioka, I., Segi, N. & Ikeda, K. (1990). Effects of monovalent metal ions and propranolol on the calcium association in calcium-induced alginate gel beads. *Chemical & Pharmaceutical Bulletin* **38**(11): 3124-3126.

You, J. O., Park, S. B., Park, H. Y., Haam, S., Chung, C. H. & Kim, W. S. (2001). Preparation of regular sized Ca-alginate microspheres using membrane emulsification method. *Journal of Microencapsulation* **18**(4): 521-532.

Zhang, S. M., Kolvek, S., Lenz, R. W. & Goodwin, S. (2003). Mechanism of the polymerization reaction initiated and catalyzed by the polyhydroxybutyrate synthase of *Ralstonia eutropha*. *Biomacromolecules* **4**(3): 504-509.

Zhang, W. (2014). Nanoparticle aggregation: Principles and modeling. Nanomaterial: Impacts on Cell Biology and Medicine. D. G. Capco & Y. Chen. **811:** 19-43.

Zhang, X. X., Wei, C. H., He, Q. C. & Ren, Y. (2010a). Enrichment of chlorobenzene and o-nitrochlorobenzene on biomimetic adsorbent prepared by poly-3-hydroxybutyrate (PHB). *Journal of Hazardous Materials* **177**(1-3): 508-515.

Zhang, X. X., Wei, C. H., He, Q. C. & Ren, Y. A. (2010b). Preparation and characterization of biomimetic adsorbent from poly-3-hydroxybutyrate. *Journal of Environmental Sciences* **22**(8): 1267-1272.

Zhang, Y. L., Wei, W., Lv, P. P., Wang, L. Y. & Ma, G. H. (2011). Preparation and evaluation of alginate-chitosan microspheres for oral delivery of insulin. *European Journal of Pharmaceutics and Biopharmaceutics* **77**(1): 11-19.

Zhao, F. H., Li, H., Wang, X. C., Wu, L., Hou, T. G., Guan, J., Jiang, Y. J., Xu, H. F. & Mu, X. D. (2015). CRGO/alginate microbeads: an enzyme immobilization system and its potential application for a continuous enzymatic reaction. *Journal of Materials Chemistry B* **3**(48): 9315-9322.

Zhao, Y. Y., Carvajal, M. T., Won, Y. Y. & Harris, M. T. (2007). Preparation of calcium alginate microgel beads in an electrodispersion reactor using an internal source of calcium carbonate nanoparticles. *Langmuir* **23**(25): 12489-12496.

Zhou, Q. S., Lin, X. Y., Qian, J., Wang, J. & Luo, X. G. (2015). Porous zirconium alginate beads adsorbent for fluoride adsorption from aqueous solutions. *Rsc Advances* **5**(3): 2100-2112.

Zhou, Y., Kajiyama, S., Masuhara, H., Hosokawa, Y., Kaji, T. & Fukui, K. (2009). A new size and shape controlling method for producing calcium alginate beads with immobilized proteins. *J Biomed Sci Eng* **2**: 287-293.

Zhu, H., Srivastava, R., Brown, J. Q. & McShane, M. J. (2005). Combined physical and chemical immobilization of glucose oxidase in alginate microspheres improves stability of encapsulation and activity. *Bioconjugate Chemistry* **16**(6): 1451-1458.

Zia, K. M., Zia, F., Zuber, M., Rehman, S. & Ahmad, M. N. (2015). Alginate based polyurethanes: A review of recent advances and perspective. *International Journal of Biological Macromolecules* **79**: 377-387.

Zou, H. B., Shi, M. X., Zhang, T. T., Li, L., Li, L. Z. & Xian, M. (2017). Natural and engineered polyhydroxyalkanoate (PHA) synthase: key enzyme in biopolyester production. *Applied Microbiology and Biotechnology* **101**(20): 7417-7426.

Zuidam, N. J. & Shimoni, E. (2010). Overview of microencapsulates for use in food products or processes and methods to make them. Encapsulation Technologies for Active Food Ingredients and Food Processing. N. J. Zuidam & V. Nedovic. New York, NY, Springer New York**:** 3-29.

Zulfikar, M. A., Afrita, S., Wahyuningrum, D. & Ledyastuti, M. (2016). Preparation of Fe3O4-chitosan hybrid nano-particles used for humic acid adsorption. *Environmental Nanotechnology, Monitoring & Management* **6**: 64-75.

Chapter 6: Appendices

Appendix I

Table 10: Summary of PHA bead characteristics used for IgG binding domain assay in stock suspension.

PHA bead Types	Protein Profile		Particle size distribution[3]					
	Protein on PHA beads (mg/g)[1]	PhaC derived protein proportion (%)[2]	D (10) (μm)	D (50) (μm)	D (90) (μm)	SPAN	Uniformity	Specific Surface Area (m^2/kg)
PhaC	5.4±0.2	36.9	0.818	6.23	18.0	2.764	0.957	2,211
ZZC	2.1±0.3	26.2	0.392	2.17	12.6	5.646	2.493	6,085

Note: [1] Protein quantified by SDS-PAGE gel densitometry. [2] Protein proportion obtained from densitometry on SDS-PAGE gel. [3] Results obtained from laser diffraction.

Table 11: Summary of PHA bead characteristics used for enzyme activity assay in stock suspension.

PHA bead Types	Protein Profile		Particle size distribution[3]					
	Protein on PHA beads (mg/g)[1]	PhaC derived protein proportion (%)[2]	D (10) (μm)	D (50) (μm)	D (90) (μm)	SPAN	Uniformity	Specific Surface Area (m^2/kg)
PhaC	5.6±0.02	40.4	2.53	6.92	46.6	6.365	1.921	1,021
PhaC-OpdA	14.2±0.4	46	5.15	13.2	33.9	2.167	0.914	559.5

Note: [1] Protein quantified by SDS-PAGE gel densitometry. [2] Protein proportion obtained from densitometry on SDS-PAGE gel. [3] Results from laser diffraction.

Appendix II

Table 12: Summary of particle size distribution of alginate microspheres in different production parameters and solutions.

		Particle size distribution characteristics					Particle size difference		
rpm	Sample Name	D (10)	D (50)	D (90)	Span	Uniformity	D (10)	D (50)	D (90)
	Alginate microspheres								
250	I-H_2O	107	186	334	1.22	0.377	-	-	-
	I+E-H_2O	47.9	82.3	144	1.037	0.323	-55%	-56%	-57%
	I+E-TBS	81.7	131	211	0.987	0.307	171%	159%	147%
	I+E-Glycine	66.5	99.6	151	0.846	0.262	144%	131%	121%
350	I-H_2O	87.5	138	220	0.96	0.296	-	-	-
	I+E-H_2O	46.3	76.3	125	1.037	0.323	-47%	-45%	-43%
	I+E-TBS	76	114	173	0.851	0.263	164%	149%	138%
	I+E-Glycine	72.8	120	203	1.087	0.334	152%	146%	141%
450	I-H_2O	56.1	90.3	147	1.004	0.31	-	-	-
	I+E-H_2O	37.6	60.3	97.1	0.987	0.306	-33%	-33%	-34%
	I+E-TBS	52.3	79.8	123	0.888	0.273	139%	132%	127%
	I+E-Glycine	48.8	74.7	116	0.893	0.276	130%	124%	119%
	PhaC PHA bead-alginate microspheres								
250	I-H_2O	125	231	450	1.407	0.443	-	-	-
	I+E-H_2O	37.4	67.8	137	1.469	0.527	-70%	-71%	-70%
	I+E-TBS	71.8	119	202	1.099	0.336	192%	176%	147%
	I+E-Glycine	63.1	109	200	1.264	0.406	169%	161%	146%
350	I-H_2O	95.9	163	289	1.184	0.367	-	-	-
	I+E-H_2O	38.8	67.2	117	1.159	0.359	-60%	-59%	-60%
	I+E-TBS	70.5	109	170	0.913	0.282	182%	162%	145%
	I+E-Glycine	60	95.1	154	0.985	0.304	155%	142%	132%
450	I-H_2O	62.1	105	183	1.16	0.399	-	-	-
	I+E-H_2O	29.9	50.5	86	1.111	0.396	-52%	-52%	-53%
	I+E-TBS	50	81.6	136	1.059	0.325	167%	162%	158%
	I+E-Glycine	47	76.1	127	1.047	0.327	157%	151%	148%
	ZZC PHA bead-alginate microspheres								
250	I-H_2O	161	292	525	1.247	0.384	-	-	-
	I+E-H_2O	38	72.7	152	1.572	0.529	-76%	-75%	-71%
	I+E-TBS	72.4	128	232	1.247	0.387	191%	176%	153%
	I+E-Glycine	67.3	119	217	1.259	0.388	177%	164%	143%
350	I-H_2O	117	197	332	1.092	0.334	-	-	-
	I+E-H_2O	39.5	69.8	123	1.192	0.368	-66%	-65%	-63%
	I+E-TBS	72.6	113	177	0.926	0.286	184%	162%	144%
	I+E-Glycine	62.1	100	163	1.007	0.313	157%	143%	133%
450	I-H_2O	77.6	128	215	1.075	0.335	-	-	-
	I+E-H_2O	31.7	53.4	89.2	1.077	0.333	-59%	-58%	-59%
	I+E-TBS	57.9	89.9	141	0.924	0.285	183%	168%	158%
	I+E-Glycine	52.1	79.8	124	0.899	0.277	164%	149%	139%

Note: “I” refers to microspheres produced by internal gelation and “I+E” refers to microspheres produced by internal gelation followed by additional gelation (double gelation). The percentage of I+E was compared with microspheres produced by internal gelation and I+E-TBS (50mM Tris and 50mM NaCl, pH7.4) and 100 Mm Glycine (pH2.5) were compared with I+E-H_2O

Table 13: Summary of particle size distribution of PHA bead-alginate microspheres in water.

PHA bead Types	D (10) (μm)	D (50) (μm)	D (90) (μm)	SPAN	Uniformity	Specific Surface Area (m^2/kg)
Alginate microspheres	60	95.2	152	0.963	0.297	66.92
PhaC PHA bead-alginate microspheres	78.9	151	294	1.425	0.448	63.19
PhaC-OpdA PHA bead-alginate microspheres	85	157	272	1.188	0.372	68.68

Note: Results from laser diffraction.

Appendix III

A

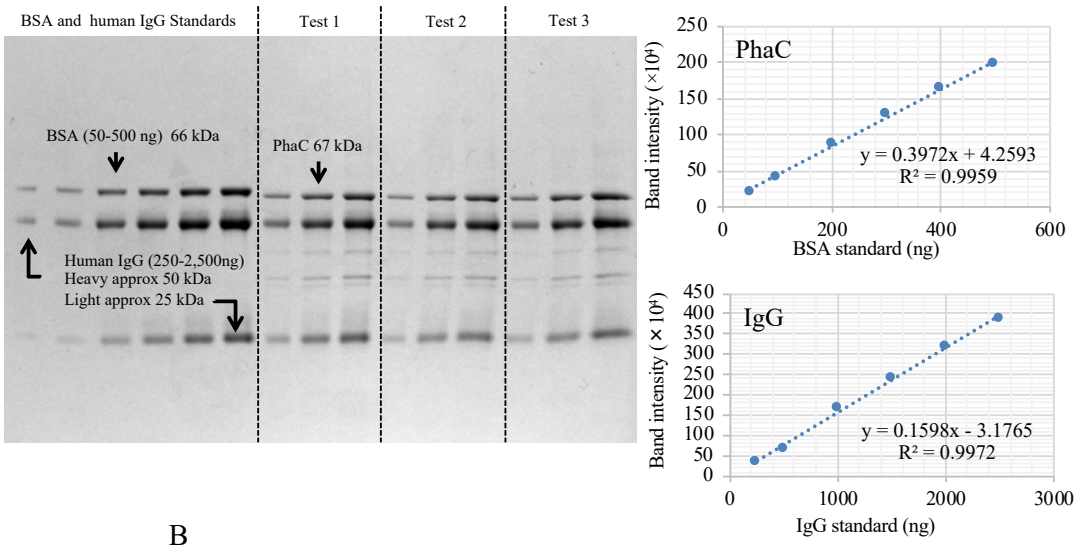

B

Sample	Phase	Bound IgG on PhaC derived protein (mg/mg)	R^2 (BSA)	R^2 (IgG)
PhaC	Binding	1.34±0.01	0.995	0.994
	Elution	1.05±0.03	0.999	0.998
ZZC	Binding	9.25±0.10	0.992	0.99
	Elution	4.16±0.13	0.999	0.995
Batch test				
PhaC-ALG	Binding	5.49±0.23	0.996	0.997
	Elution	8.64±0.87	0.999	0.998
ZZC-ALG	Binding	21.77±0.21	0.991	0.995
	Elution	27.30±1.59	0.992	0.994
Column test				
PhaC-ALG	Binding	6.40±0.43	0.995	0.993
	Elution	11.21±1.87	0.996	0.997
ZZC-ALG	Binding	19.96±1.70	0.991	0.984
	Elution	28.65±1.96	0.975	0.977

Figure 43: Quantification of bound IgG on the PhaC derived proteins by SDS-PAGE densitometry method. A: representative SDS-PAGE gel for quantifying bound IgG on PhaC derived protein on PHA beads by densitometry method, B: Summary of the amount of bound IgG on PhaC derived proteins after binding and elution phase and coefficient correlation of the densitometry test. PhaC indicates free PhaC PHA beads, ZZC indicates free ZZC PHA bead, PhaC-ALG indicates PhaC PHA bead-alginate microspheres, ZZC-ALG indicates ZZC PHA bead-alginate microspheres.

Appendix IV

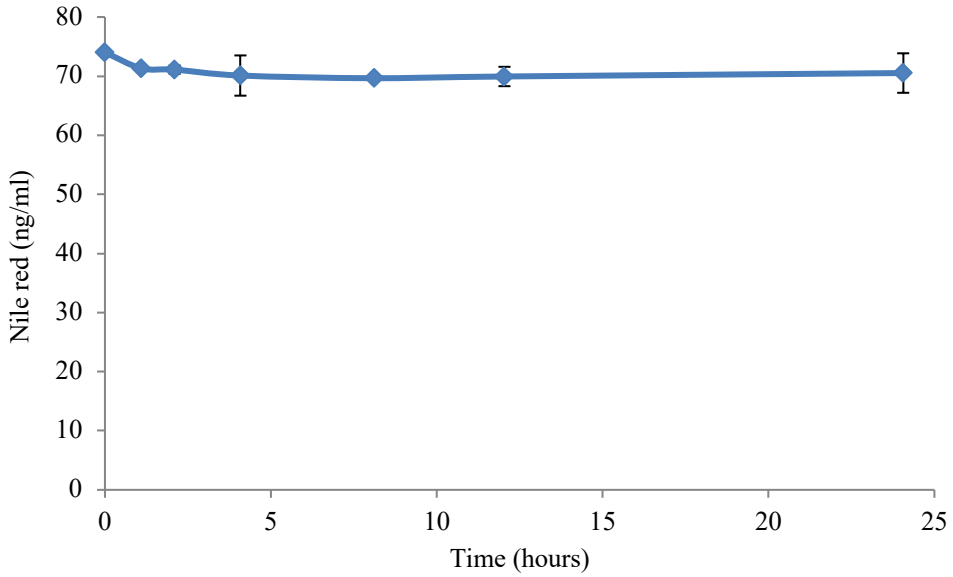

Figure 44: Quality control of Nile red solution in a flask over 24 hours incubation for adsorption kinetic test. The initial concentration of Nile red solution containing 10% v/v DMSO: 70 ng/ml; incubation: 25°C with 100rpm shaking for 24 hours. The measurement was done in triplicate and mean±standard deviation is reported.

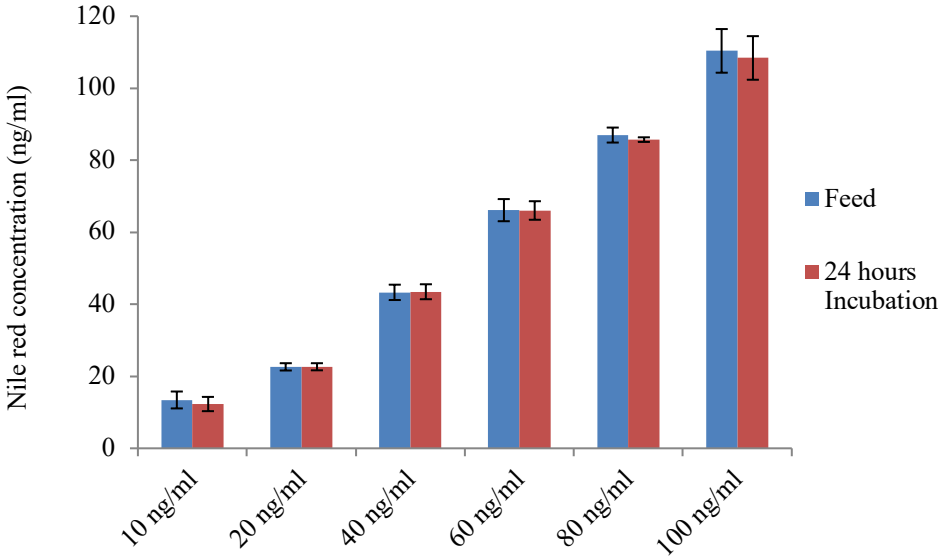

Figure 45: Quality control of Nile red solution in a flask after 24 hours incubation for adsorption isotherm test. The initial concentration of Nile red solution containing 10% v/v DMSO: 10-100 ng/ml; incubation: 25°C with 100rpm shaking for 24 hours. The measurement was done in triplicate and mean±standard deviation is reported.